The Passive Control of Machine Tool Vibration with a Piezoelectric Actuator

by

Cornelius Johannes Stander

A dissertation submitted in partial fulfilment of

the requirements for the degree

Master of Engineering

in the Department of Mechanical and Aeronautical Engineering

of the Faculty of Engineering

of the

University of Pretoria

January 2000

The Passive Control of Machine Tool Vibration with a Piezoelectric Actuator

by

Cornelius Johannes Stander

Supervisor	:	Prof. P.S. Heyns
Department	:	Mechanical and Aeronautical Engineering
Degree	:	M.Eng.

Summary

The vibration of a machine tool structure reduces the life expectancy of tool tips, the quality of the surface finish and the tolerances obtained by the machining process. The problem is related to the dynamic stiffness of the machine tool structure. Mechanical absorbers were traditionally implemented to improve the dynamic stiffness, however, active control systems have in recent years proved to be more effective. The active control of vibration is a cost intensive solution to the problem of machine tool vibration. A passively shunted piezoelectric stack actuator proved to be an intermediate solution between a mechanical absorber and an active control system. The device is less cost intensive and its adaptation ability is superior to that of the mechanical absorber. A mathematical model of the device was derived and verified experimentally. The objective of the research was set to improve the dynamic stiffness of a CNC lathe's tool changer. A modal analysis was conducted to determine the dynamic properties of the structure and was verified by an operational deflection shape analysis. The shunted piezoelectric actuator was implemented on the tool changer and attenuation of up to 17 percent was obtained at one of the structural modes. Reasonable correlation was obtained between the experimental and simulation results.

Keywords: Absorber, attenuation, control, damper, machine tool, piezoelectric, passive, smart materials.

Die Passiewe Beheer van Masjiengereedskap Vibrasie met 'n Piezoelektriese Aktueerder

deur

Cornelius Johannes Stander

Studie leier : Prof. P.S. Heyns
Departement : Meganiese en Lugvaartkundige Ingenieurswese
Graad : M.Ing.

Opsomming

Die vibrasie van masjiengereedskapstrukture verkort die verwagte lewensduur van snypunte, verswak die gehalte van die oppervlakafwerking, en vergroot die haalbare toleransiewaardes. Die vlakke van vibrasie wat tydens masjinering ondervind word is afhanklik van die dinamiese styfheid van die struktuur. Meganiese absorbeerders is tradisioneel geïmplementeer om die dinamiese styfheidseienskappe te verbeter. Die aktiewe beheer van vibrasie is 'n meer moderne oplossing tot die probleem, maar dit is koste-intensief. Die navorsing toon aan dat 'n multilaag-piezoelektriese aktueerder 'n intermediêre oplossing tot die probleem is, as daar 'n passiewe elektriese stroombaan aan die pole gekoppel word. Die toestel is goedkoper en is meer aanpasbaar as 'n meganiese absorbeerder. 'n Wiskundige model is afgelei en eksperimenteel geverifiëer vir die toestel. Die doelstelling van die navorsing was om die dinamiese styfheid van 'n gereedskapwisselaar, wat op 'n numeries beheerde draaibank gemonteer is, te verbeter. 'n Modale analise is op die struktuur uitgevoer om die dinamiese eienskappe daarvan te bepaal. Die dinamiese gedrag van die struktuur onder masjineringstoestande is bestudeer met 'n operasionele defleksie-analise. Die toestel is geïmplementeer op die gereedskaphouer en sewentien persent attenuasie is verkry by een van die struktuurmodusse. Redelike korrelasie is verkry tussen eksperimentele en gesimuleerde resultate.

Sleutelwoorde: Absorbeerder, attenuasie, beheer, demper, masjiengereedskap, piezoelektrisiteit, passief, slim materiale.

Acknowledgements

A word of gratitude to the following people and institution who enabled me to conduct and complete the research:

- Professor Stephan Heyns my supervisor for the opportunity and support in making the research possible.
- Mr Frans Windell for his assistance during the experimental tests.
- Ms Steynberg, Ehlers and Boshoff at the academic information services.
- To the NRF for the financial support of the project.
- My parents for their endless support, love and encouragement during my studies.

Table of contents

Nomenclature

Piezoelectric

A	Area of the piezoelectric element perpendicular to the poling direction
C_p^T	Inherent capacitance of the piezoelectric element
D	Electrical displacement
E	Electrical field in the material
I	Electrical current
K	Static stiffness of the piezoelectric actuators / element
K_{33}^{ME}	Relation between the applied force and displacement for the uniaxial loading case
L	Length of the piezoelectric element in the poling direction
L_i	Electrical inductance
R	Electrical resistance
S	Material engineering strain
S^{SU}	Compliance of the shunted piezoelectric element
T	Material stress
V	Electrical voltage (Tension)
Y^D	Open circuit admittance due to the inherent capacitance of the piezoelectric element
Y^{EL}	Electrical admittance of the shunted piezoelectric
Y^{SU}	Admittance of the shunt circuit
Z^{EL}	Electrical impedance equal to the inverse of the electrical admittance
ε^T	Dielectric constant
d_{33}	Piezoelectric constant with poling and deformation in the three direction
s	Laplace parameter
s^E	Piezoelectric material compliance at constant field
φ	Mode shape matrix

Structural Dynamic Response Reconstruction

N	Number of sampled time intervals
T	Sampling interval
V_N	Loss function
a	Input parameter
b	Output parameter
$e(t)$	Innovation term at time t
na	Number of input parameters
nb	Number of output parameters
nk	Time delay
$u(t)$	System input at time t
$y(t)$	System response at time t
$\hat{y}(t)$	Estimated output at time t

Abbreviations

ARX	Auto Regressive model with eXternal input
EMA	Experimental Modal Analysis
FEM	Finite Element Model
FRF	Frequency Response Function
ODS	Operational Deflection Shapes
SDRR	Structural Dynamic Response Reconstruction
emf	Electromotive Force

Chapter 1

Introduction and literature survey

1.1 Introduction

The attenuation of machine tool vibration is a field of research that has been the concern of many engineers over the past few decades. The driving force behind the ongoing research can be related to the fact that the level of vibration at the tool tip, limits the tool life as well as tolerances and the surface finish obtained by the machining process. Traditionally, the rate of material removal is reduced to obtain the required tolerances and surface finish. The reduction in rate of material removal reduces the efficiency of the machine, since the component manufacturing time is increased and lower production is obtained from the machine over a period of time. The objective of the vibration attenuation is to improve the dynamic stiffness of the machine tool structure, to increase the rate of material removal and thereby prolonging the life of the tool tip.

Acoustic noise emission during the machining process results from the relative motion between the tool tip and work piece. High levels of acoustic noise can cause discomfort in the working environment. The problem is related to the dynamic stiffness of the machine tool structure. By improving the dynamic stiffness of the structure, the level of noise emission from the machining process can be reduced.

During the material removal or cutting process, the toolholder and machine structure is subjected to dynamic excitation forces. If the dynamic force excites the modes of the structure, the response of the structure may reach hazardous proportions due to the excitation, depending on the amount of inherent damping in the structure. The problem of extreme structure response is addressed by adding artificial damping to the structure, or by shifting the modes of the structure to alternative frequencies which the dynamic force does not excite. The frequency shift is implemented with absorbers, and has limited frequency shift ability. However the frequencies may shift to a frequency that is still within the excitation frequency band and a damped vibration absorber is usually implemented to improve the attenuation results.

Active control of the tool tip response has become rather fashionable in both internal and external cutting processes over the past decade. The control design is either a feedback control system or a feed-forward control system, for the more advanced applications. The active control of machine tool vibration produces excellent results. The actuators used in the active control of machine tool vibration are usually piezoelectric actuators or magnetostrictive actuators. Piezoelectric ceramic materials are materials, which produce an electric field when strained by a force. When an electrical field is applied to the material, the material produces a strain. If the strain is restricted, a force is applied to the constraint by the material.

The magnetostrictive actuator consists of a magnetostrictive rod surrounded by an annular coil and a permanent magnet. If an electrical field is applied to the coil, the magnetostrictive rod produces a strain, as in the case of the piezoelectric actuator. These actuators are chosen for their high force per unit volume and operational frequency band characteristics. The control system consists of transducers, actuators, gain amplifiers, computation devices or electrical circuitry. Therefore considerable costs are involved in the implementation of such a system.

The properties of the piezoelectric and magnetostrictive actuators make them extremely attractive for the attenuation process. However, the cost of their implementation in the active control environment lessens this appeal. Recent advances in the field of research have lead to the implementation of these actuators as passive dampers and absorbers. The actuators are attached to a structure to alter the dynamic characteristics of the structure. A passive electrical circuit is connected in parallel to the poles of the actuators to adjust the dynamic behaviour of the actuator, and hence that of the structure. A vibration damper can be constructed by placing a resistor over the poles of the actuator. A vibration absorber can be constructed by adding an inductor in series with the resistor. The frequency of the absorber can be adjusted by varying the inductance of the circuit. The small size of the actuators, and the simplicity with which the absorption frequency can be changed, gives the concept an advantage over mechanical absorbers.

The technology has previously been implemented on beams and plates by various researchers. ACX Ltd. commercially implements the concept on snowboards, ski's and baseball bats to reduce the vibrations experienced by the sportsman. However, the challenge remains to determine the feasibility of implementing these actuators as passive structural elements in the attenuation of machine tool vibration.

1.2 Literature survey

The objective of this research was to implement a smart actuator with a passive electrical network, to attenuate machine tool vibration. The literature survey addressed the following topics:

- Passive damping features of the various smart actuators.
- Vibration attenuation with piezoelectric actuators.
- Active and passive control of machine tool vibration.

1.2.1 Passive damping features of the various smart actuators

An article by Smith and Anderson [2], on passive damping by the use of smart materials, deals with the selection of a suitable type of actuator for passive damping applications. The smart actuators considered in the paper were the piezoelectric, electrostrictive and magnetostrictive types. The article deals with the specific mechanisms used for the energy dissipation. A distinction is made between cases were the energy is dissipated internally, or externally, to the material of the attenuation device. In contrast to the traditional viscoelastic or viscous fluids where the energy dissipation occurs internally, the smart actuators that were considered employed external dissipation.

According to the article the viscoelastic materials and viscous fluids possess an internal structure which facilitates the dissipation of energy. The advantage of external energy dissipation is related to properties of the materials used in the vibration attenuation device. The properties of most materials vary with temperature change. The change might reduce the dissipation characteristics of some of the devices and in other cases it might complicate the design of the attenuation device. If the energy is dissipated externally, the characteristics of the attenuation device become insensitive to temperature change during the dissipation of the vibration energy.

The smart actuators are used as energy couplers to convert mechanical energy into electrical energy. The electrical energy is dissipated externally in an electric circuit. The electrical circuit consists of a resistive element, which is used to dissipate the electrical energy. In some of the electrical circuits, an inductor is added in series to the resistive element. The addition of the inductor causes the electrical circuit to resonate. By tuning the resonant frequency, additional vibration attenuation can be obtained. If a resistive element is placed over the poles of an actuator, the article states that the actuator is shunted resistively. In the case where an inductor and a resistive element are placed over the poles of the actuator, the article states that the actuator is shunted resistive–inductive. An actuator that is shunted resistively is called a damper and is analog to the design of viscoelastic materials as vibration dampers. An actuator that is shunted resistive–inductive is analog to a mechanically tuned damped mass absorber.

Piezoelectric actuators are perhaps the most straightforward to implement as passive dampers and absorbers, since the electromechanical coupling is linear and no external stimuli are required. The non-linear characteristics of the material can usually be ignored. The ceramic material, from which the piezoelectric actuator is built, is brittle and has high stiffness properties. Therefore, the actuators are less attractive for use as structural elements. The electromechanical coupling is relatively temperature insensitive, compared to the loss-producing mechanisms in viscous and viscoelastic materials. The use of piezoelectric elements in the longitudinal direction is preferred to the transverse direction for passive damping applications, since the electromechanical coupling is much higher in the longitudinal direction. The term longitudinal refers to the instance were the deformation of the material is perpendicular to the electrodes of the element. The transverse case refers to the instance where the deformation of the material occurs in parallel with the electrodes of the element. In general practice, the transverse case is referred to as a wafer and a piezoelectric stack actuator is the term used for a multi layered longitudinal configuration co-fired into one solid.

Electrostrictive materials appear to be feasible for passive vibration damping, but have limited use. Smith and Anderson indicate that electrostrictive materials such as lead-magnesium-niobate are often used as direct replacements for piezoelectric actuators in micro-positioning systems. The electrostrictive material has the disadvantages of high permittivity and relatively strong temperature dependence.

Due to the non-linear characteristic of the electromechanical coupling, the electrostrictive materials cannot be used to couple energy to an external dissipation system, without the addition of an external DC electric field. The field biases the electrostrictive coupler to a point of nonzero slope on the quadratic field-strain curve. The electrostrictive actuator is therefore biased and shunted with an electrical circuit to attenuate vibration. The shunting circuit resembles that of the piezoelectric case. The DC field is added in series with the shunt circuit, which in turn is coupled in parallel over the poles of the actuator. The lower the shunt frequency, the higher the required inductance value for resistive–inductive shunted piezoelectric and electrostrictive actuators. The relatively higher capacitance value of the electrostrictive actuator, in comparison with the piezoelectric actuators, reduces the required inductance value for the shunt circuit. The property of reduced inductance requirement is attractive but the necessity of an external electric field makes the option less so. The required inductance value versus actuator capacitance value will be dealt with in chapter 2 of the dissertation. The effectiveness of the circuit has not been verified experimentally.

Magnetostriction is a transduction process in which magnetic energy is converted to mechanical energy. It is also possible to invert the process. The transduction from mechanical to electrical energy in the magnetostrictive actuator is attained when the material of the actuator is stressed. When the material is stressed, the magnetic domains within the material rotate and alter the permeability of the material. In the presence of an electric bias field, the magnetic flux in the vicinity of the magnetostrictive varies as the external load varies. The change in the flux induces an electromotive force (emf) in the adjacent coil. The induced emf drives a current through the resistor. The magnetostrictive actuators are shunted with resistors as in the case of piezoelectric and electrostrictive actuators, however they are not shunted with resistive–inductance circuits. The most commonly available example of a magnetostrictive material must be Terfenol-D. Terfenol-D has the ability to extract large amounts of strain energy from a structure. The material has high stiffness, high power density, low operating voltages, and is thermal-insensitive.

The magnetostrictive and electrostrictive actuators impose difficulties due to the non-linear characteristics and external stimuli. The advantages of smart materials are the tuning ability and the temperature insensitivity. Of the three materials considered, the piezoelectric actuator is the most practical.

1.2.2 Vibration attenuation with piezoelectric actuators

The possibility of using piezoelectric materials as passive elements to attenuate vibration was first proposed by Forward [3] in 1979. Forward bonded piezoelectric elements to a beam and shunted the elements with an inductor. He significantly reduced the vibration levels of the beam at a resonant mode frequency of the beam.

A respected paper in the field of passive piezoelectric vibration attenuation is that of Hagood and Von Flotow [4]. They presented the first research that implemented a resistor shunt to enhance the damping of the structure to which the piezoelectric actuator is attached. The article derives a complete mathematical model for the piezoelectric damper and absorber. The article focuses on the piezoelectric wafers and verifies the mathematical model by implementing the wafers on an aluminium-cantilevered beam. The first mode of the beam was damped and absorbed experimentally. The article presents techniques to determine the optimal resistance and inductance values for the damper and absorber based on the implementation of a piezoelectric wafer element on a structure.

The amount of damping added to a structural mode of a plate structure, through the addition of shunted piezoelectric wafer element, is related to the ratio of strain energy captured by the piezoelectric element to the modal strain energy in the system. The concept is known as the modal strain energy approach and was initially proposed by Hagood and Von Flotow [4] for a single degree of freedom model. Davis and Lesieutre [5] did further development on the modal strain energy approach too extend its use too finite element modelling. Therefore, the amount of damping obtained can be improved by increasing the amount of wafers, to capture more of the strain energy. The modal strain energy approach is used to optimise the positioning of shunted wafer elements, on plate structures, to obtain optimal damping results.

A literature survey conveying the evolution of piezoelectric shunting analysis is presented by Lesieutre [6]. The survey presents two new forms of shunting analysis namely the capacitive and switched shunts. The capacitive circuit is used to alter the stiffness of the piezoelectric element. The concept is implemented by Davis and Lesieutre [7] to develop an active tuned mechanical vibration absorber. The piezoelectric element provided the stiffness of the device, which granted the researchers the ability to electrically tune the stiffness of their damper. The switched shunt circuit apparently offers the possibility of controlling the energy transfer to reduce frequency dependent behaviour. The concept of switch shunt circuits refers to the research of Warkentin and Hagood [8]. According to Lesieure little research has addressed the topics of capacitive and switched shunting.

In his literature survey Inman [9] reports on the use of smart actuators as passive and active structural elements to solve structural vibration problems. The body of the article focuses on piezoelectric actuators to attenuate vibration. The article reviews the use of piezoelectric actuators as passive dampers, absorbers, and active control actuators. The working principle and implementation of the passive piezoelectric damper and absorber described correspond to that of Smith and Anderson [2]. The article states that passive electronic damping has become a viable alternative to passive viscoelastic damping. The article reveals an experimental case study where the first two modes of a cantilevered beam is suppressed individually by shunting two piezoelectric wafers resistive–inductive. The vibration amplitudes of the beam were decreased about 25 dB and 20 dB at the first and second mode frequencies, respectively.

Browning and Woodson [10] indicated that it is possible to attenuate twelve different modes of a clamped-clamped steel plate with four piezoelectric wafer elements. They developed a wide band passive electronic shunt circuit for each of the four piezoelectric wafer elements that are coupled to attenuate the twelve structural modes.

A reduction of 20 dB for some of the structural modes is measured simultaneously over the frequency band. Browning and Wynn [10] admit that their finite element model of the plate suffered from potential inaccuracies in geometric and boundary condition modelling. Therefore, they based their analysis on an experimental modal model of the assembled test system. The system was exited with an electrodynamic shaker driven by a white noise signal, and a transfer function analysis was used to identify optimal wafer placement.

Edberg *et al.* [11] attenuated multiple modes of a structure with a single piezoelectric element. Variable synthetic inductors were used in the system. The synthetic inductor is known as a gyrator [12, 13] which is an electronic circuit consisting of one or two operational amplifiers, a real capacitor and a number of resistors. Edberg and colleagues substituted one of the feedback resistors with a variable resistor to obtain a variable synthetic inductor.

The Active Control Experts from Cambridge, Massachusetts designed the only known commercial implementations of the passive piezoelectric dampers and absorbers in their snowboards, ski's and baseball bats. The article regarding their snowboard design [14] states, that the piezoelectric based dampers outperform conventional dampers in a more compact package. The vibration in snowboards lessens the contact area between the board edge and snow surface. The reduced contact area leads to loss of control, stability and the maximum board speed. The resistive shunted piezoelectric actuators convert about 10 % of mechanical vibration energy into heat, which is on par with other passive dampers. A comparison of piezoelectric dampers to conventional options such as constrained layer viscoelastic dampers and absorbing foams shows piezoelectric damping systems are more expensive and require more design effort. Therefore, the concept is not cost-effective for small vibration control applications. It is recommended that the piezoelectric actuator should be mounted at areas of maximum strain for the modes of interest. A detailed structural model and modal analysis are required to optimise placement. The more piezoelectric material incorporated in the design, the larger the amount of strain energy captured. The more the strain energy captured, the higher the damping levels obtained. An optimal design point with respect to cost and performance can be found.

The active control of vibration with piezoelectric stack actuators was investigated by Smit [16]. Smit adopted a mathematical model for a piezoelectric stack actuator from the work of Sumali and Cudney [17, 18]. The influence of the various properties of the actuator was simulated with the model to obtain the information required to design an appropriate actuator. Various control strategies were simulated and verified experimentally.

The experimental verification was conducted on a beam, which was excited with random force. A reduction of 12 dB in the frequency response was obtained with velocity feedback and a reduction of 18 dB was obtained with a state feedback algorithm.

Inman [9] presents a case study of store flutter suppression. If an external load such as a fuel tank or a missile is attached to a fighter aircraft wing, the attached structure causes the bending and torsion modes of the wing to couple. (The attachments to the wing are referred to as stores.) Coupling of these modes causes flutter to occur at lower speeds which reduces the efficiency of the aircraft. The pylon of the attachment is substituted with an active pylon consisting of a piezoelectric based wafer actuator to restore the original flutter speed of the aircraft. The system was modelled for an F16 aircraft. Unfortunately, the results of the implementation are not clear in the article and the reader should consult the references.

Fuller, Elliott and Nelson [19] wrote a complete text on the active control of vibration. Chapter 5 of the book is devoted to the use of piezoelectric actuators in the active control of vibration. The book of Beards [20] on the active control of vibration contains relevant matter of interest.

1.2.3 Active and passive control of machine tool vibration

Chatter is a phenomenon in the machining industry that refers to the instance where the cutting process induces a force onto the structure of the machine tool at a frequency near to or at one of the structural modes of the system. Boring bars are slender cutting tools used in a turning operation on a lathe to create cylindrical inner surfaces. These tools operate with a long overhang when machining long cylindrical pieces, therefore boring bars are prone to resonate at their first modes during the machining process. Increasing the stiffness or the damping factor of the boring bar can reduce the chatter. Browning and Woodson [21] proposed a reaction mass actuator to add additional damping to the boring bar as an alternative to active control, which is a cost intensive-solution to the problem. The reaction mass actuator consists of a piezoelectric stack actuator, a mass, a return spring and a hinge. The reaction mass actuator is attached near the cutting tip of the boring bar to alter the dynamic characteristics of the boring bar. The reaction mass actuator's influence on the boring bar is altered by shunting the piezoelectric stack actuator. The piezoelectric stack actuator was shunted with a resistive–inductive or resonant shunt and a negative capacitance shunt. A reduction of 20 dB in the response of the boring bar was obtained by implementing the reaction mass actuator with the negative capacitance shunt, and a 14 dB reduction in the response was obtained with the resonant shunt circuit. The negative capacitance circuit consists of an operational amplifier, a capacitor, and a few resistors. The operational amplifier requires an external electrical power supply, therefore the circuit is referred to as being semi-active. A conceptual drawing of the reaction mass actuator is shown in figure 1.1.

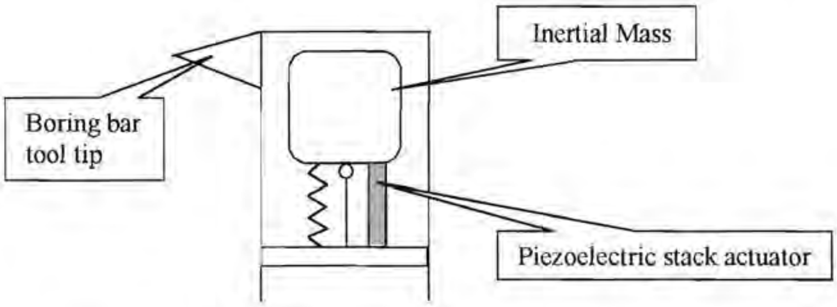

Figure 1.1 *Piezoelectric reaction mass actuator*

Pratt and Nayfeh [22, 23, and 24] have researched the active control of boring bar chatter. The objective of their research was to increase the stability envelope of the boring bar by implementing active control. They implemented two Terfenol-D actuators to exert the control forces at the base of the boring bar near its attachment, to counteract the unwanted vibration. The actuators are mounted in a plane perpendicular to the feed direction of the lathe. Figure 1.2 presents a schematic diagram of the system.

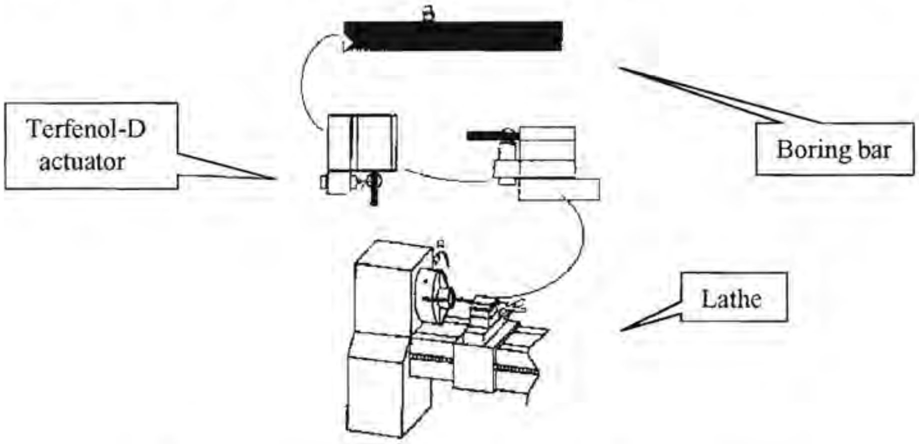

Figure 1.2 *Active boring bar control system [22]*

The system utilises two actuators in the transverse directions since chatter can occur in both the directions. Pratt and Nayfeh applied an experimental system identification technique to develop a reduced order model for the structural dynamics of the resulting smart machine tool system. The transfer function is determined from the voltage input of the actuator to the voltage output of the accelerometer. The vertical and horizontal control loops are orthogonal to each other and the authors assumed that no coupling exists in the absence of a cutting force. The system identification was conducted by exciting the Terfenol-D actuator with a random voltage signal and measuring the accelerometer response voltage. The amplifier gain was set at mid range to ignore the effects of system saturation. The data was used to identify a linear system model.

The frequency response function of the system indicated that the first mode of the boring bar dominates the response of the system and therefore the system was simplified as a single degree of freedom model with a natural frequency at the dominant mode frequency of the identified model. The simplified model was used to develop an appropriate control strategy. The remaining research addressed more advanced control strategies and extended the structural model to incorporate non-linear behaviour to predict chatter stability and instability.

According to Hakansson, Claesson, Sturesson and Lago [25, 26, 27, 28, 29 and 30] the machine tool vibration problem in the external cutting process can be related to the dynamic stiffness of the machine tool structure. Normal mode analysis was used to investigate the dynamic properties of the tool shank and holder. The authors state that the dynamic response of a machine tool structure can not be described adequately by a single degree-of-freedom model. The comment arises from the fact that most of the pioneering work in the field has been based on single and two degree-of-freedom models that are used in the different models that predict the occurrence of chatter or machine tool vibration. Tobias [31] and Tlusty [32] presented these models in their work.

The authors built a finite element model of the tool holder and shank with MSC/Nastran to describe the dynamic behaviour of the machine tool structure, which was assumed to be linear. The model was built with solid brick elements. The model was verified by comparing the mode frequencies with spectral density data measured on the tool during various cutting processes. The feed rate and other properties of the cutting process was changed for each cut and the peaks of the spectral densities that remained constant was taken to be the natural frequencies of the system. The model enabled the authors to place the actuators at the appropriate positions in an integrated tool holder system. The design used four Terfenol-D actuators to produce the counter force. A schematic diagram of the system is shown in figure 1.3. A large current 5 kW amplifier drove the actuators of the system. An accelerometer was placed on the shank for feedback into the controller of the system. The acceleration levels of the shank were reduced by 40 dB at the 1500 Hz and 3000 Hz modes.

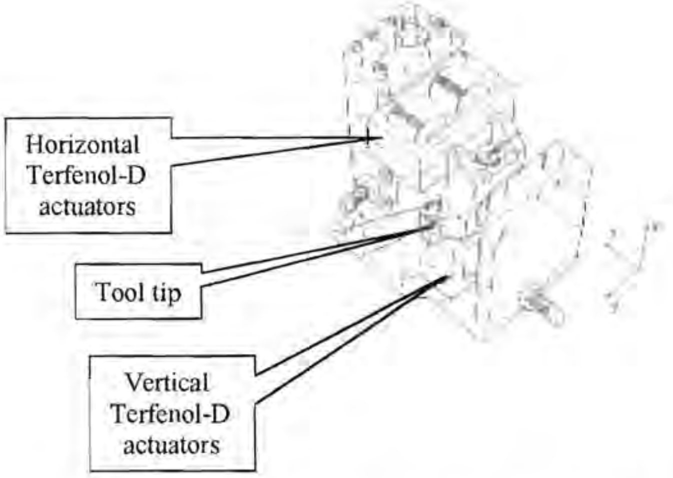

Figure 1.3 *Active vibration controlled tool system [25]*

Zatarain and Leizaola [33] improved the dynamic stiffness of a numerically controlled milling machine with a tuned dynamic absorber. The natural mode frequencies of the structure varies due to the fact that the work piece is moved on the axis of the machine tool while the mass and stiffness of the work piece is reduced as machining take place. A detailed modal analysis was done on the structure, and a change of 6 Hz in the mode frequencies was measured. Therefore the absorber had to retune itself as the machining took place. The absorber consisted of a mass, which was attached to the structure with nitrile rubber elements. The nitrile rubber elements were used to obtain the required stiffness and damping affect. The stiffness was tuned by the variation of the preload with hydraulic cylinders. The pressure of the cylinders was varied between 10 bar and 70 bar to control the absorber frequency. Both open and closed loop control systems were tested and the dynamic responses of the structure at crucial locations were reduced considerably. Unfortunately, the exact working principle of the absorber is not clearly documented.

A combination between a damper and active vibration control was implemented by Chung, Smith and Tlusty [34] on a high-speed machine tool. The system takes the form of a conventional damped absorber with the exception that an actuation force is applied between the system mass and the absorber mass. The acceleration of the system is used as an input to a feedback control system that controls the actuation force exerted between the system and the absorber. The design implements an electromagnetic actuator, which was designed to exert a maximum force of 1000 N over a frequency band of 300 Hz. The system was implemented to attenuate the structural modes of the machine since the size of the system is too large to implement near the spindle of the machine tool. The frequency response of the targeted mode is reduced by a factor of 2.6 and 5.3 depending on the gain of the control system.

In order to control the spindle vibration of a milling machine, it is necessary to implement actuators on the spindle itself. Martinez, Hinnerichs and Redmond [35] implemented imbedded piezoelectric actuators in a beam that was used as a surrogate machine tool structure. The objective of their study was to determine optimal actuator positions for the active control of the spindle vibration. The authors state that improved methods are required for incorporating smart material actuators in cutting tools without a loss of static stiffness, before active control systems can be implemented on a milling machine spindle.

Riehle and Brown [36] developed a conventional damped absorber for an automatic boring machine to attenuate the first bending mode of the spindle at 300 Hz. The boring machine was used to machine aluminium covers. The components required a surface finish of 50μin and values of over a hundred were obtained without the damped absorber. A viscoelastic material element was used for the damping and spring stiffness of the damper. The article contains information on the appropriate selection of the geometry and material for the application. The damper was mounted on the spindle and the surface finish was improved to 36 μin.

1.3 Research objectives

The focus of the research was to attenuate the structural modes of the machine tool. However, it is acknowledged that the component, that is being machined, influences the vibration levels experienced during machining. The attenuation of the vibration of the machine tool structure is practically feasible. The vibration attenuation of the component that is machined remains a challenge and will not be addressed in this research. The research was conducted on a Cholechester CNC 2000L horizontal lathe fitted with a diplomatic tool changer *(TRM120 series 10)*.

The research of Hakansson, Claesson, Sturesson and Lago [25, 26, 27, 28, 29 and 30] indicated that the vibration levels near the tool tip of a lathe can be reduced considerably by the implementation of an active vibration control system that utilises smart actuators to exert the control forces. The global objective of the research was set to determine whether the passive shunting of the smart actuators could be used to improve the dynamic stiffness of the machine tool structure near the tool tip. The first objective of the literature survey was to establish which type of actuator to use in the application.

The article of Smith and Anderson [2], on passive damping by the use of smart materials, addressed the selection of a suitable type of actuator. A piezoelectric actuator was selected for the application based on the fact that it is less expensive than Terfenol-D actuators, the actuator does not require external stimuli in the shunt and its behaviour can be assumed to be linear.

The work of Browning and Woodson [21] indicated that it is possible to shunt a stack actuator since they implemented a shunted piezoelectric stack actuator in their reaction mass actuator. The detail of the mathematical model of the shunt was not documented in their publication and it did not involve the implementation of the piezoelectric actuator as a discrete damper or absorber.

Therefore the first objective of this research was to derive and validate a mathematical model to simulate the effect of the shunted piezoelectric stack actuator on a structure.

Insight into the dynamic behaviour of the lathe structure under machining conditions had to be obtained in order to implement the vibration attenuation device. Therefore the operational deflection shapes of the lathe structure should be measured under machining conditions, in accordance with the technique proposed by Døssing *et al.* [1]. The dynamic characteristics of the lathe structure had to be determined though experimental modal analysis to verify the behaviour of the structure under machining conditions. The two tests should yield the necessary information to understand the behaviour of the structure and to build a mathematical model of the structure for simulation purposes.

The dynamic input force on to the structure should be determined under machining conditions, in order to construct a mathematical simulation of the machining process on the lathe. The mathematical simulation of the machining process can be used to investigate the influence of the absorber on the machine tool structure in a repeatable environment.

The piezoelectric absorber should be implemented on the lathe to verify the mathematical modelling.

1.4 Document overview

The mathematical models of the piezoelectric damper and absorber are derived in chapter 2. The chapter presents various simulations, which indicate the influence of the model parameters on the dynamic stiffness of the structure. The experimental verification of the mathematical model on an aluminium beam is documented.

The operational deflection shapes of the lathe as well as the experimental modal analysis results are documented in chapter 3.

The process of estimating the dynamic force that is exerted onto the tool tip is presented in chapter 4.

The experimental implementation of the absorber on the lathe is described in chapter 5. The chapter is further dedicated to the simulation of the absorber implementation on the lathe.

A conclusion to the research is given in chapter 6 as well as recommendations for further research and development.

Chapter 2

Mathematical model

2.1 Piezoelectric terminology and concepts

At this point it has been made clear that a piezoelectric element deforms when an electrical field is placed over the element. The direction of the electrical field is determined by the placement of the electrodes on the element. The direction in which the electrical field is applied is referred to as the poling direction. It is evident that multiple poling directions are possible in an element. The electrical field has maximum effect in the poling direction but also influences the behaviour of the element in the other directions. To account for the effects of various poling directions, the constitutive relation for the piezoelectric element is written in a matrix format. The format resembles the use of the material compliance in the field of non-isotropic material modelling. The material properties in this case are not determined by, for example, the material lay-up, but rather the electrical field lay-up on the element. The number of electrical fields and the directions, in which they are applied, are determined by the application.

The constitutive relations and conventions for piezoelectric elements are applied in the same way for a damped vibration absorber as for an actuator. The fact that the material is strained by an applied stress to produce an electrical field does not change the use of the constitutive relation and its convention.

Damped vibration absorbers are based on a uniaxial loading case where the piezoelectric element is subjected to a shear or a normal stress and only one pair of electrodes is present to provide an external electric field. The literature refers to two modes of operation. The longitudinal case where the stress is applied in the electrical field development direction and the transverse case where the directions differ.

2.2 Specification for the mathematical model

The model originates from the work of Hagood and Von Flotow [4]. They derived and verified a single layered transverse case model for a shunted piezoelectric absorber on a cantilevered aluminium beam.

A piezoelectric stack actuator is a multi-layered longitudinal configuration. According to Hagood and Von Flotow [4] the longitudinal configuration of the piezoelectric is more effective than that of the transverse configuration, when implemented as a damped absorber. The higher effectiveness is contributed to the fact that the direction of poling and deformation of the piezoelectric material coincide.

The multiple layers are introduced to improve the attenuation device's ability to convert mechanical deformation into electrical energy, as well as to increase the capacitance value of the piezoelectric actuator. The relevance of the capacitance value will be dealt with further in section 2.4. The objective was to derive a mathematical damped absorber model for a multi-layered longitudinal piezoelectric actuator (Stack actuator). The model was validated by experimental procedure.

2.3 Derivation of the mathematical model

The constitutive relation for the material constants of a linear three-dimensional piezoelectric solid in accordance with reference [4] is presented by equation (2.1).

$$\begin{bmatrix} \bar{\mathrm{D}} \\ \bar{\mathrm{S}} \end{bmatrix} = \begin{bmatrix} \bar{\varepsilon}^{\mathrm{T}} & \bar{\mathrm{d}} \\ \bar{\mathrm{d}}_{\mathrm{t}} & \bar{\mathrm{s}}^{\mathrm{E}} \end{bmatrix} \begin{bmatrix} \bar{\mathrm{E}} \\ \bar{\mathrm{T}} \end{bmatrix} \tag{2.1}$$

with:

D: Electrical displacements (charge/area).
E: Electrical field in the material (volt/meter).
S: Material engineering strain.
T: Material stress (force/area).

ε : Dielectric constant.
s: Compliance.
d: Piezoelectric constant.

The lowercase entries are matrices defining the material properties of the non-isotropic material. The uppercase entries denote the variable vectors. The superscripts on the material property denote the mechanical or electrical boundary condition under which the constants are valid and the subscript t denotes the conventional matrix transpose.

According to Hagood and Von Flotow [5], the material property matrices in equation (2.1) can be simplified to single value material properties when the piezoelectric element is loaded uniaxially with a normal stress and only one pair of electrodes is present on the element to develop the external electrical field in the same direction.

The piezoelectric properties for the longitudinal application are denoted by a subscript '33', which indicates that, the direction of loading and electrical field development is in the '3' direction in accordance with piezoelectric convention.

$$\begin{bmatrix} \mathrm{D}_3 \\ \mathrm{S}_3 \end{bmatrix} = \begin{bmatrix} \varepsilon_{33}^{\mathrm{T}} & \mathrm{d}_{33} \\ \mathrm{d}_{33} & \mathrm{s}_{33}^{\mathrm{E}} \end{bmatrix} \begin{bmatrix} \mathrm{E}_3 \\ \mathrm{T}_3 \end{bmatrix} \tag{2.2}$$

The entries into equation (2.2) are scalars.

To incorporate traditional concepts, such as admittance and impedance, into the shunting analysis, a change of variables are required. The definitions for voltage and current are used for this purpose and are defined by equations (2.3) and (2.4).

$$I = \int_A \frac{\partial}{\partial t} D \cdot da \tag{2.3}$$

$$V = \int_0^L E \cdot dx \tag{2.4}$$

The assumption is made that the field within and the electrical displacement on the surface are uniform for the piezoelectric material. The linear relationships can be defined in the Laplace domain by equations (2.5) and (2.6).

$$I(s) = sA \cdot D(s) \tag{2.5}$$

$$V(s) = L \cdot E(s) \tag{2.6}$$

with:

L: Length of the material in the poling directions.
A: Area perpendicular to the direction of poling.
s: Laplace parameter.

By taking the Laplace transform of equation 2.2 and using equations 2.5 and 2.6 to eliminate E and D, the constitutive relation for a piezoelectric in terms of the external current input and applied voltage is obtained.

$$\begin{bmatrix} I_3 \\ S_3 \end{bmatrix} = \begin{bmatrix} sAL^{-1}\varepsilon^T & sAd_{33} \\ d_{33}L^{-1} & s_{33}^E \end{bmatrix} \begin{bmatrix} V_3 \\ T_3 \end{bmatrix} \tag{2.7}$$

The upper left partition of the constitutive relation matrix can be defined as the capacitance between the surfaces that are perpendicular to the poling direction. Therefore the constitutive relation can be written as.

$$\begin{bmatrix} I_3 \\ S_3 \end{bmatrix} = \begin{bmatrix} sC_P^T & sAd_{33} \\ d_{33}L^{-1} & s_{33}^E \end{bmatrix} \begin{bmatrix} V_3 \\ T_3 \end{bmatrix} \tag{2.8}$$

The open circuit admittance of the piezoelectric due to the inherent capacitance with free boundary conditions is defined as,

$$Y^D = sC_P^T \tag{2.9}$$

For shunted piezoelectric applications, a passive electrical circuit is connected in parallel with the surface electrodes of the piezoelectric.

The circuit is in parallel with the inherent capacitance of the piezoelectric. The admittance in parallel adds and therefore the constitutive relation for a shunted piezoelectric can be written as.

$$Y^{EL} = Y^{D} + Y^{SU} \tag{2.10}$$

$$\begin{bmatrix} I_3 \\ S_3 \end{bmatrix} = \begin{bmatrix} Y^{EL} & sAd_{33} \\ d_{33}L^{-1} & s_{33}^{E} \end{bmatrix} \begin{bmatrix} V_3 \\ T_3 \end{bmatrix} \tag{2.11}$$

with:

Y^{D} : Open circuit electrical admittance of the piezoelectric.
Y^{SU} : Shunting admittance of the piezoelectric.
Y^{EL} : Electrical admittance of the shunted piezoelectric.

Figure 2.1 displays a schematic diagram of a shunted uniaxial piezoelectric element.

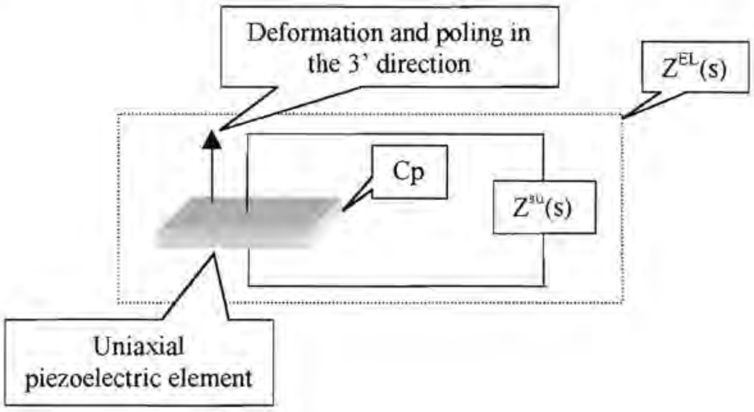

Figure 2.1 *Schematic diagram of the shunted uniaxial piezoelectric element*

The piezoelectric elements in a stack actuator are mechanically in series and electrically in parallel. Therefore the constitutive relation for a multi layered shunted piezoelectric stack can be written in the form of equation (2.12).

$$\begin{bmatrix} I_3 \\ S_3 \end{bmatrix} = \begin{bmatrix} Y^{EL} & nsAd_{33} \\ nd_{33}L^{-1} & ns_{33}^{E} \end{bmatrix} \begin{bmatrix} V_3 \\ T_3 \end{bmatrix} \tag{2.12}$$

$$Y^{EL} = n \cdot C_p^{T} + Y^{SU}$$

The variable n refers to the number of layers in the stack. An expression for the shunted compliance of the multi-layered piezoelectric actuator is derived from equation (2.12). Equation (2.13) and (2.14) is written from equation (2.12).

$$I_3 = Y^{EL}V_3 + nsAd_{33}T_3 \tag{2.13}$$

$$S_3 = nd_{33}L^{-1}V_3 + ns_{33}^{E}T_3 \tag{2.14}$$

Equation (2.13) can be written as an expression for the applied voltage and substituted in to equation (2.14) to obtain equation (2.16)

$$V_3 = Z^{EL} \cdot \{I_3 - nsAd_{33}T_3\} \tag{2.15}$$

with:

Z^{EL} : Electrical impedance, equal to the inverse of the electrical admittance.

$$S_3 = [ns_{33}^{E} - n^2 d_{33}^2 L^{-1} Z^{EL} sA]T_3 + nd_{33} L^{-1} Z^{EL}]I_3 \tag{2.16}$$

From equation (2.16) the shunted piezoelectric compliance can be defined from the terms in brackets that relates the material strain to the applied stress.

$$s^{su} = ns_{33}^{E} - n^2 d_{33}^2 L^{-1} Z^{EL} sA \tag{2.17}$$

The relation between applied force and displacement, for the uniaxial loading case of the stack actuator, is expressed in equation (2.18).

$$\begin{gathered} K_{33}^{ME} = \frac{A}{s^{su}L} \\ K_{33}^{ME} = \frac{A}{L \cdot [ns_{33}^{E} - n^2 d_{33}^2 L^{-1} Z^{EL} sA]} \end{gathered} \tag{2.18}$$

By altering the electrical impedance term, the passive characteristics of the stack actuator is altered. The process of altering the passive characteristics of the actuator has been referred to as shunting. As indicated in chapter 1, there are two types of electrical networks that are used for shunting the actuator, the first of which is resistive shunting where a resistor is placed in parallel over the actuator poles, and the second where a inductor is added in series with the resistance. The second shunt is referred to as a resonant shunting since the circuit resonates. The expression of electrical impedance for the resistively shunted actuator is expressed by equation (2.19) and the expression for the resonant shunted actuator is expressed by equation (2.20).

$$Z^{EL} = \frac{R}{RnC_p^T s + 1} \tag{2.19}$$

$$Z^{EL} = \frac{L_i s + R}{L_i n C_p^T s^2 + RnC_p^T s + 1} \tag{2.20}$$

with:

R: Resistance of the shunt circuit
L_i : Inductance of the shunt circuit

The actuator is implemented as a damper or a damped absorber on a structure through the use of the relation between the applied force and displacement as a transfer function in a feedback loop to the force input of the structure model. The transfer function is obtained by substituting either equation (2.19) or (2.20) into equation (2.18) and manipulating to obtain equation (2.21) for the resistive shunt case or equation (2.22) for the resonant shunt case.

$$K_{33}^{ME} = \frac{\{nAC_P^T R\}s + A}{\{n^3 Ls_{33}^E C_P^T R - n^3 d_{33}^2 AR\}s + \{n^2 Ls_{33}^E\}} \tag{2.21}$$

$$K_{33}^{ME} = \frac{\{nAC_P^T L_i\}s^2 + \{nAC_P^T R\}s + A}{\{n^3 Ls_{33}^E C_P^T L_i - n^3 d_{33}^2 AL_i\}s^2 + \{n^3 Ls_{33}^E C_P^T R - n^3 d_{33}^2 AR\}s + \{n^2 Ls_{33}^E\}} \tag{2.22}$$

The transfer function does not take the static stiffness of the structure that surrounds the piezoelectric elements in to account. A second transfer function of static stiffness is used in a feedback loop to the force input of the structural model to account for the additional stiffness. A diagram of the closed-loop system is presented in figure 2.2.

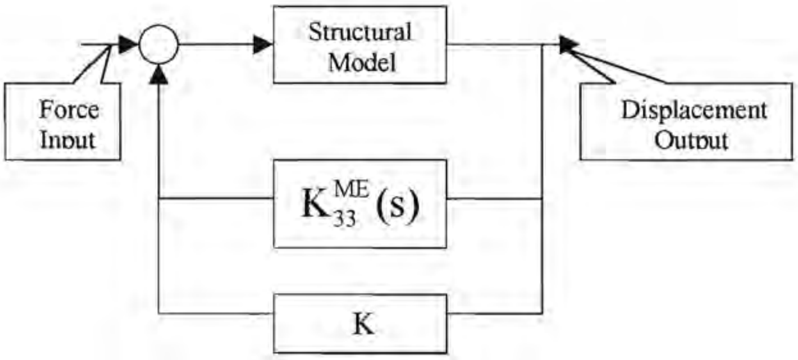

Figure 2.2 *Flow diagram of the closed loop system*

The inherent structural damping of the structure is increased when the actuator, without the shunt, is added to the structure. The feedback loop does not account for the increase in structural damping. Therefore, the model updating procedure of the structural model itself addresses the increase in structural damping. The influence of the static stiffness and inherent damping, which the actuator adds to the structure as a structural element, will be explained in more detail with the experimental verification further on in the chapter.

2.4 Implementation of the model on a discrete spring mass system

The objective of the implementation simulations was to investigate the influence of the various parameters such as the resistance, inductance, capacitance, structural damping and stiffness on the model.

The model is implemented on the spring mass system as indicated in figures 2.2 and 2.3. The actuator was placed in parallel with the spring of the system. An additional stiffness coefficient was not incorporated in the feedback loop, to compensate for the additional stiffness that is added to the system when the actuator is incorporated as a structural element. The additional stiffness would only change the natural frequency of the system, which was chosen at 1000 Hz. The natural frequency of the system was kept constant at 1000 Hz throughout the simulations and therefore the mass of the system was increased when the stiffness was increased.

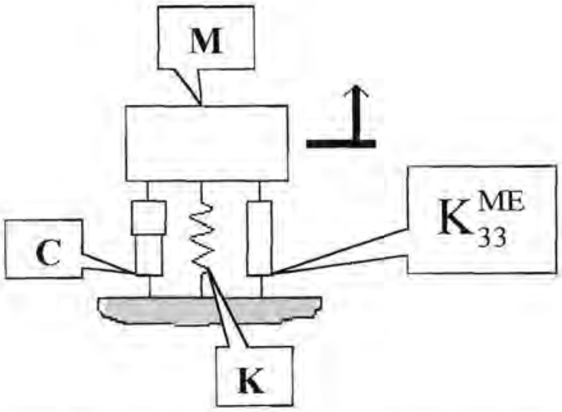

Figure 2.3 *Discrete spring mass system with piezoelectric stack actuator*

2.4.1 Damper model

A piezoelectric stack actuator resembles the properties of a discrete damper when shunted with a resistor. The degree of attenuation obtained through its application is far less than that obtained through the resonant shunt. However, it still remains interesting to examine its behaviour. Figure 2.4 indicates the effect that the damper has on the Frequency Response Function (FRF) of the system. With an increase in resistance, the amount of attenuation is increased. The specifications of the system used in the simulation of figure 2.4 is shown in table 2.1 (a) while the attenuation versus resistance data is shown in table 2.1 (b). The amount of attenuation is defined as the reduction in the peak FRF value throughout the text.

Table 2.1 (a) Specification of the simulated system displayed in figure 2.3

Mass	1 kg
Damping	1 %
Capacitance	100×10^{-9} F

Table 2.1 (b) The resistance versus the attenuation for the simulation in figure 2.3

Resistance [Ω]	Attenuation [m/N]
400	0.2591×10^{-6}
800	0.3974×10^{-6}
1200	0.4775×10^{-6}
1600	0.5210×10^{-6}

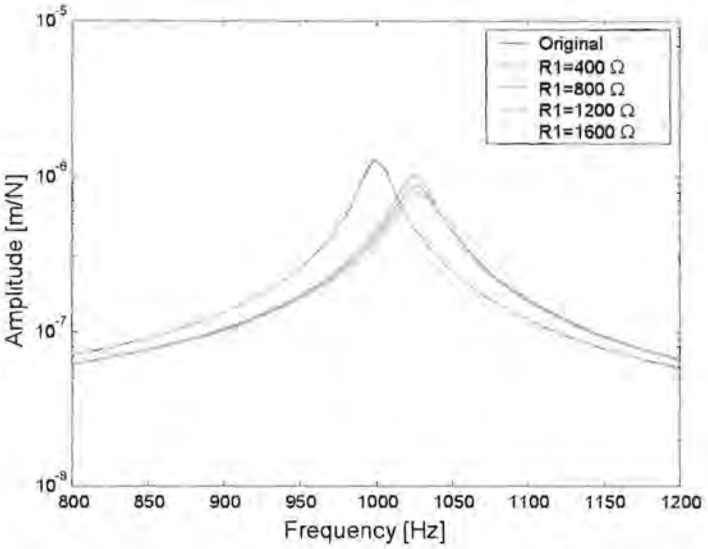

Figure 2.4 *FRF of the damped structure and the original structure*

The natural frequency of the system increases as the shunt resistance was increased due to the stiffening of the piezoelectric material. An increase in the resistance improves the amount of attenuation obtained. However, there is an optimum resistance value. Figure 2.5 reveals the resistance versus attenuation behaviour of the system. An optimum resistance value is obtained at 2400 Ω. An increase in the system mass and stiffness will decrease the amount of attenuation, but does not influence the optimum resistance value. The stiffness versus attenuation results is shown in table 2.2.

Table 2.2 Stiffness versus the attenuation at 2400 Ω, for the simulation in figure 2.5

Stiffness [N/m]	Attenuation [m/N]
39.478×10^{6}	5.47×10^{-7}
78.957×10^{6}	1.75×10^{-7}
118.435×10^{6}	8.55×10^{-8}

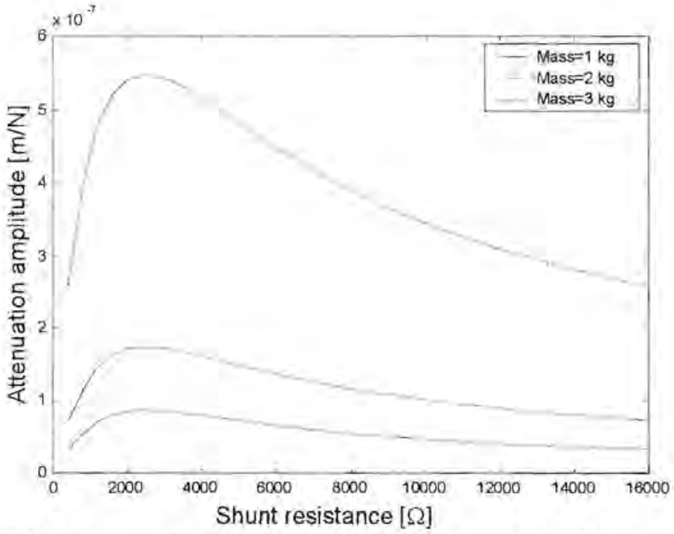

Figure 2.5 *Attenuation versus shunt resistance and system mass*

The optimum resistance occurs between the open and closed circuit scenarios. In the open circuit scenario no current will flow from the piezoelectric element since the network path is not closed. As the resistance is increased towards the closed circuit scenario less current will flow from the piezoelectric element. Therefore the amount of energy which is transferred to the external dissipation circuit is reduced as well as the effectiveness of the piezoelectric damper.

The amount of attenuation is restricted by the amount of inherent damping present in the system. Figure 2.6 represent a simulation where the mass and stiffness of the system is kept constant while the percentage inherent damping is increased. The specifications of the system used in the simulation of figure 2.6 are noted in table 2.3 (a) while the attenuation versus inherent damping data is noted in table 2.3 (b). Note that the optimum resistance still remains at 2400 Ω.

Table 2.3 (a) Specification of the simulated system displayed in figure 2.6

Mass	1 kg
Capacitance	100×10^{-9} F

Table 2.3 (b) The resistance versus the attenuation for the simulation in figure 2.6

Inherent damping [%]	Attenuation [m/N]
1	5.47×10^{-7}
1.3	3.63×10^{-7}
2	1.8×10^{-7}

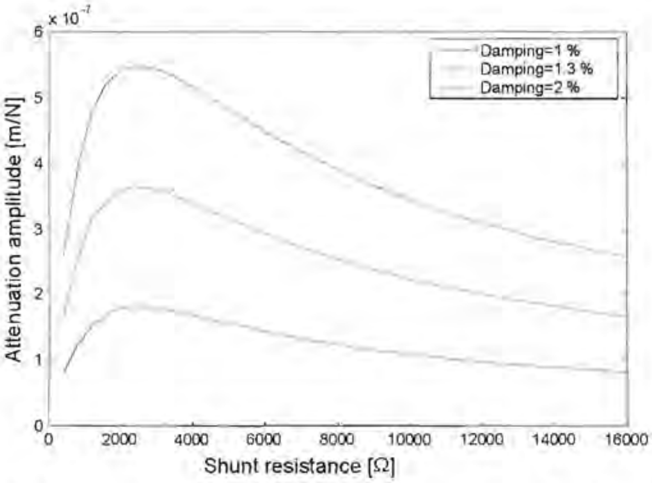

Figure 2.6 *Attenuation versus shunt resistance and system damping*

Increasing the capacitance of the actuator can increase the amount of attenuation. Figure 2.7 shows the increase in the attenuation as a function of the capacitance. The specifications for the simulated system are shown in table 2.4.

Table 2.4 Specification of the simulated system displayed in figure 2.7

Mass	1 kg
Damping	1 %
Resistance	2400 Ω

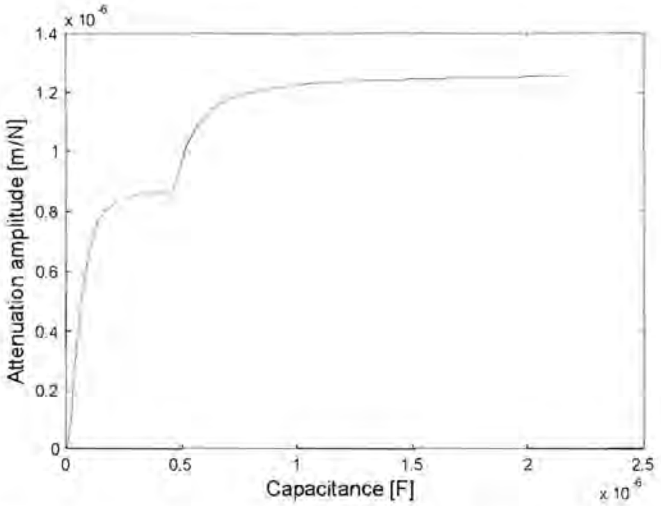

Figure 2.7 *Attenuation versus the actuator capacitance*

It is unclear why the curve in figure 2.7 has the peculiar shape. No further attention was given to the shape since better attenuation could be obtained with the piezoelectric absorber. The one prominent aspect shown by the curve is that an increase in the capacitance value increases the amount of attenuation. The cost of the actuator should be taken into account when selecting an optimal capacitance value.

2.4.2 Absorber model

The term piezoelectric absorber refers to the resonant shunting case of the stack actuator. The piezoelectric absorber is a damped absorber which transforms the resonant frequency of the system to two resonant frequencies, one lower than the natural frequency of the original system, and the other higher. Figure 2.8 (a) is a frequency response function plot that indicates the addition of the piezoelectric absorber on the discrete spring mass system. A Bode diagram of the shunted piezoelectric stack actuator's transfer function is shown in figure 2.8 (b). The specification of the simulated system is presented in table 2.5.

Table 2.5 Specification of the simulated system displayed in figures 2.8 (a) and (b)

Mass	50 kg
Damping	1 %
Resistance	1 Ω
Inductance	0.378 H
Capacitance	100×10^{-9} F

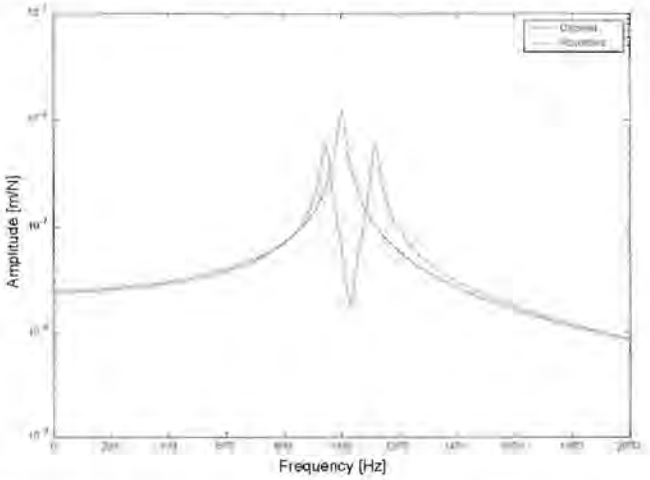

Figure 2.8 (a) *FRF of the absorbed structure and the original structure*

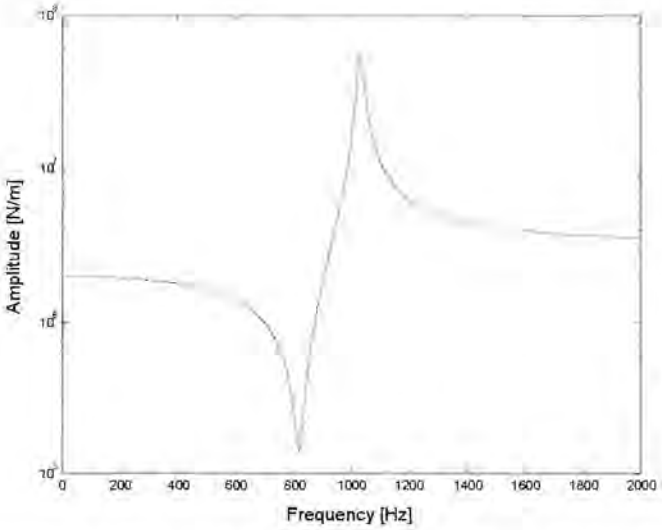

Figure 2.8 (b) *Bode diagram of the shunted piezoelectric stack actuator's transfer function*

The absorber frequency is tuned by adjusting the inductance value of the resonant circuit. An increase in the inductance value reduces the resonant frequency. The inductance value is decreased to obtain a higher resonant frequency. The absorber is optimally tuned, when both the natural frequencies of the absorbed system have the same amplitude on the frequency response function plot. The appropriate inductance value, to tune the absorber to a natural frequency of the structure, is obtained through inspection. Figures 2.9 (a) and 2.9 (b) indicate how the transfer function and frequency response function changes with a change in the inductance. The optimum inductance value for the discrete spring mass system is 378×10^{-3} H. The specification for the system in figures 2.9(a) and (b) is shown in table 2.5 The change in inductance values are shown along with the resonant frequencies of the system in table 2.6.

Table 2.6 Natural frequencies of the system with variation in the inductance value

Inductance value [H]	**First mode frequency [Hz] of the absorber**	**Spring mass resonant frequency [Hz]**	**Second mode frequency [Hz] of the absorber**
0.378	945	1000	1117
0.3	985	1000	1203
0.52	841	1000	1067

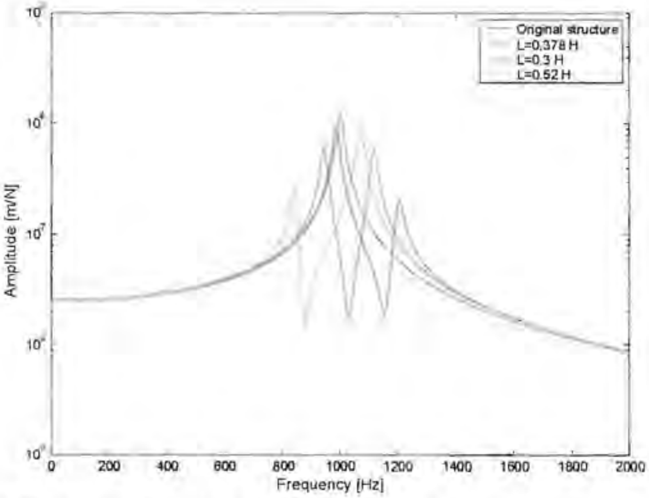

Figure 2.9 (a) *FRF of the absorbed structural mode with variation in the inductance value*

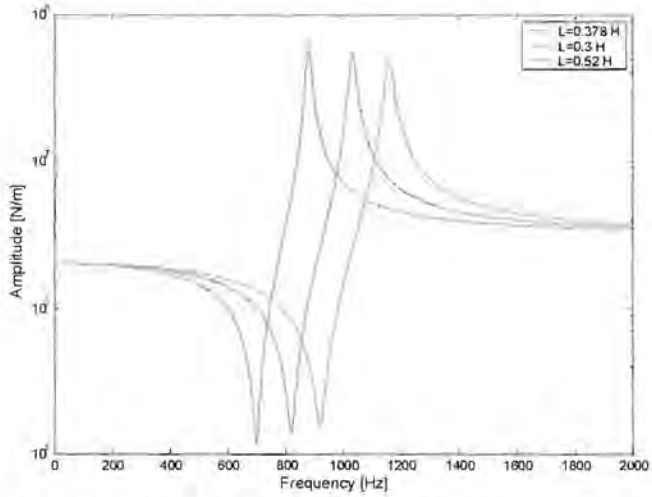

Figure 2.9 (b) *Bode diagram of the shunted piezoelectric stack actuators transfer function with variation in the inductance value*

The resistance of the shunt circuit determines the amount of damping in the system. The higher the resistance value, the more damping is present in the system. Care should be taken not to increase the resistance too much, since too much damping will cause the system to form one resonant pick near the original natural frequency of the system. The absorber therefore loses its effect when the resistance value is increased too much.

The optimal resistance value is obtained through inspection as indicated in section 2.4.1. Figures 2.10 (a) and (b) indicate the effect of the increase in the shunt resistance. The specification of the system in figures 2.10 (a) and (b) is shown in table 2.7 (a).

The increase in the amount of attenuation with the increase in resistance is shown in table 2.7 (b).

Table 2.7 (a) Specification of the simulated system displayed in figures 2.10 (a) and (b)

Mass	1 kg
Damping	1 %
Inductance	0.378 H
Capacitance	100×10^{-9} F

Table 2.7 (b) The amount of attenuation in the system for the shunt resistance

Resistance [Ω]	**Attenuation [m/N]**
50	6.4513×10^{-7}
100	8.5428×10^{-7}
150	9.4966×10^{-7}
200	1.0003×10^{-6}
250	1.0316×10^{-6}

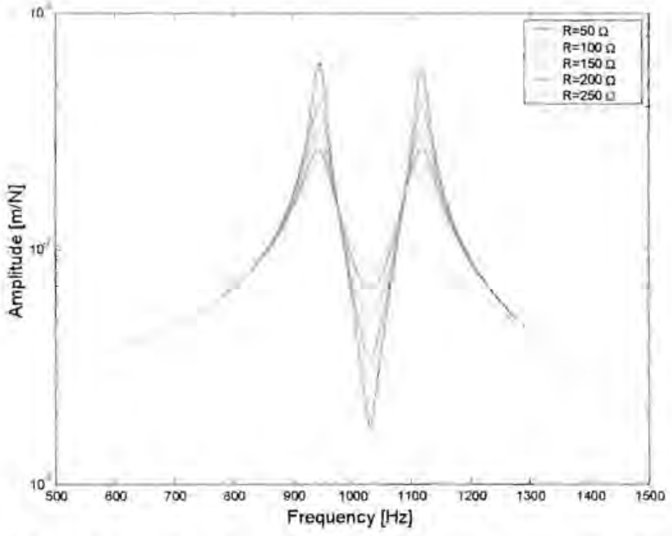

Figure 2.10 (a) *FRF of the absorbed structure with variation in the resistance value*

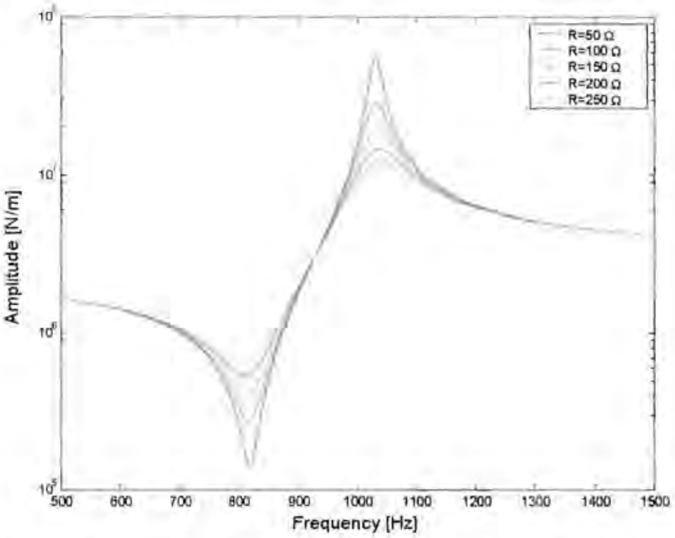

Figure 2.10 (b) *Bode diagram of the shunted piezoelectric stack actuators transfer function with variation in the resistance value*

The amount of attenuation obtained through the implementation of the absorber is a function of the structure mass, stiffness, the amount of inherent structural damping and the capacitance value of the actuator. The capacitance value of the actuator is related to the area perpendicular to the poling direction of the piezoelectric element and the number of layers in the stack. Figure 2.11 (a) indicates the reduction of the amount of attenuation as the mass and stiffness of the discrete spring mass system is increased while the inductance, resistance and capacitance are held constant. The values of the simulation are presented in tables 2.8 (a) and (b).

Table 2.8 (a) Mass and stiffness values for the simulations

Mass [kg]	Stiffness [N/m]
50	1.9739×10^9
40	1.5791×10^9
30	1.1844×10^9
20	0.7896×10^9
10	0.3948×10^9

Table 2.8 (b) Constant model values for the variation in system mass and stiffness simulations.

Resistance	100 Ω
Inductance	0.4005 H
Capacitance	100×10^{-9} F

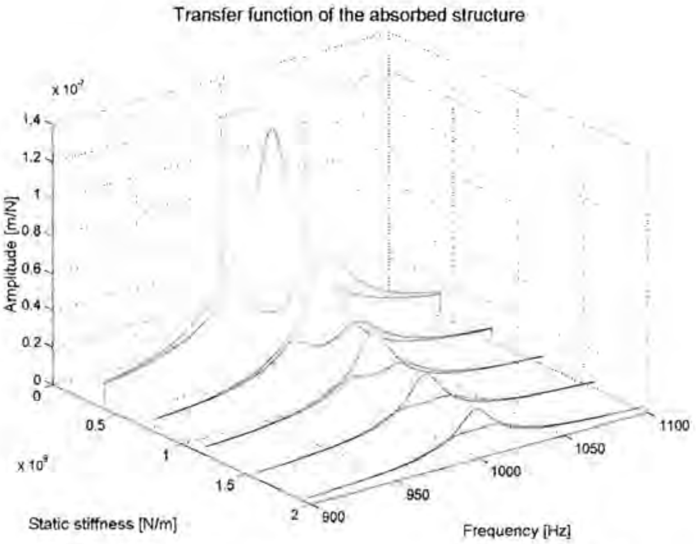

Figure 2.11 (a) *FRF of the absorbed structure with variation in the mass and stiffness values. Resistance of 100 Ω*

The simulation was repeated with a 10 Ω resistance and figure 2.11 (b) indicates that the anti-resonant at low damping levels are less susceptible to the phenomena, compared to cases were the absorber is more heavily damped. The amplitude of the resonant peaks is higher for the lightly damped case, which is undesirable for wide frequency band excitation.

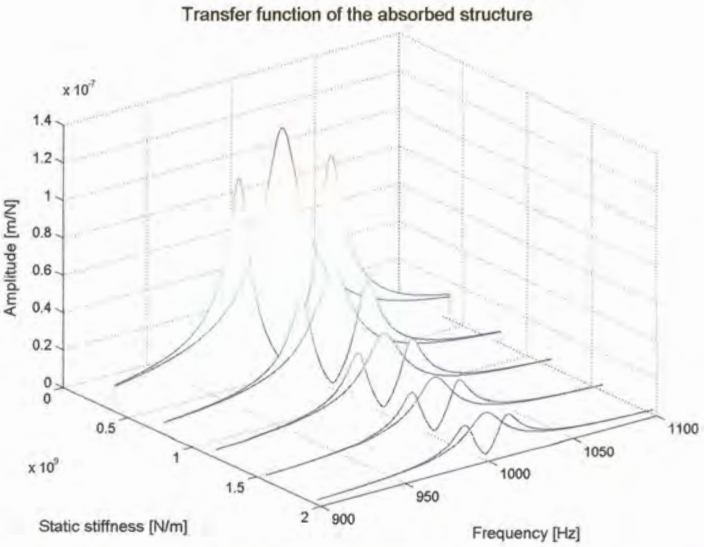

Figure 2.11 (b) *FRF of the absorbed structure with variation in the mass and stiffness values. Resistance of 10 Ω*

The influence of the structure's damping is indicated in figure 2.11 (c) where the simulations were repeated for 5 % structural damping and a shunt resistance of 100 Ω. The results of figure 2.10 (b) and (c) indicate that the amount of attenuation decreases as the structural damping increases.

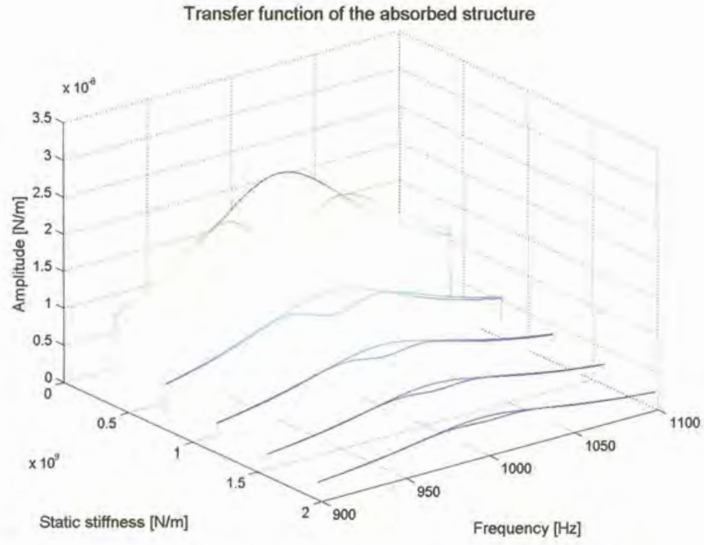

Figure 2.11 (c) *FRF of the absorbed structure with variation in the mass and stiffness values. Resistance of 10 Ω Structural damping 5 %*

The influence of the capacitance is demonstrated in the simulations that produced the frequency response functions in figure 2.12 (a).

The mass of the discrete spring mass system was increased to 10 kg for visualisation purposes and was kept constant. The resistance of the shunt circuit was set to 10 Ω. The inductance values had to change with the capacitance values to obtain optimum resonant absorption frequency. The specification for the system in figure 2.12 (a) and (b) is presented in tables 2.9 (a) and (b).

Table 2.9 (a) Specification of the simulated system displayed in figure 2.12 (a) and (b)

Mass	10 kg
Damping	1 %
Resistance	10 Ω

Table 2.9 (b) Variation of the inductance with change in capacitance

Inductance [H]	Capacitance [F]
0.504	87×10^{-9}
0.123	347×10^{-9}
0.0535	781×10^{-9}
0.029	1.388×10^{-6}
0.0175	2.169×10^{-6}

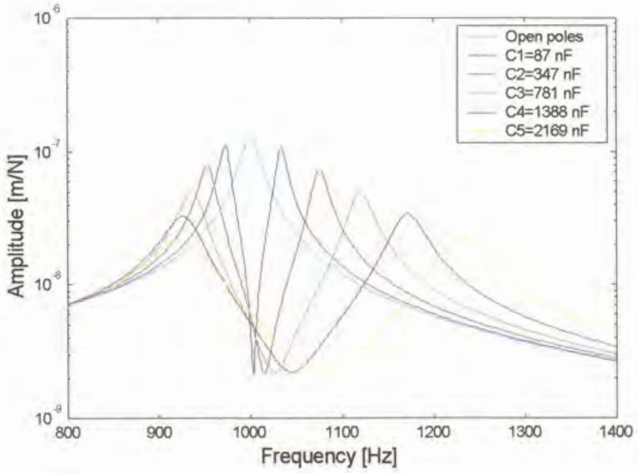

Figure 2.12(a) *FRF of the absorbed structure with variation in the capacitance and inductance mass = 10 kg*

Note the change in the anti-resonant frequency with the increase in the capacitance value of the stack actuator. The amount of attenuation increased for the increase in capacitance. Figure 2.12 (b) shows the decrease in the inductance value as the capacitance is increased to obtain optimum resonant absorption frequency.

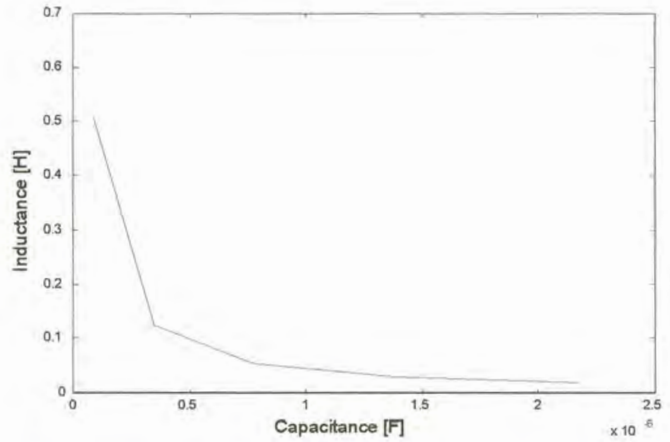

Figure 2.12 (b) *The variation of the shunt inductance as the capacitance increases*

The amount of attenuation for a given shunt resistance value decreases as the system mass and stiffness increases. Figure 2.13 shows the simulation result of the previous system, where the mass was increased to 50 kg. Note the reduced shift in the anti-resonant frequency of the system with the increase in mass and stiffness.

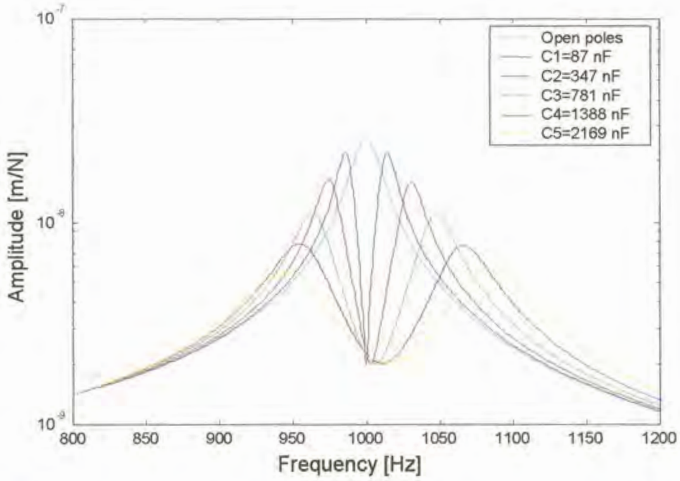

Figure 2.13 *FRF of the absorbed structure with variation in the capacitance and inductance mass = 50 kg*

It has been proven that the amount of attenuation for a piezoelectric absorber configuration decreases for an increase in system mass and stiffness. The amount of attenuation may be improved by increasing the capacitance of the piezoelectric stack actuator. Figures 2.14 (a) presents simulation results where the system mass and stiffness were kept constant and the capacitance value was increased. The system mass was increased to 50 kg for visualisation purposes. The specification of the system in figures 2.14 (a) and (b) is presented in tables 2.10 (a) and (b).

Table 2.10 (a) Specification of the simulated system displayed in figures 2.14 (a) and (b)

Mass	50 kg
Damping	1 %
Resistance	10 Ω

Table 2.10 (b) Variation of the inductance with change in capacitance

Resistance [Ω]	Inductance [H]	Capacitance [F]
100	0.504	87×10^{-9}
50	0.123	347×10^{-9}
35	0.0535	781×10^{-9}
25	0.029	1.388×10^{-6}
20	0.0175	2.169×10^{-6}

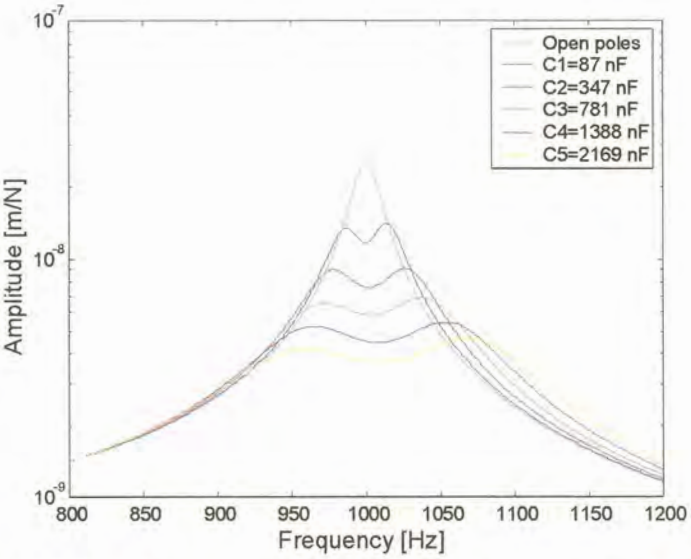

Figure 2.14 (a) *FRF of the absorbed structure with variation in the capacitance, inductance and resistance*

The simulation was repeated for a system mass of 100 kg. The results are displayed in figure 2.14 (b) and clearly show the decrease in the amount of attenuation for the same amount of capacitance.

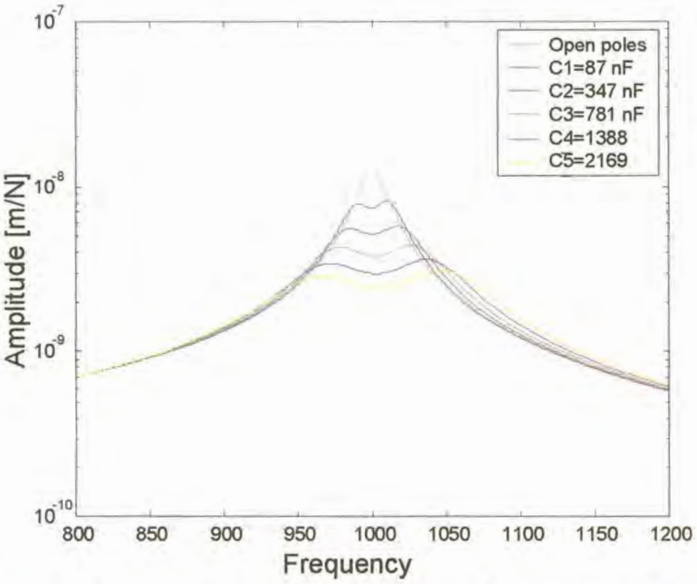

Figure 2.14 (b) *FRF of the absorbed structure with variation in the capacitance, inductance and resistance Mass = 100 kg*

Figures 2.14 (c) and (d) show the variation in the resistance as the capacitance was increased. Notice that there is little to no difference in the resistance requirements for the variation in mass. The required resistance values are slightly lower for the increases in system mass and stiffness.

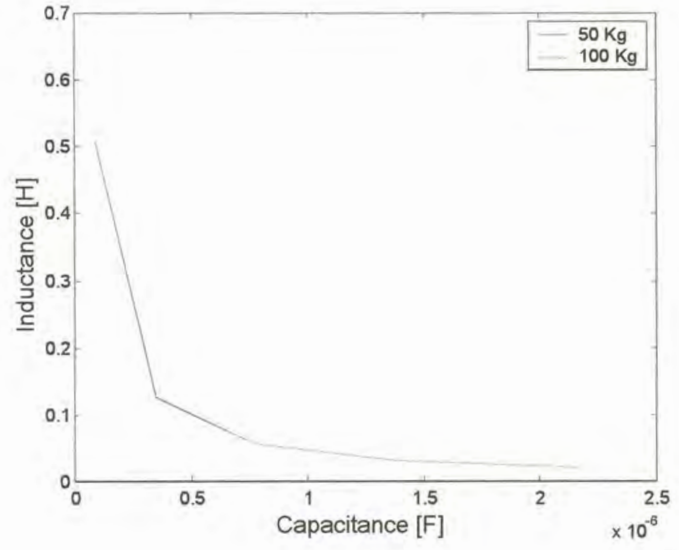

Figure 2.14 (c) *Variation of the inductance value as a function the capacitance for the simulations presented in figures 2.14 (a) and (b)*

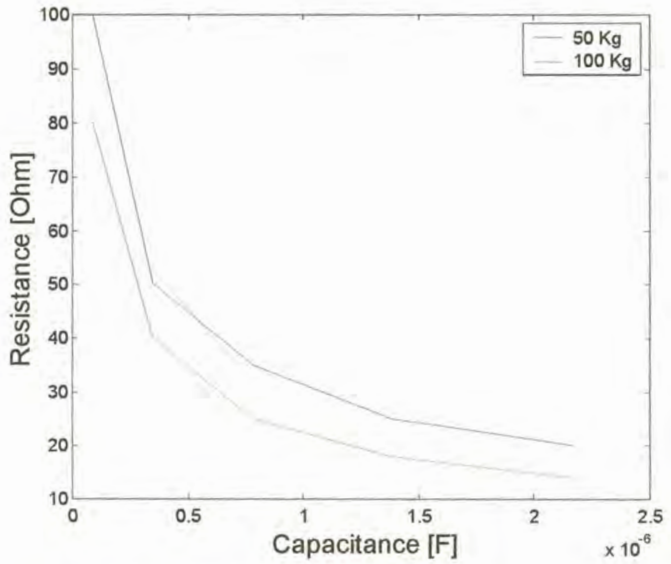

Figure 2.14 (d) *Variation of the resistance value as a function the capacitance for the simulations presented in figures 2.14 (a) and (b)*

2.5 Experimental verification of the mathematical model

2.5.1 Experimental procedure and test rig

The experimental verification was conducted on a cantilevered aluminium beam. The model was verified for the piezoelectric absorber and not for the damper. The experimental set-up is shown in figure 2.15 (a), (b) and (c). A modal analysis was conducted on the beam in the vertical direction with two different configurations. The first modal analysis was conducted only on the beam without the actuator. The piezoelectric stack actuator was added to the second experimental test rig as a structural element with the poles of the actuator open. The objective of the second modal analysis was to estimate the influence of the actuator on the cantilevered beam. The second modal analysis was followed by various modal analyses in which the piezoelectric actuator was shunted with an equivalent inductance and resistance.

The modal measurements were taken through the use of a digital signal processor and data logger. An electrodynamic shaker driven with a random signal induced the force input onto the structure. A list of the equipment used in the measurements is presented in table 2.11. The dimensions of the aluminium beam are tabled in table 2.12.

Table 2.11 Modal measurement equipment list

Item number	Item	Model
1	DSP Siglab signal processor and generator	20-42
2	IMV Vibropet electrodynamic shaker	PET-01
3	Rotel amplifier	RA-970BX
4	PCB miniature high frequency accelerometer	353B17
5	PCB impedance head	288D01
6	PCB Battery powered signal conditioner	480E09
7	Notebook computer	Intel 486 DX2-66
8	Piezomechanik piezoelectric stack actuator	Pst 500/5/15 VS10

Table 2.12 Dimensions of the aluminium beam

Length	490 mm
Height	10 mm
Width	30 mm

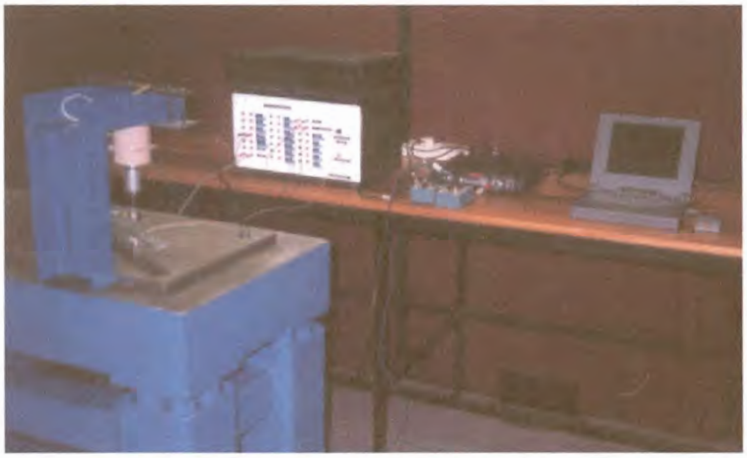

Figure 2.15 (a) *Experimental test rig and instrumentation*

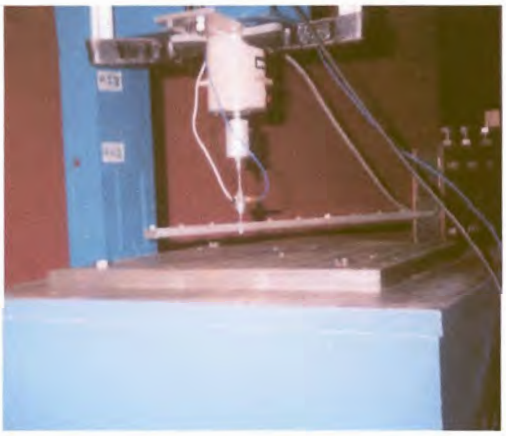

Figure 2.15 (b) *Experimental test rig without the piezoelectric stack actuator*

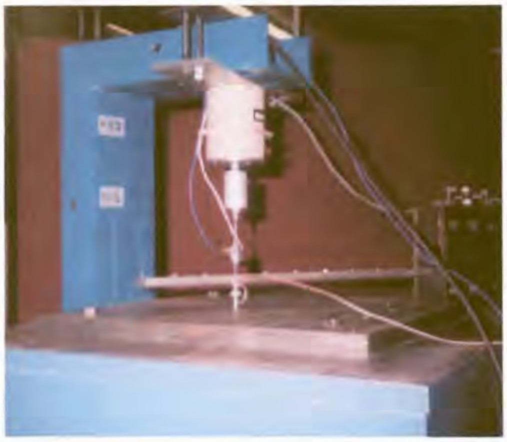

Figure 2.15 (c) *Experimental test rig with the piezoelectric stack actuator.*

The shunt circuit comprised of a variable resistance pot and a number of custom made inductors. The inductors were wound on ferromagnetic E cores. The current rating of the circuit was 1A. The inductance values of the various inductors were specified so that any inductance value between 1×10^{-3}H and 1H could be obtained in discrete steps of 1×10^{-3}H by connecting the various inductors in series. Toroid cores were implemented in the shunting circuit but for some reason did not work. The phenomenon was not investigated further since the E cores worked well, but it is still worth mentioning for further reference. An attempt was made to simulate a variable inductor with an electronic circuit comprising of two operational amplifies a few resistors and a capacitor. The circuit is commonly referred to as a gyrator. A diagram of the gyrator is shown in figure 2.16 and the equivalent inductance in terms of the resistance and capacitor values are expressed in equation 2.23.

$$\mathrm{Leq} = \frac{\mathrm{R_1 \cdot R_3 \cdot R_4 \cdot C}}{\mathrm{R_2}} \tag{2.23}$$

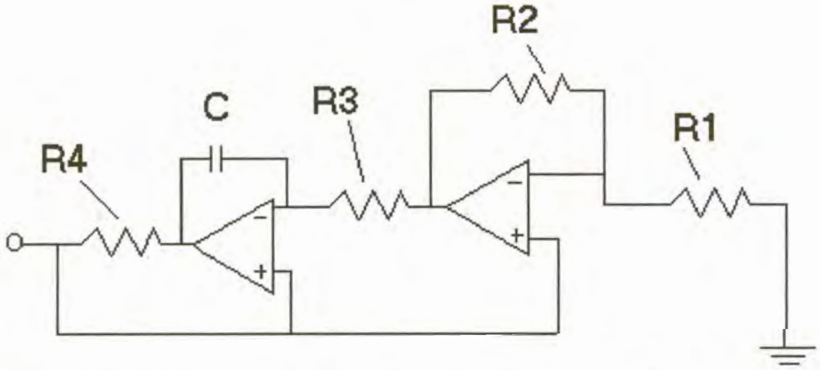

Figure 2.16 *Gyrator diagram / Synthetic inductor diagram [12]*

The successful design of the circuit is strongly dependent on the characteristics of the operational amplifiers.

The idea of varying one of the resistance values with a pot to obtain a variable inductor failed due to the limited ability or characteristics of the operational amplifiers. The concept works for a limited band, but is too unstable to use in the shunting analysis. Proper design of the circuit at a designated inductance value still makes the gyrator an attractive option to use when large inductance values are required and the size of real inductors become too large for the application. Edburg *et al.* [11] apparently implemented variable synthetic inductors with success. For further information on the gyrator please refer to references [12] and [13].

2.5.2 Verification of the mathematical model

The feedback loop transfer functions of the piezoelectric damper and absorber were derived so that the actuator could be modelled in the state space environment. It is possible to convert a finite element model as well as a modal model into the state space format. The model of the actuator can therefore be implemented on a measured model or on a finite element model that has been verified or updated by experimental data. An updated finite element model was used to verify the mathematical model of the actuator. In order to verify the influence of the actuator as a structural element, the finite element model was constructed without the influence of the feedback stiffness loop indicated in figure 2.2. The beam was modelled within the structural dynamic toolbox environment of Matlab [40]. Twenty, twelve degree of freedom, Bernoulli-Euler beam-elements were used in the model. It is necessary to determine which mode shapes of the finite element model coincide with the mode shapes of the Experimental Modal Analysis (EMA) in order to update the finite element model with experimental modal data. The modal assurance criteria proposed by Allemang and Brown [38] was used to establish which of the mode pairs coincide. The criterion provides a quantitative evaluation of the quality of the comparison between the mode shape pairs. The Modal Assurance Criterion (MAC) between the predicted mode and measured modes are defined by equation (2.24).

$$\mathrm{MAC}\,(\varphi_{\mathrm{iA}},\varphi_{\mathrm{jX}}) = \frac{|\{\varphi_{\mathrm{iX}}\}^{\mathrm{T}}\{\varphi_{\mathrm{jA}}\}|^{2}}{\{\varphi_{\mathrm{iX}}\}^{\mathrm{T}}\{\varphi_{\mathrm{iX}}\}\{\varphi_{\mathrm{jA}}\}^{\mathrm{T}}\{\varphi_{\mathrm{jA}}\}} \qquad (2.24)$$

with:

φ : Mode shape matrix

The first subscript index of the mode shape matrix indicates the mode number and the second subscript denotes the measured co-ordinate point. The superscript T denotes the conventional matrix transpose. The subscript (i) denote the predicted mode shape matrix column number, and the (j) subscript the modal mode shapes matrix column number.

The modal assurance criteria compare all the measured mode shapes to all the finite element mode shapes and renders a value between one and zero to indicate how well the modes compare. The values are presented in a matrix format. A value above 0.7 indicates that the two modes have approximately the same shape.

In order to obtain a good comparison of the modes it is required that a finite element mode shape will coincide with only one experimental modal mode shape. This implies that only one of the values in each matrix column should have a value above 0.7. The remaining values in the matrix columns should have values less than 0.3.

The modal analysis of the beam was conducted only in the vertical direction. Therefore there were more finite element modes than modal modes, since the finite element model took in to account the horizontal and torsional modes. The modal analysis rendered six modes in the frequency band that was measured and the finite element modes which coincide with these modes, were determined by the use of the modal assurance criteria. The frequency response data measured at the collocated point as well as the corresponding finite element data of the updated model is presented in figure 2.17. A visual representation of the modal assurance criteria test is shown in figure 2.18. The finite element modes that corresponded to the measured modes are shown in table 2.13.

Table 2.13 Mode numbers of the modes that coincide

Modal mode number	Finite element mode number
1	3
2	4
3	6
4	9
5	11
6	13

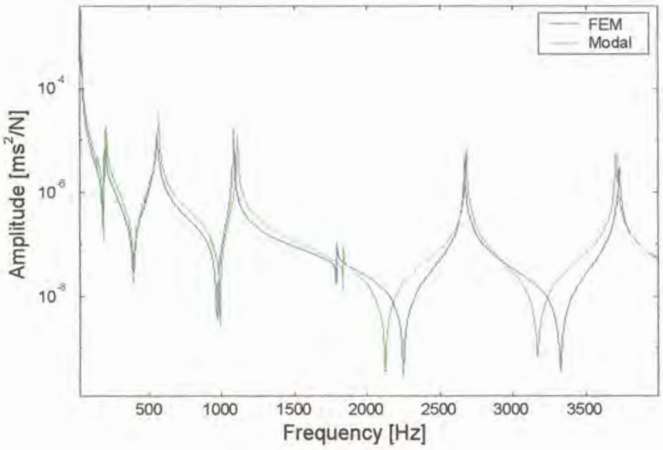

Figure 2.17 *Frequency response data at the collocated point without the actuator present as a structural element*

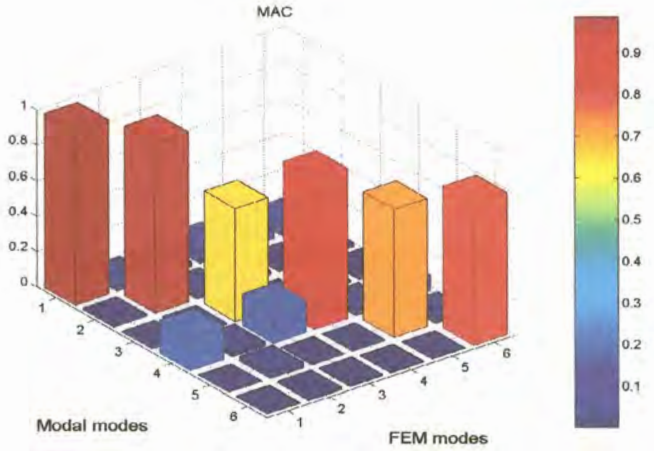

Figure 2.18 *MAC matrix*

The model was updated through the use of an optimisation algorithm that implements a simplex search method. The method is robust and can handle discontinuities in the objective function. The algorithm does not use analytical or numerical gradient information, which makes it less efficient, and increases the number of function evaluations required to obtain the local minimum. The more efficient methods, such as the quasi-Newton and the conjugate gradient variants cannot deal with discontinuities in the objective function. The MATLAB optimisation toolbox [45] was used to perform the model updating. The objective function was written as the sum of the absolute differences between the natural frequency values of the modes proposed by the modal assurance criteria. The objective of the optimisation was to minimise the objective function value. The finite element model parameters used in the updating process was the Young's modulus, density, beam height and width. The result of the model updating is presented in table 2.14 and the updated frequency response plot is compared to the measured data in figure 2.17.

Table 2.14 Results of the model updating.

Modal mode number	EMA frequency [Hz]	FEM mode number	FEM frequency [Hz]
1	200.4	3	196.9
2	558.6	4	551.3
3	1106.6	6	1080.3
4	1827.5	9	1786.0
5	2673.0	11	2668.6
6	2695.9	13	3707.04

The objective function value versus the number of function evaluations is shown in figure 2.19. The variables of the model updating process versus the number of function evaluation are shown in Appendix A.

The addition of the actuator to the structure rendered it necessary to update the model with the additional stiffness of the actuator. The same procedure was used. The objective function was compiled by the sum of the absolute differences between the 11th, 13th and 15th mode frequencies. The frequencies of the 11th and 13th modes increased due to the additional stiffness of the actuator. Priority was given to these modes since they were the modes that were attenuated for the experimental verification. The frequencies are tabled in table 2.15 (a). The result of the model updating parameters is presented in table 2.15 (b). Figures 2.20 and 2.21 show the results obtained by the model updating.

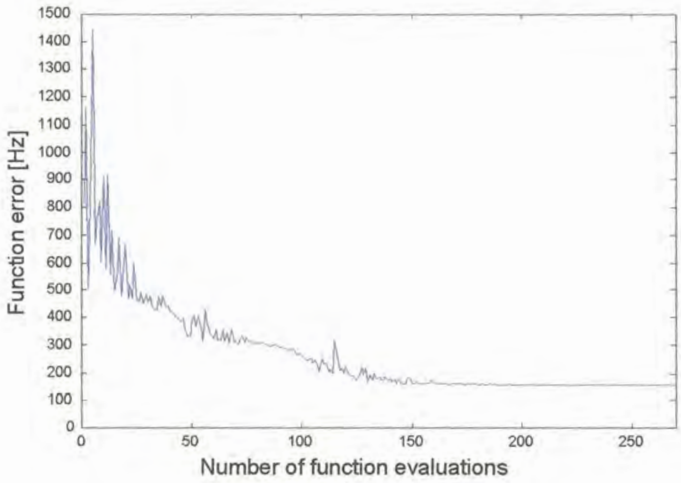

Figure 2.19 *The objective function value versus the number of function evaluations for the model without the actuator present as a structural element*

Table 2.15 (a) Comparison between the modal and finite element mode frequencies for the model updating, with the actuator present as a structural element

Mode number	FEM frequency [Hz]	Modal frequency [Hz]
11	2875	2942
13	3910	3910

Table 2.15 (b) Model parameters after model updating with and without the actuator present as a structural element.

Model updating parameter	Model without the actuator	Model with the actuator
Actuator stiffness [N/m]		1.0419×10^7
Young's modulus [Pa]	44.928×10^9	81.511×10^9
Density $[kg/m^3]$	2916.7	2737.8
Width [m]	0.0343	0.03
Height [m]	0.0118	0.01

An additional amount of inherent damping is added to the structure due to the incorporation of the actuator as a structural element. The effect can be seen when comparing figure 2.20 to figure 2.17. The dynamic characteristics of the beam are influenced to a large extent since the cantilevered beam is a structure with low stiffness at the point where the actuator is implemented. The extent to which the structure is influenced by the actuator can be related to the properties of the structure itself and the implementation of the actuator. The implementation of the feedback stiffness loop is required to simulate the normal stiffness of the actuator structure on the beam. The boundary conditions in the FEM of the cantilevered beam were assumed to be rigid. However in practice this is not the case and therefore the model updating process reduced the Young's modulus to an unrealistic value in order to compensate for the reduced stiffness in the boundary conditions. The effect is less prominent when the actuator is added to the structure since the number of boundary conditions is increased. The data in table 2.15 (b) shows that an increase in the stiffness of the finite elements is required to obtain the measured frequency response.

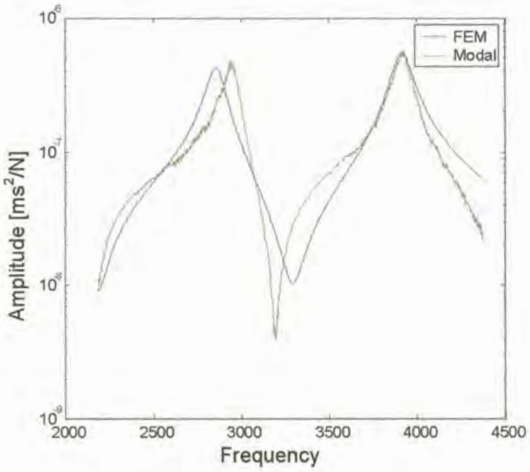

Figure 2.20 *Frequency response data at the collocated point with the actuator present as a structural element*

The piezoelectric absorber was implemented to attenuate the modes shown in figure 2.20. The experimental and mathematical model results are shown in figures 2.22 (a) to (c) and 2.23 (a) to (c). The inductance and resistance values for the various figures are tabled in tables 2.16 and 2.17.

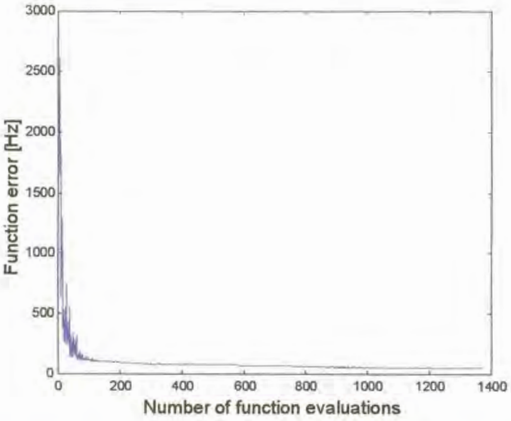

Figure 2.21 *The objective function value versus the number of function evaluations for the model with the actuator present as a structural element*

Table 2.16 The resistance and inductance values of the experiments and mathematical model

Figure number	Experimental resistance value [Ω]	Model resistance value [Ω]	Experimental inductance value at 1000 Hz [H]	Model inductance value [H]
2.22 (a)	100.0	190	0.0461	0.042
2.22 (b)	51.3	120	0.0461	0.042
2.22 (c)	1.2	10	0.0461	0.042

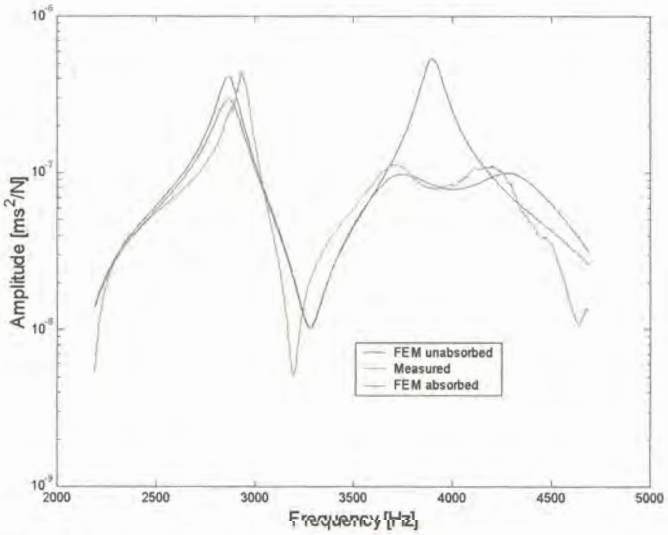

Figure 2.22 (a) *Experimental and mathematical absorber implementation*

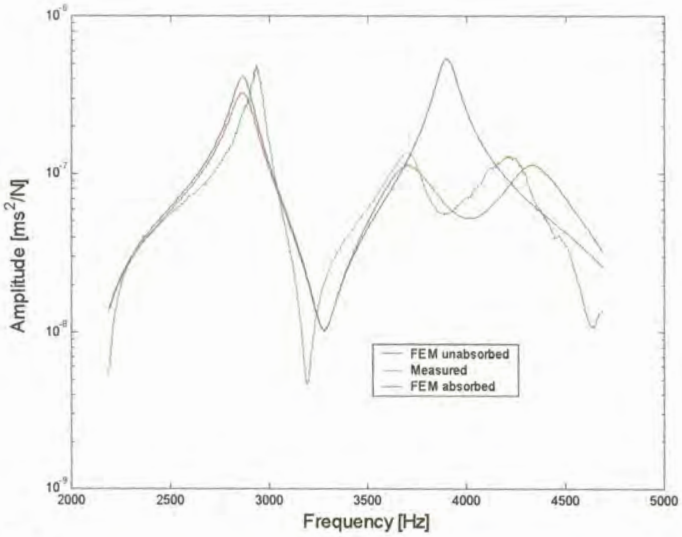

Figure 2.22 (b) *Experimental and mathematical absorber implementation*

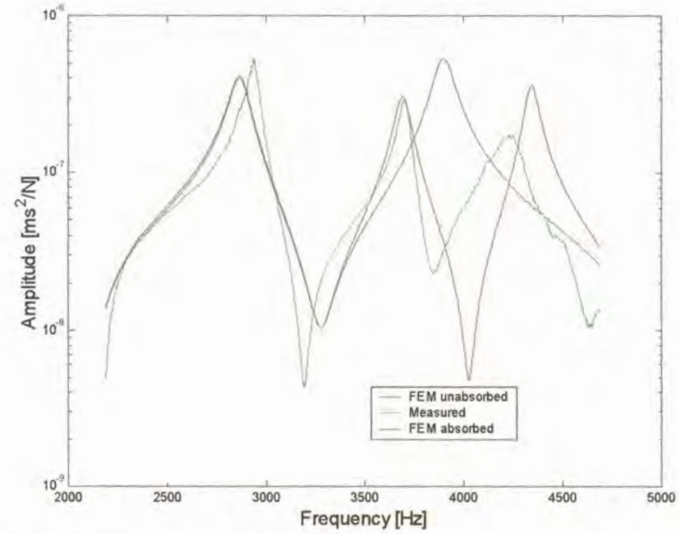

Figure 2.22 (c) *Experimental and mathematical absorber implementation*

Table 2.17 The resistance and inductance values of the experiments and mathematical model

Figure number	**Experimental resistance value [Ω]**	**Model resistance value [Ω]**	**Experimental inductance value at 1000 Hz [H]**	**Model inductance value [H]**
2.23 (a)	230.0	350	0.0808	0.0808
2.23 (b)	70.0	160	0.0808	0.0808
2.23 (c)	1.3	5	0.0808	0.0808

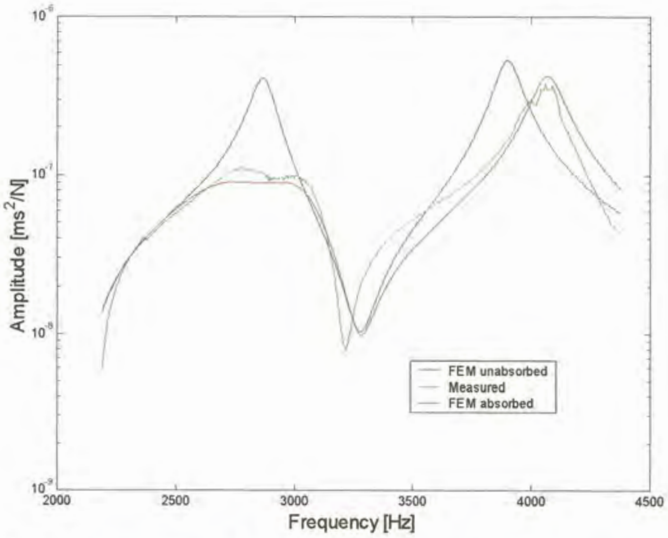

Figure 2.23 (a) *Experimental and mathematical absorber implementation*

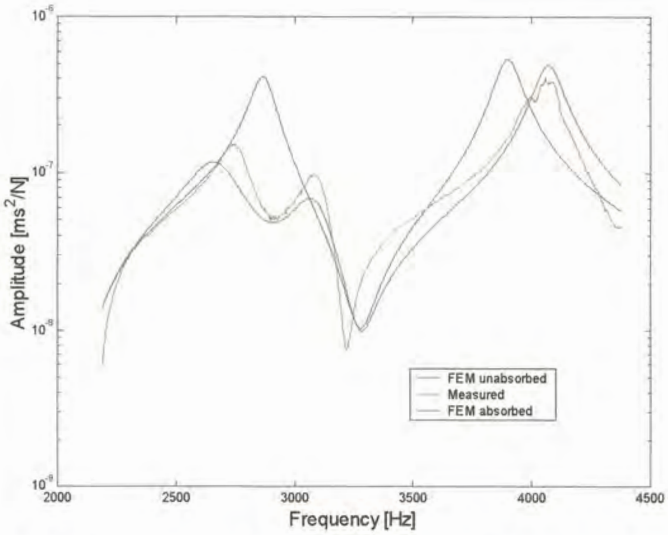

Figure 2.23 (b) *Experimental and mathematical absorber implementation*

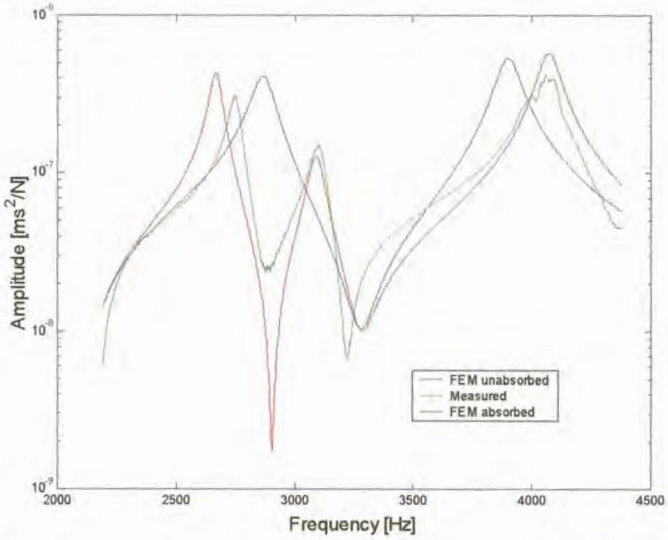

Figure 2.23 (c) *Experimental and mathematical absorber implementation*

The results of the experimental measurements compare fairly well to the mathematical model. The feedback loop of the absorber does not account for the inherent structural damping of the actuator. Therefore the resistance of the shunt circuit model was increased to accommodate the inherent structural damping in the mathematical model. As a result the experimental resistance values were lower than the resistance values of the mathematical model. The accuracy of the structural model and the accuracy of the actuator material properties determine the performance of the piezoelectric damper model. It is evident that the stiffness of the actuator is increased by the shunt. The optimum attenuation results are shown in table 2.18.

Table 2.18 Optimum attenuation results

Frequency region [Hz]	Attenuation [m/N]	Attenuation [%]
2875	319×10^{-9}	77.9
3910	437×10^{-9}	81.7

Chapter 3

Machine tool dynamics

Hakansson *et al.* [25, 26, 27, 28, 29 and 30] indicated that the weak link of a lathe structure is situated at the tool post. Their observation was verified on a Diplomatic TRM120 series 10 tool changer. A modal analysis was conducted to determine the dynamic properties of the tool changer. The behaviour of the tool changer under machining conditions was investigated using an Operational Deflection Shape (ODS) analysis. The tool shank was fitted with an "MTJNR-2020K-16W" external tip tool holder for the tests.

3.1 Operational deflection shape analysis

The ODS analysis was conducted in accordance with Døssing and Staker [1]. The ODSs may be predicted from the modal model, the boundary conditions and the operational forces. However it is utilised to assist the evaluation of the dynamic behaviour when the exact operational forces are difficult to measure and the structure is suspected of being non-linear. In the application of machine tools, the analysis provides a simple and efficient method of obtaining reliable information regarding the dynamic behaviour of a machine tool structure. The information can assist the design of the modal analysis test procedure and can be extended to verify modal analysis results.

The ODS analysis is based on the measurement of transmissibility functions. A transmissibility function is defined as a dimensionless ratio of relative movement between two points, on a structure. The transmissibility is measured in the same direction under the structure's operational conditions. ODSs are constructed from a variety of transmissibility functions that are measured relative to a reference point on the structure. The reference point is chosen at a position on the structure that exhibits large displacement, when compared to the rest of the structure, under operational conditions. The roving response is divided by the larger reference response values to minimise the occurrence of ill-conditioned transmissibility functions. A second set of transmissibility functions, can be measured in a plane perpendicular to the first, to construct an ODS with two-dimensional movement. The movement of the reference point in the two directions is scaled by a ratio of displacement. The displacements are selected at the operational frequency from spectral measurements at the reference point, to obtain the correct ratio of movement in the planes

The measurement and computation of transmissibility functions are closely related to that of frequency response functions and therefore the data is presented in the same frequency domain format. The amplitudes of relative motion are extracted from the transmissibility functions at the operational frequency to construct the graphical representation of the ODSs. Multiple ODSs at different operational frequencies can be constructed to obtain insight into the analysis at hand.

The magnitude of the acceleration levels measured on the lathe bed was negligible in comparison to the levels measured on the tool changer. Therefore the experimental effort was focused on the tool changer and cross slide. The transmissibility functions were measured on the tool changer and cross slide during the machining of a shaft.

Details of the experimental set-up as well as the instrumentation used are presented in tables 3.1(a) and (b). The accelerometer at the tool tip was used as the reference since it is the point on the structure that exhibits the highest vibration levels. The tool changer was instrumented as indicated in figure 3.1.

Figure 3.1 *Tool changer instrumentation for the transmissibility measurement*

Table 3.1 Details of the experimental procedure

Shaft length between tailstock and chuck	250 mm
Shaft diameter	30 mm
Shaft material	Mild steel
Feed rate	0.125 mm/rev
Rotational speed	470 rpm
Cut depth	1.5 mm

Table 3.1 (b) Instrumentation used to measure the operational deflection shape data

Item number	Item	Model
1	Diagnostics Instruments spectrum analyser	PL202
2	PCB miniature high frequency accelerometers	353B17
3	PCB battery powered signal conditioners	480e09

A schematic diagram of the measuring points is presented in figure 3.2.

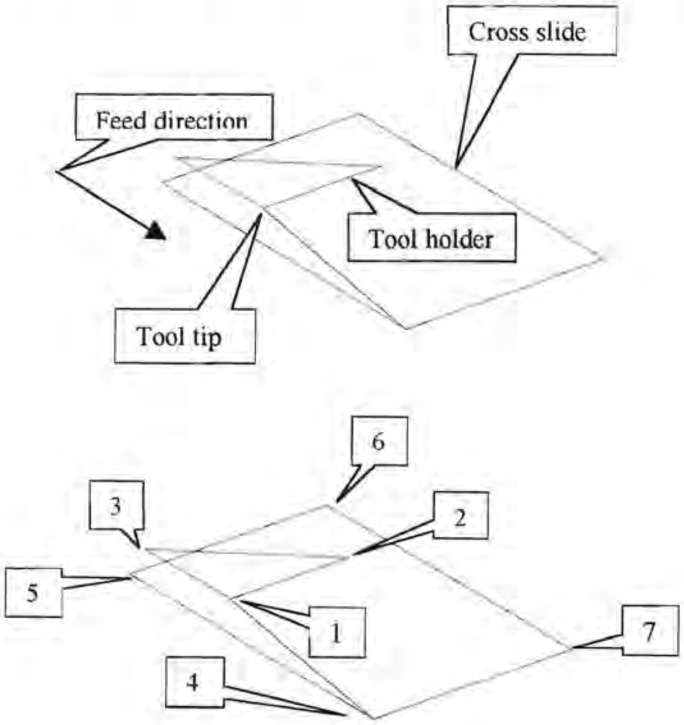

Figure 3.2 *Schematic diagram of the measuring points*

The machining process of a lathe is a non-stationary process due to the movement of the tool post, the loss in machined component mass, the deviancies in the alignment of the component along the lathe bed, and the variation in the material properties of the machined component. These facts also contribute to the poor measurement repeatability of the process. The technique of ODS analysis proposed by Døssing and Staker [1] requires that the process be stationary.

To accommodate the stationary theory a number of processing averages were computed from the measured signals during the machining process. The transmissibility functions and spectra, which were measured during machining on the lathe, are therefore an average representation of the machining process. The data can be assumed to be stationary for the purpose of the research.

The operational frequencies are usually selected from the spectrum of the reference point at frequencies with peak values indicating the presence of energy in the structure. The spectrum at the tip of the tool is shown in figures 3.3(a) and (b). The ODS analysis was conducted in the vertical and horizontal directions of the lathe. The response of the tip in the vertical direction is higher than the response in the horizontal direction. Most of the response of the structure is concentrated between 500 and 2000 Hz. The spectrum was measured and calculated with a Diagnostics Instrument PL202.

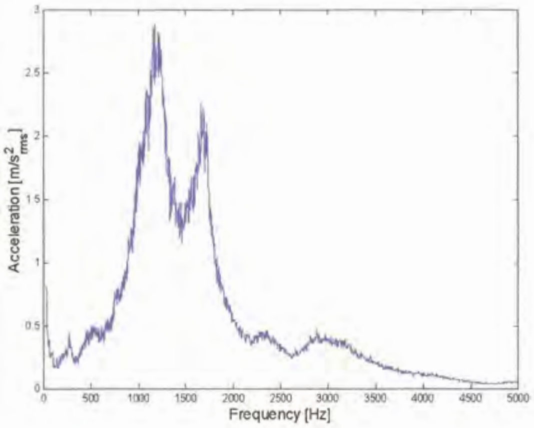

Figure 3.3 (a) Vertical spectrum at the reference point

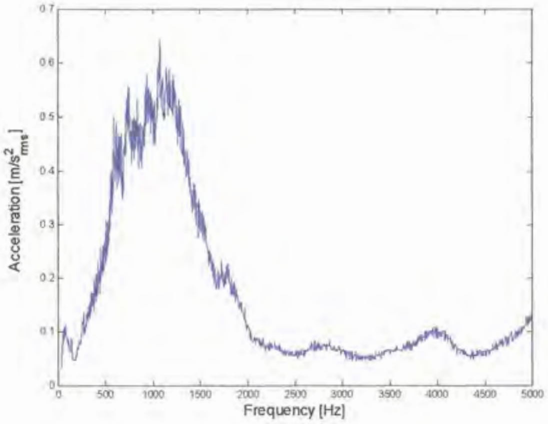

Figure 3.3 (b) *Horizontal spectrum at the reference point*

The operating frequencies that were selected for the operational deflection shape analysis, based on their high levels of response on the spectrum, are displayed in table 3.2.

Table 3.2 Operating frequencies

Frequencies observed in vertical spectrum [Hz]	**Frequencies observed in horizontal spectrum [Hz]**
1200	934
1660	1070

The transmissibility functions on the tool changer were measured during different machining runs to validate the stationary assumption. The results obtained from the transmissibility measurements between the front and the end of the tool holder are presented in figures 3.4 (a) and (b).

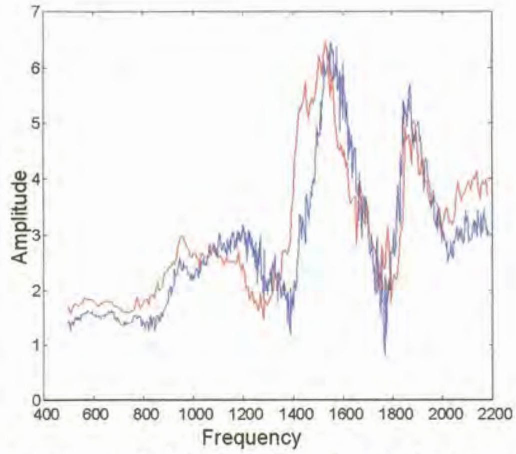

Figure 3.4 (a) *Transmissibility function T_{21} in the horizontal direction*

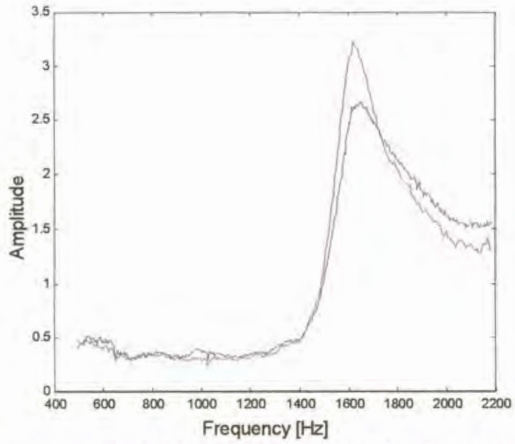

Figure 3.4 (b) *Transmissibility function T_{21} in the vertical direction*

The results indicate a deviation between the two processes. However, the trend of the data remained the same. The trends predicted by the ODSs can therefore be used to indicate the behaviour of the machine tool at the operating frequencies. The complete sets of transmissibility functions are presented in appendix B.

The operational deflection shapes are presented in figures 3.5 (a) to (d).

(a) *ODS at 934 Hz operational frequency (Horizontal)*

(b) *ODS at 1070 Hz operational frequency (Horizontal)*

(c) *ODS at 1200 Hz operational frequency (Vertical)*

(d) *ODS at 1660 Hz operational frequency (Vertical)*

Figure 3.5(b) *ODSs of the toolchanger and cross slide of the lathe*

The ODSs indicate that the motion of the lathe's cross slide is negligible in comparison with the motion of the tool shank and holder.

3.2 Modal analysis

The objective of the experimental modal analysis was to obtain the natural frequency and mode shape information that describes the inherent dynamic behaviour of the tool changer. The tool changer was removed from the lathe for the initial modal analysis and was inserted in to a laboratory test rig to measure the frequency response functions (FRFs). The test rig is shown in figures 3.6 (a) and (b). The instrumentation used for the frequency response measurements of the aluminium beam in chapter 2, was also used for the frequency response measurements on the tool changer. Refer to table 2.11 for the equipment list.

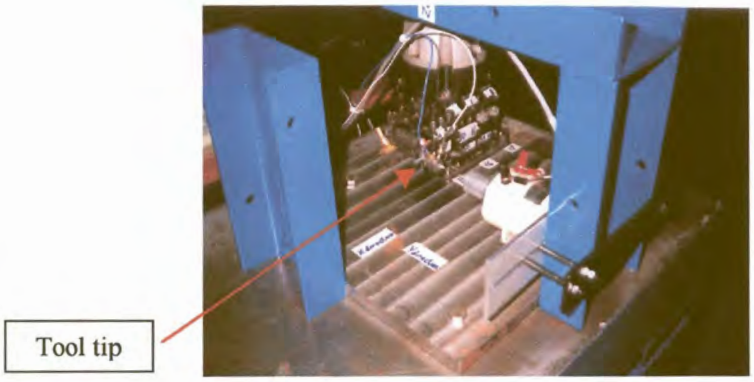

Figure 3.6 (a) *Horizontal FRF measurement set-up*

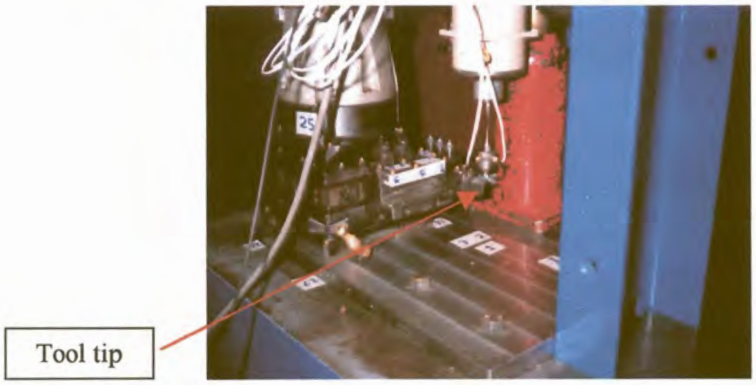

Figure 3.6 (b) *Vertical FRF measurement set-up*

Two separate modal analyses were performed on the structure in each direction. The tool tip was taken to be the collocated point for the modal analyses. A custom-made tool insert was fixed to the tool tip holder to attach the impedance head on to the structure. The results of the modal analyses in the two directions are presented in tables 3.3 (a) and (b). The measured and fitted FRFs at the collocated point for each analysis is presented in figures 3.7 (a) and (b).

Table 3.3 (a) Modal analysis result in the horizontal direction

Mode number	**Frequency [Hz]**	**Damping [%]**
1	1055.0	1.55
2	1098.1	22.67
3	1215.4	24.97
4	1520.3	3.79
5	1692.9	1.05

Table 3.3 (b) Modal analysis result in the vertical direction

Mode number	Frequency [Hz]	Damping [%]
1	772.3	17.25
2	1068.1	2.24
3	1374.4	1.99
4	1470.2	5.83
5	1699.3	1.74
6	2121.1	4.32

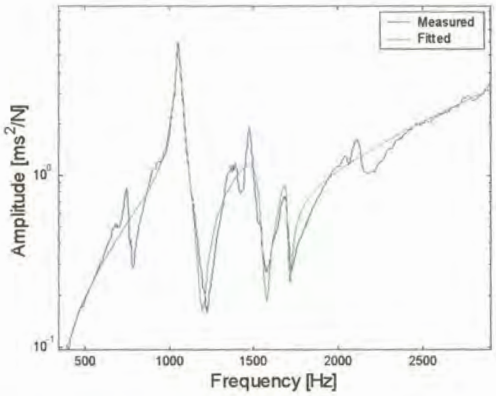

Figure 3.7 (a) *FRF at the collocated point in the horizontal direction*

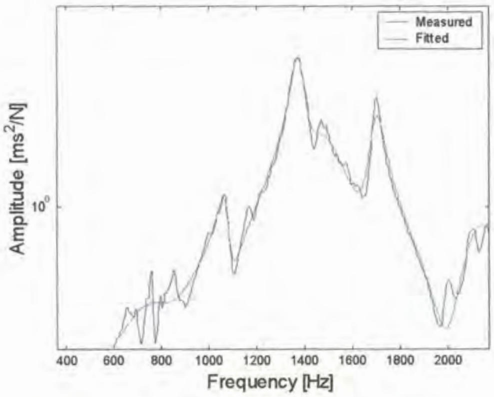

Figure 3.7 (b) *FRF at the collocated point in the vertical direction*

The mode shapes that were extracted from the modal analyses are presented in figures 3.8 (a) to (e) and 3.9 (a) to (f).

(a) *Mode shape 1* (b) *Mode shape 2*

(c) *Mode shape 3* (d) *Mode shape 4*

(e) *Mode shape 5*

Figure 3.8 *Mode shapes of the horizontal modal analysis*

(a) *Mode shape 1* (b) *Mode shape 2*

(c) *Mode shape 3* (d) *Mode shape 4*

(e) *Mode shape 5* (f) *Mode shape 6*

Figure 3.9 *Mode shapes of the vertical modal analysis*

The mode shapes of the modal analyses exhibited excessive movement at the tool shank and holder which verified the ODS analysis results. However the FRFs were fitted with inaccurate results to some of the modes. A further complication is the fact that none of the modal frequencies was observed in both the analyses.

A second set of FRFs was measured with the tool changer fitted onto the lathe in a bid to improve the results. The impedance head was bolted directly onto the tool holder, to omit the dynamics of the tool tip insert, since the objective was to attenuate the structural modes and not those of the tool tip insert.

The second modal analysis was extended to render response results in the horizontal and vertical directions for the horizontal and vertical excitation cases. The experimental set-up is displayed in figures 3.10 (a) to (c).

Figure 3.10 (a) *Horizontal FRF measurement in the lathe environment*

Figure 3.10 (b) *Vertical FRF measurement in the lathe environment*

A Modal 50 electrodynamic shaker was used to excite the system. The larger electrodynamic shaker was used to induce an amount of energy in to the system, which is comparable with the amount of energy induced by the machining operation. The modal model fitted to the FRF data would be an improved linear approximation of the system under machining conditions, since the FRF data was measured at comparable force levels. The only change in the equipment list of table 2.11 is that of the electrodynamic shaker and its amplifier.

The results of the second modal analyses in the two directions are presented in tables 3.4 (a) and (b). The measured and fitted FRFs at the collocated point for each analysis is presented in figures 3.11 (a) and (b).

Table 3.4 (a) Modal analysis results in the horizontal direction within the lathe environment

Mode number	Frequency [Hz]	Damping [%]
1	556.8	5.15
2	804.6	37.80
3	942.6	3.78
4	1452.9	7.14
5	1884.9	33.68
6	1955.2	4.73

Table 3.4 (b) Modal analysis results in the vertical direction within the lathe environment

Mode number	Frequency [Hz]	Damping [%]
1	930.1	7.35
2	1098.7	3.99
3	1303.5	6.51
4	1582.2	2.74
5	1639.9	10.91
6	1847.2	5.28
7	2058.3	7.19
8	2452.3	3.79

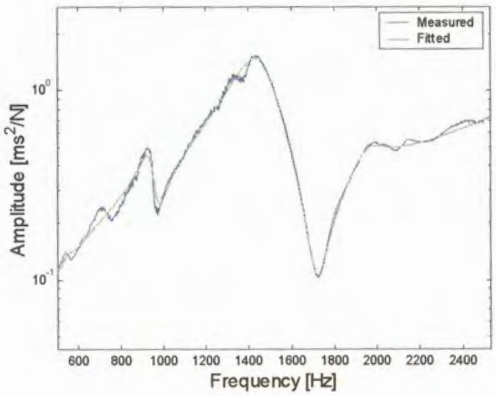

Figure 3.11 (a) *FRF at the collocated point in the horizontal direction within the lathe environment*

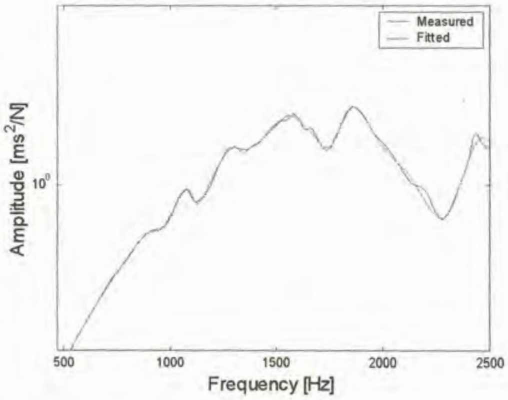

Figure 3.11 (b) *FRF at the collocated point in the vertical direction within the lathe environment*

The mode shapes that were extracted from the second modal analysis are displayed in figure's 3.12 (a) to (g) and 3.13 (a) to (f).

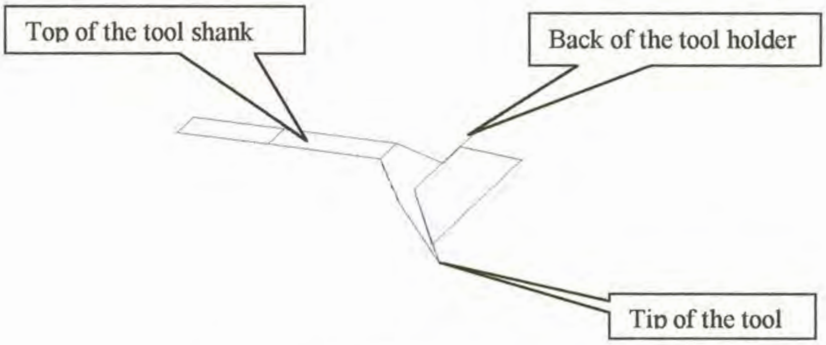

(a) *Mode shape diagram*

(b) *Mode shape 1*

(c) *Mode shape 2*

Figure 3.12 Mode *shapes of the horizontal modal analysis within the lathe environment*

(d) *Mode shape 3* (e) *Mode shape 4*

(f) *Mode shape 5* (g) *Mode shape 6*

Figure 3.12 *Mode shapes of the horizontal modal analysis within the lathe environment*

(a) *Mode shape 1* (b) *Mode shape 2*

Figure 3.13 *Mode shapes of the vertical modal analysis within the lathe environment*

(c) *Mode shape 3*

(d) *Mode shape 4*

(e) *Mode shape 5*

(f) *Mode shape 6*

Figure 3.13 *Mode shapes of the vertical modal analysis within the lathe environment*

The second set of FRFs revealed a system with higher levels of damping. The modal frequencies of the first and second modal analyses deviated significantly from one another. However the accuracy with which the FRFs were fitted in the modal analyses were increased. The prominent peak at a 1068 Hz of the first modal analysis in the horizontal excitation direction was not present in the second set of FRFs. This could be attributed to the fact that the tool insert was omitted. Due to these facts the modes obtained from the second vertical excitation modal analysis were chosen to be representative of the system since the system exhibited larger displacement in the vertical direction during the machining operation and the research aim was set to attenuate the vertical response of the tool.

3.3 Finite element models

A finite element model of the tool holder and shank was built with the objective to update the model with the modal analysis results. The absorber was supposed to be implemented on the updated finite model to predict the influence of the damper on the tool holder and shank. The finite element models suffered from inaccuracies. Nonetheless the modelling attempt was considered useful and was documented for further reference and development.

3.3.1 Solid model of the tool holder and shank

A solid model of the tool holder and shank was constructed in Abaqus CAE. The model was meshed with first order linear tetrahedral elements. Several attempts were made to mesh the geometry with brick elements, but the mesh generator of Abaqus CAE failed each time. A mesh convergence study was conducted to obtain a converged mesh. The tetrahedral mesh converged at 55936 elements. Figures 3.14 (a) to (c) display the solid model of the tool holder and shank.

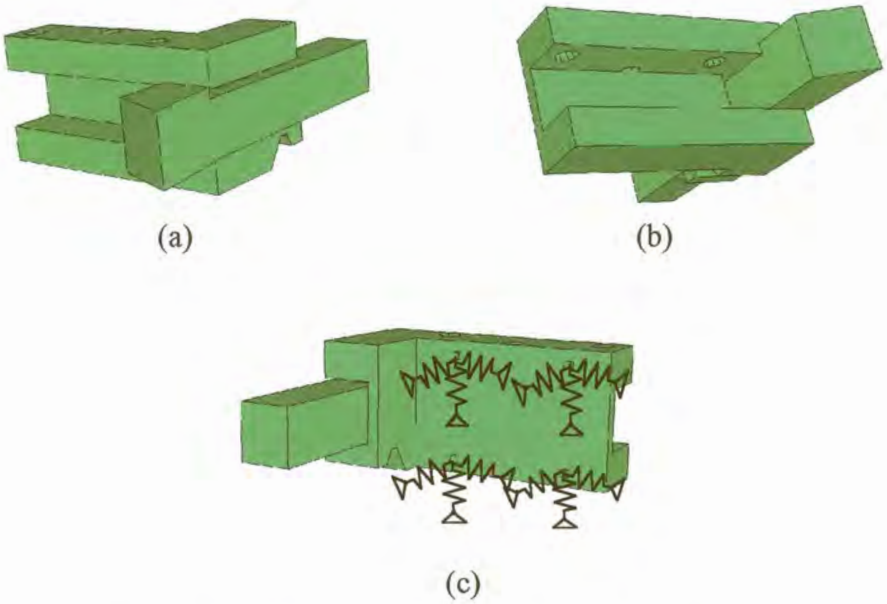

(a) (b)

(c)

Figure 3.14 *Solid model of the tool shank and holder*

The stiffness of the bolted connection was approximated with twelve spring elements at the four positions of the bolts. A number of analyses were conducted, where each of the stiffness coefficients was increased by a constant amount so that the change in the modal frequencies could be monitored. The data was used to establish which modes were sensitive to which spring stiffness and to quantify the sensitivity. The stiffness coefficients were tuned in accordance with the spring sensitivity study to obtain the desired modal frequencies.

An optimisation algorithm approach was implemented to find the optimal spring stiffness values. However it was abandoned since it required too much function evaluations and a function evaluation entailed an eigen value extraction of the model which took a fair amount of computational time since the model consisted of 55936 elements.

The first four finite element mode frequencies were tuned to four of the Experimental Modal Analysis frequencies presented in table 3.4 b. The frequencies and mode numbers are tabled in table 3.5.

Table 3.5 Finite element model update results

FEM mode number	FEM mode frequency [Hz]	EMA mode number	EMA frequency [Hz]
1	1099.7	2	1098.7
2	1580.6	4	1582.2
3	1846.9	6	1847.2
4	2060.1	7	2058.3

A MAC test was conducted on the first five modes of the finite element model to estimate which mode shapes coincide with the experimental modes. The result of the test is presented in figure 3.15 and the mode shapes of the finite element model are displayed in figures 3.16 (a) to (e).

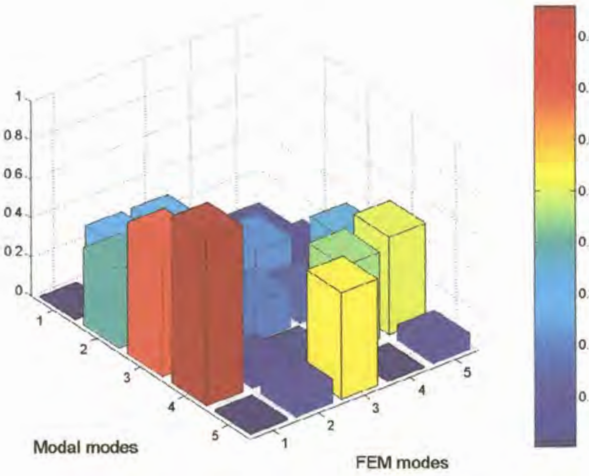

Figure 3.15 *MAC matrix results*

Figure 3.15 indicates that the finite element model failed to construct a prominent set of diagonal values in the MAC matrix even though the mode shapes slightly resembled those of the modal analysis. It is essential that the FRF of the finite element model fit the measured FRF, however it can be anticipated from the MAC that the FRFs would fit poorly. The FRF at the tip of the tool in the vertical direction is shown in figure 3.17. The performance of the finite element model could not be improved by adjusting the spring stiffnesses, density and modulus of the model. A decrease in the spring stiffnesses resulted in unrealisable mode shapes while an increase in the stiffnesses caused the modal frequencies to rise above the measured values.

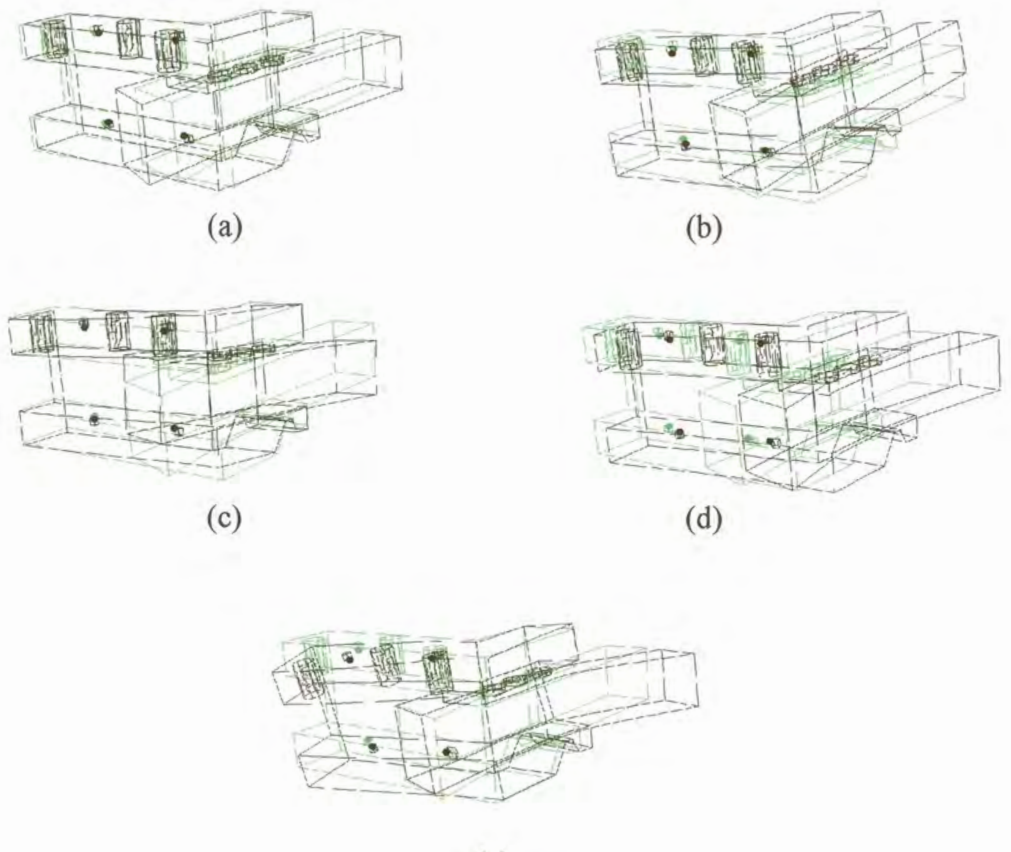

(a) (b)

(c) (d)

(e)

Figure 3.16 *Mode shapes of the finite element model*

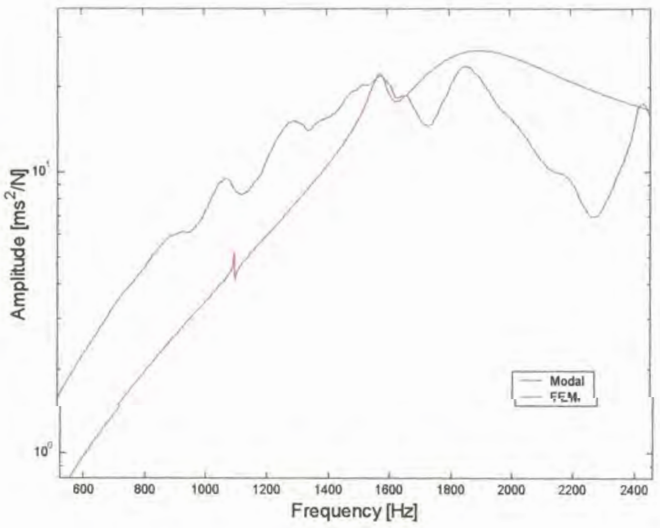

Figure 3.17 *FRF at the tool tip in the vertical direction*

3.3.2 Beam element model of the tool holder

The bolted connection between the tool holder and shank was modelled as a solid connection in the previous model. Therefore the approximation of the stiffness between the two components was incorrect. The approximation was improved by the modelling of the tool holder with Bernoulli-Euler beam-elements while the bolted connection stiffness was approximated with nine spring elements at the bolt positions on the tool holder. The simplified finite element model was updated with the procedure presented in section 2.5.2 that was used to update the finite element model of the cantilevered aluminium beam. The various stiffness coefficients, beam height, beam width, density and modules were used as variables parameters in the optimisation algorithm of the model updating process. The model updating process failed to produce a model that matched all of the modes, but produced a model that improved on the approximation of the measured FRFs. Figure 3.18 indicates the FRF fit at the collocated point on the tip of the tool. The modes that were used in the model updating process are presented in table 3.6.

Table 3.6 Model updating data and results

FEM mode number	FEM mode frequency [Hz]	EMA mode frequency	Excitation direction in which the mode was observed
2	806.6	804.6	Horizontal
3	1283.7	1303.5	Vertical
4	1640.8	1639.9	Vertical
5	1933.6	1955.2	Horizontal

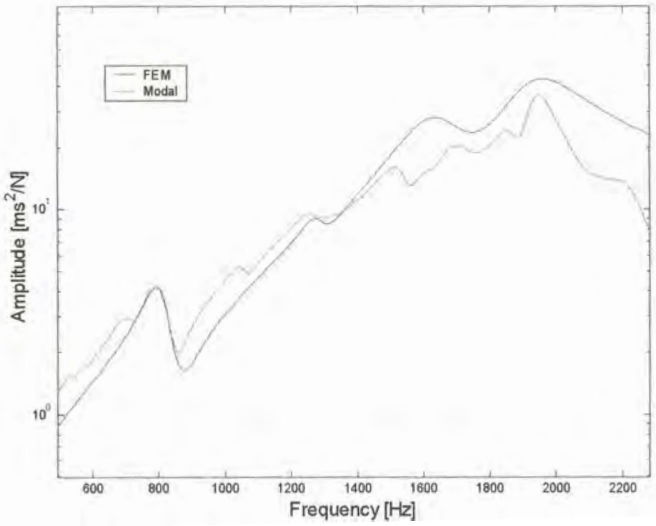

Figure 3.18 *FRF at the tip of the tool in the vertical direction*

The MAC test of the modes improved somewhat but still remains unacceptable. The result of the objective function value versus the number of function evaluations is presented in figure 3.20. Detail results of the model updating process are given in Appendix A.

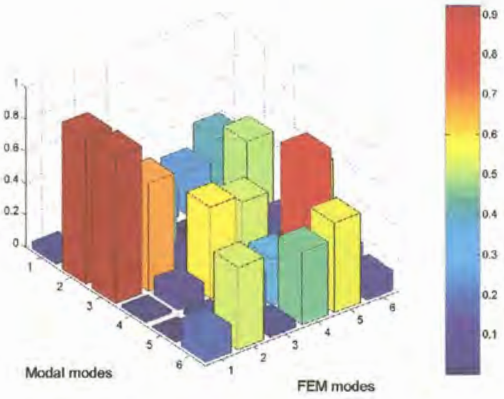

Figure 3.19 *MAC matrix results*

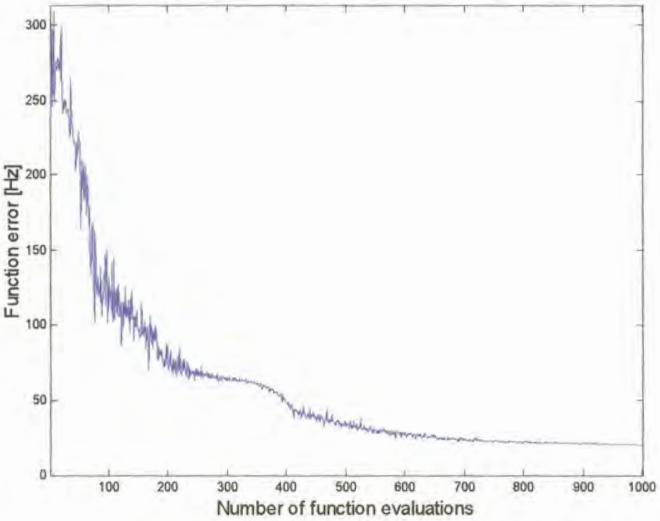

Figure 3.20 *The objective function value versus the number of function evaluations*

The poor performance of the FEM can be attributed to the inability of the spring element configuration to model the stiffness of the bolted connection between the tool holder and shank. Due to time constraints further investigation in to the use of finite element models were discontinued. The remaining research was conducted on an experimental modal model.

Chapter 4

Structural dynamic response reconstruction

The dynamic forces exerted on the cutting tool during the machining process have to be acquired in order to perform a mathematical simulation of the cutting process. The forces exerted on to the tool tip of a lathe during the machining operation are traditionally measured with a dynamometer. However, the introduction of a load sell will alter the dynamic properties of the system considered in chapter 3. The problem of accurate dynamic force measurement is experienced in a number of structural research fields. In most cases the structural response is measured under operational conditions and an inverse model is used to calculate the input forces from the measured response. However, it is not that simple to obtain an inverse model. Most of the dynamic models of structures in practice suffer from ill conditioning when the inverse of the model is calculated. Therefore, special techniques have to be implemented to obtain the dynamic inverse model and input forces.

4.1 Structural dynamic response reconstruction

The concept of dynamic force estimation from the measured structural response is referred to as Structural Dynamic Response Reconstruction (SDRR). The techniques of SDRR are widely used in the service load industry for the durability testing of structures. The work of Raath [43] presents a thorough overview of the concepts and issues involved in the SDRR process.

Raath [43] proposed a system identification approach that is used to construct an inverse model of the structure from measured process data. The approach produces a stable inverse model which can be used to estimate the input forces. Certain changes were incorporated in the implementation of the technique to accommodate the model structure of the tool holder and shank in the force calculation process.

4.2 Response measurement

The objective was set to determine the horizontal and vertical forces on the tool tip. Therefore the response of the tool holder was measured in the vertical and horizontal directions, to obtain a reference response to each cutting force. The measurements were taken near the tip of the tool during a machining operation. Figure 4.1 indicates the measurement positions on the holder. Further details on the response measurements and machining conditions are presented in tables 4.1(a) and (b).

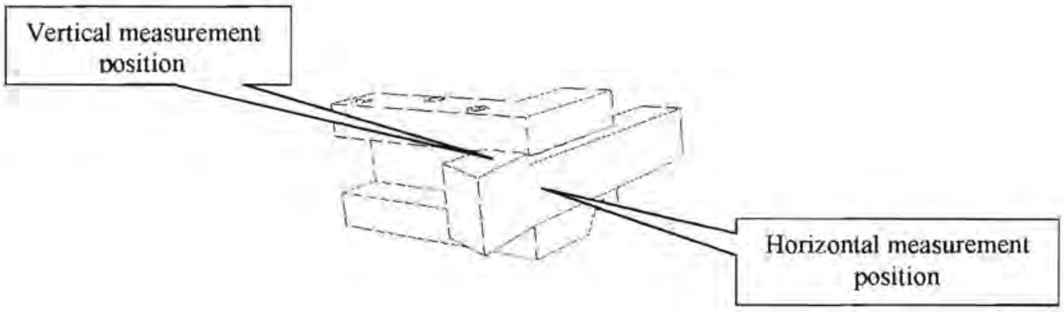

Figure 4.1 *Response measurement positions*

Table 4.1 (a) Details of the machining operation

Shaft length between the tailstock and the chuck	250 mm
Shaft diameter	40 mm
Shaft material	EN 8
Feed rate	0.2 mm/rev
Rotational speed	840 rpm
Cut depth	1.5 mm

Table 4.1 (b) Instrumentation used in the response measurement

Item number	Item	Model
1	DSP Siglab signal processor	20-42
2	Notebook computer	Intel 486 DX2-66
3	PCB miniature high frequency accelerometer	353B17
4	PCB battery powered signal conditioner	480E09

4.3.1 System identification overview

System identification techniques are used to build dynamic process models. The techniques construct transfer functions from measured input and output time signals. Only discrete time points are considered since the signals are recorded at discrete time instances. A schematic representation of the system is shown in figure 4.2.

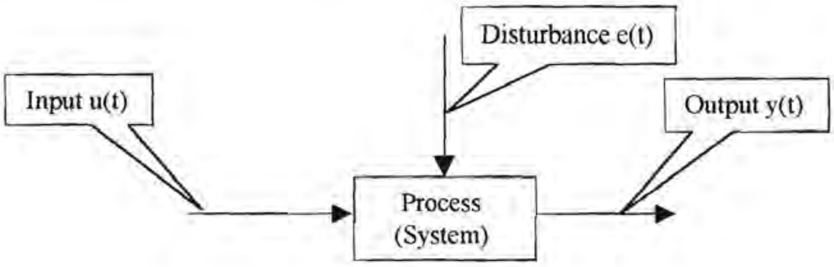

Figure 4.2 *System model*

A system identification model is described by a difference equation that relates the response of the system to the input of the system through a combination of past input and output instances. Several of these difference equations exist with their own unique properties, which accommodate the modelling of process noise and non-linearity.

The Auto Regressive model with eXternal input (ARX) is a linear model formulation known for its simplicity and ease of use. Raath proposed a convenient procedure to estimate a stable inverse model of a system that becomes ill conditioned when attempting to invert its dynamic model. The inverse ARX model facilitates the dynamic force calculation. The difference equation of a Single Input Single Output (SISO) ARX model is presented in equation 4.1.

$$\begin{gathered} y(t)+a_1 y(t-T)+\ldots+a_{na} y(t-na\times T)= \\ b_1 u(t-nk\times T)+\ldots+b_{nb} u(t-nk\times T-nb\times T+1)+e(t) \end{gathered} \tag{4.1}$$

with:

$u(t)$: System input
$y(t)$: System response
$e(t)$: Innovation term
a : Input parameter
b : Output parameter

na : Number of input parameters
nb : Number of output parameters
T : Sampling interval
nk : Time delay

The difference equation of the ARX model can be rewritten to produce the output at time t as a linear combination of past inputs and outputs.

$$\begin{gathered} y(t)=-a_1 y(t-T)-\ldots-a_{na} y(t-na\times T)+ \\ b_1 u(t-nk\times T)+\ldots+b_{nb} u(t-nk\times T-nb\times T+1)+e(t) \end{gathered} \tag{4.2}$$

The system identification process entails the estimation of parameter values, the number of parameters required and a time delay. The time delay refers to the time that passes until a change in the input influences the output. The parameters of the difference equation are estimated by a least squares estimate procedure. The innovation term represents the part of the output that cannot be determined from past and present data. Equation 4.3 represents the innovation term.

$$\begin{aligned} e(t) &= y(t) - \hat{y}(t) \\ e(t) &= y(t) - a_1 y(t-T) - \ldots - a_{na} y(t - na \times T) + \\ & b_1 u(t - nk \times T) + \ldots + b_{nb} u(t - nk \times T - nb \times T + 1) \end{aligned} \tag{4.3}$$

with:

$\hat{y}(t)$: Output estimate

The least squares parameter estimation procedure employs a loss function, which is minimised to obtain a set of equations. The loss function is presented in equation 4.4.

$$V_N = \frac{1}{N} \sum_{t=1}^{N} e^2(t) \tag{4.4}$$

with:

N : Number of sampled time intervals

The advantage of the least squares parameter estimation is the fact that the quadratic loss function can be minimised analytically with respect to the parameters as indicated by equation 4.5.

$$\frac{\partial V_n}{\partial a_1} = \ldots = \frac{\partial V_n}{\partial a_{na}} = \frac{\partial V_n}{\partial b_1} = \ldots = \frac{\partial V_n}{\partial b_{nb}} = 0 \tag{4.5}$$

The partial differentiation of the loss function with respect to the various parameters results in a number of equations that are solved simultaneously to obtain the various parameter values. The number of parameters and time delay required to simulate the system is obtained though inspection.

4.3.2 Reverse inverse model

A forward ARX model is estimated from the measured input output data of a system. The input and output data signals are swapped in the estimation of the inverse model. However the inverse model violates the concept of causality, meaning that the system is required to respond to input which has not been induced. Raath [43] proposed the estimation of a reverse inverse model that does not violate the concept of causality. Sufficient proof is given by Raath [43] to validate the reverse inverse technique.

The reverse inverse model estimation requires that the input output data signals are swapped and reversed in order. The reverse inverse technique that Raath [43] proposed is only valid on Multiple Input Single Output (MISO) models. A number of MISO models are estimated to accommodate Multiple Input Multiple Output models (MIMO).

4.3.3 Force computation with the reverse inverse ARX model technique

The first step in the force computation process is to obtain input output data from the forward model. A white noise signal is used to excite the forward model in order to obtain model response data. The input output data is filtered with a high pass filter to remove trends from the data. The data is filtered with a low pass filter to omit the higher frequency data where no response is observed in the structural response measurements.

The order of the data is reversed and the input output signals are swapped to estimate the reverse inverse ARX model parameters. Two thirds of the data is used to estimate the model. The remaining third of the response data is used to calculate the known force input with the reverse inverse ARX model. The reverse inverse ARX model is validated by the correlation between the identification force and the force calculated with the reverse inverse ARX model.

The forces calculated for a MIMO system are dependent on each other. A number of MISO reverse inverse ARX models are estimated to approximate the MIMO model. Each MISO model is used to calculate a force input of the forward model. The output of the various reverse inverse MISO models are fed back to the model inputs in a finite difference feedback loop to accommodate the influence of the various calculated forces on each other. Figure 4.3 shows a flow diagram of the finite difference feedback loop for a reverse inverse ARX model with two inputs and two outputs.

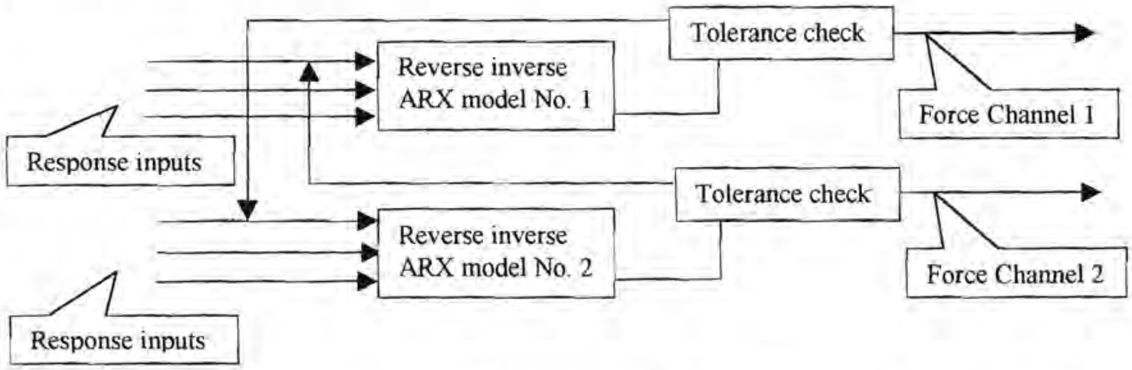

Figure 4.3 *MIMO reverse inverse ARX model with finite difference feedback loop*

Random force signals are initially used as inputs to the system to simulate the force input signals of the forward model. The force signals obtained from the previous simulation are used as the force input signals to the next simulation. The simulation loop is continued until the difference between the force signals used as the force inputs to the simulation and the force signals obtained from the simulation is less than a specified tolerance.

The number of input and output parameters as well as the time delay needs to be specified by the user in the model estimation process. Raath [43] states that the number of input parameters should equal the number of output parameters of the model. The number of parameters is referred to as the model order. No time delay is specified since most structural systems react fast enough to the system input.

An iteration process may improve the accuracy of the force estimation. The initial force estimate is used to excite the forward model in order to obtain the response to the initial force estimate. The difference between the response obtained from the simulation and the operational response is calculated and is used as an input to the reverse inverse model to compute the error in the force estimate. The error in the force is added to the previous force estimate and is used as an input to the forward simulation. The iteration response is compared to the measured response to determine whether the error in the response has diverged. The procedure is repeated as long as the error between the measured and iteration response converges. The error will diverge in certain cases. A diagram of the process is shown in figure 4.4.

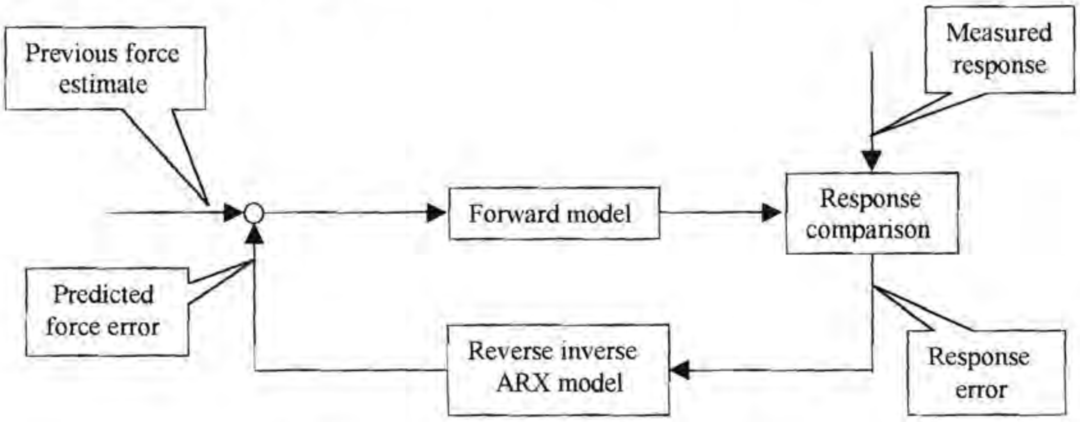

Figure 4.4 *Force iteration diagram*

4.3.4 Evaluation criteria

The error between the measured and calculated response signals is evaluated with a standard statistic correlation. However a more sensitive parameter was required to evaluate the iteration or simulation error. Therefore a new parameter or expression, in terms of the Root Mean Square (RMS) amplitude values of the signals, were defined to evaluate the results. The expression is defined in equation 4.6.

$$Simulation\ Error\,[\%] = \frac{MRA_{RMS} - CRA_{RMS}}{MRA_{RMS}} \times 100 \tag{4.6}$$

with:

MRA_{RMS} : RMS value of the Measured Response signal Amplitude

CRA_{RMS} : RMS value of the Calculated Response signal Amplitude

The reverse inverse ARX model is validated by a comparison between a white noise reference force and a calculated force as explained in section 4.3.3. Therefore equation 4.6 is redefined as equation 4.7 to accommodate the model validation process .

$$Model\ Error\,[\%] = \frac{RFA_{RMS} - CFA_{RMS}}{RFA_{RMS}} \times 100 \tag{4.7}$$

with:

RFA_{RMS} : RMS value of the Reference Force signal Amplitude

CFA_{RMS} : RMS value of the Calculated Force signal Amplitude

4.3.5 Force computation results with the reverse inverse ARX technique

A number of reverse inverse ARX models were estimated and validated to determine the optimal model order. The model order values were selected between one and eight. Figure 4.5 reveals the validation results of the various model order simulations. The combined model error is the sum of the vertical and horizontal model error. The optimal model was obtained at an order of four.

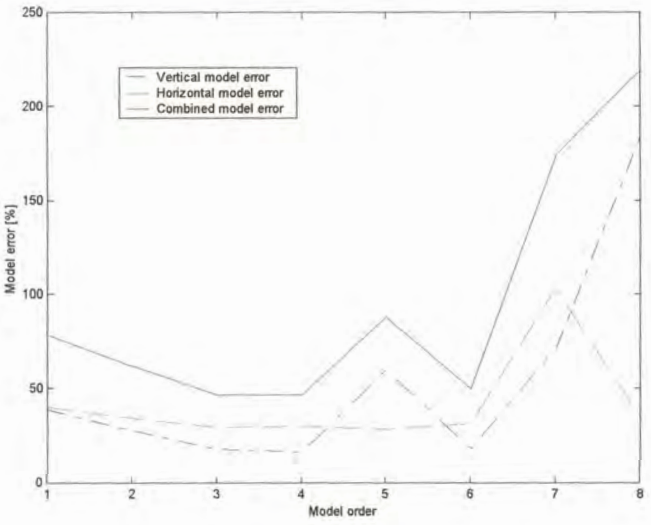

Figure 4.5 *Model order simulation results*

The simulation iteration results for the various models in terms of the simulation error is presented in figures 4.6 (a) and (b). The simulation error is defined by equation 4.6. The figures indicate that the iteration process was unsuccessful since the simulation error diverged in the simulation process. The more accurate the model the less the divergence.

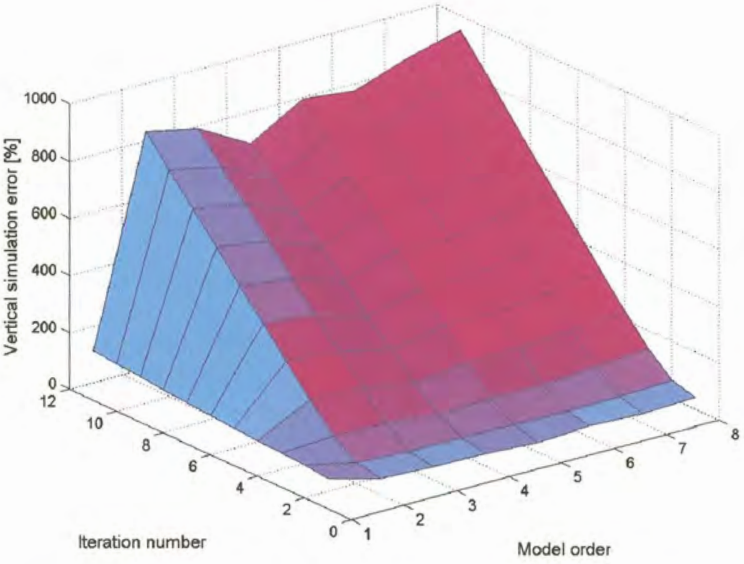

Figure 4.6 (a) *Vertical simulation error*

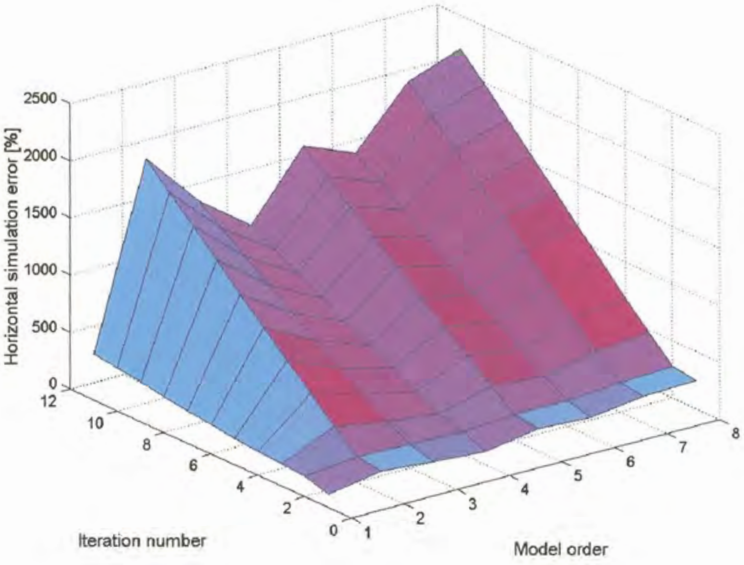

Figure 4.6 (b) *Horizontal simulation error*

Figures 4.7 (a) and (b) indicate the correlation coefficients for the simulations in figures 4.6 (a) and (b). The correlation coefficient does not indicate the reduction in the accuracy of the response reconstruction as well as the simulation error criteria during the simulation process.

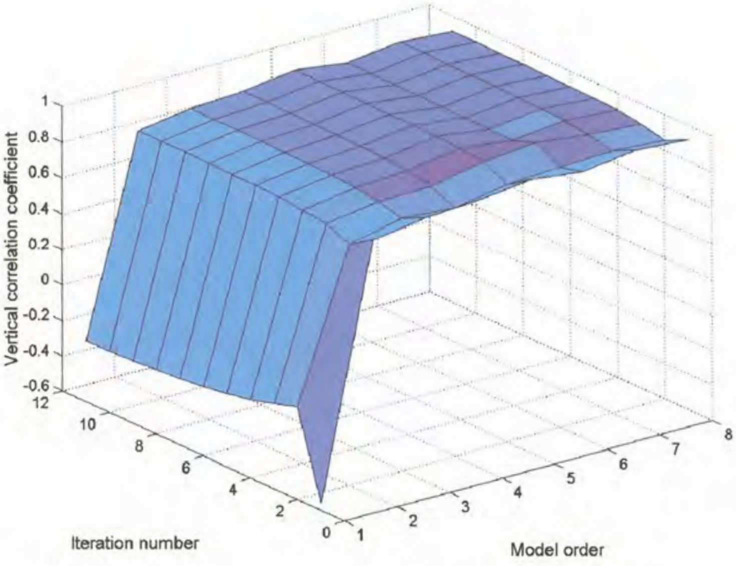

Figure 4.7(a) *Vertical correlation coefficient*

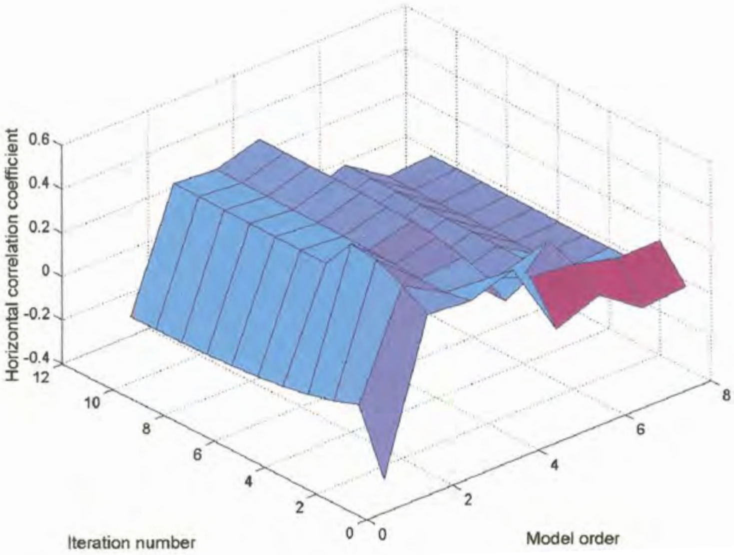

Figure 4.7 (b) *Horizontal correlation coefficient*

The optimum results of the SDRR process on the tool holder and shank is indicated in table 4.2.

Table 4.2 Optimum results of the SDRR process

Direction	Simulation Error [%]	Correlation coefficient [%]
Vertical	42.62	90.72
Horizontal	123.35	36.95

The optimum reconstructed response is compared to the measured response data in figures 4.8 (a) to (d). The time signals and Fast Fourier Transforms (FFT) of the signals are presented.

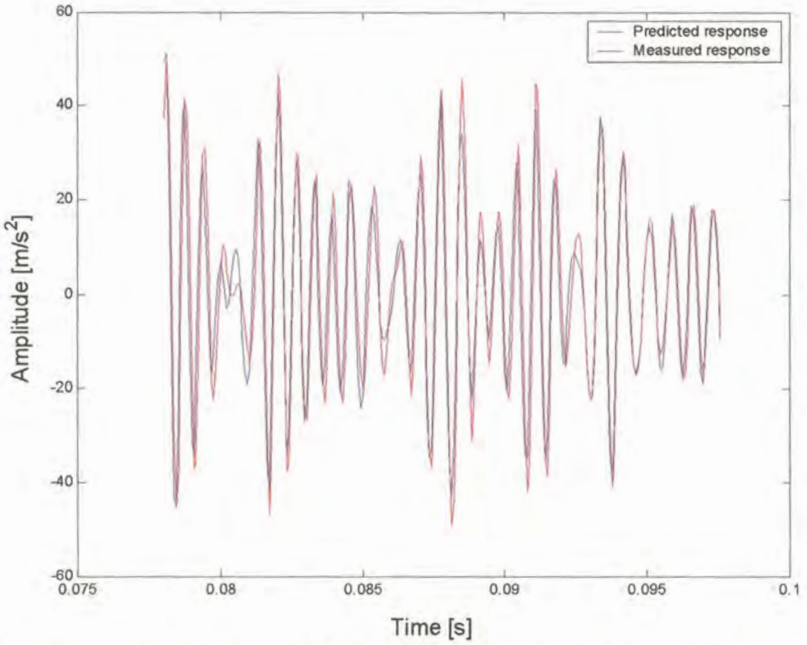

Figure 4.8 (a) *Comparison between the measured and predicted response in the vertical direction*

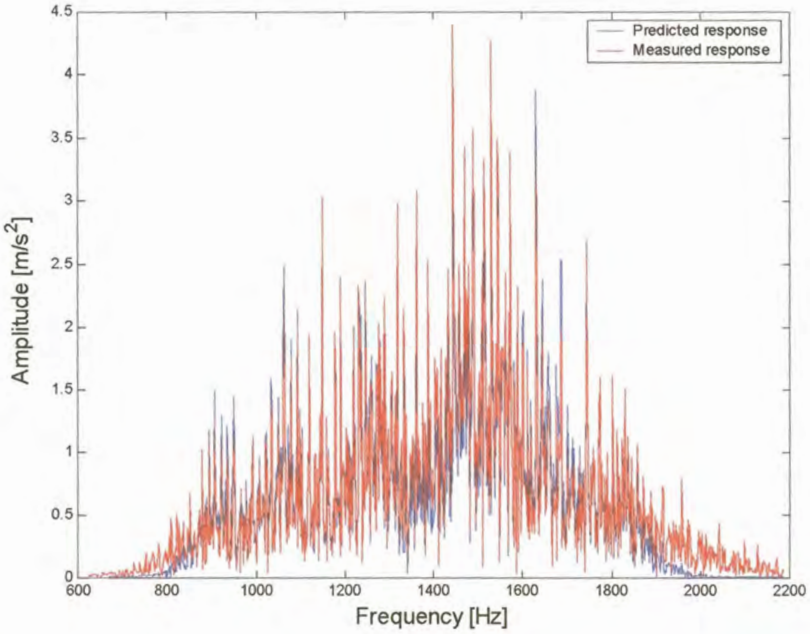

Figure 4.8 (b) *Comparison between the measured and predicted response in the vertical direction*

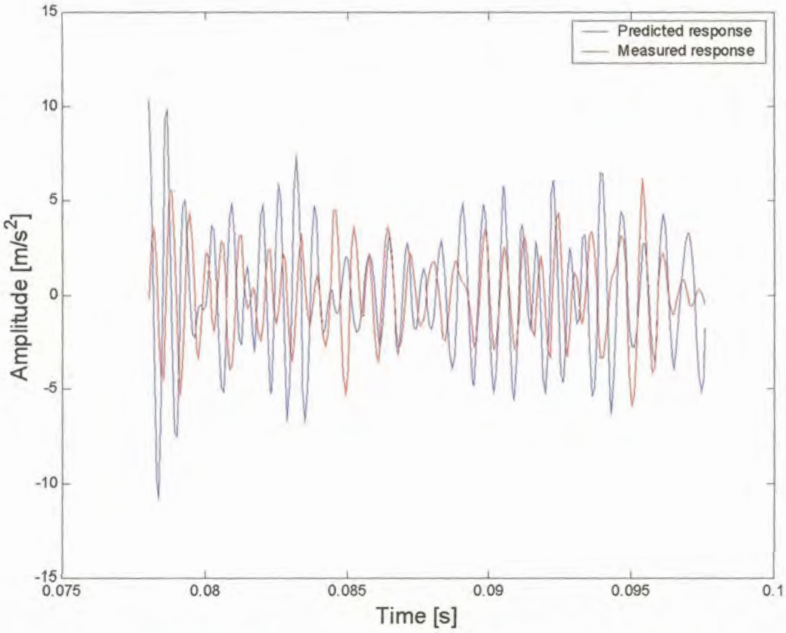

Figure 4.8 (c) *Comparison between the measured and predicted response in the horizontal direction*

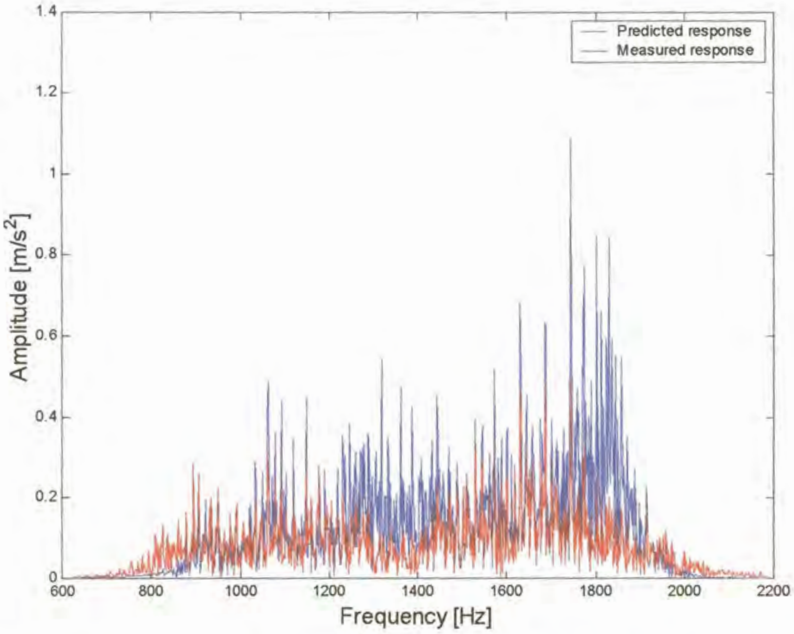

Figure 4.8 (d) *Comparison between the measured and predicted response in the horizontal direction*

The response of the structure in the vertical direction was reconstructed with a correlation of 90.72 percent. Figures 4.8 (a) and (b) indicate the accuracy with which the response was reconstructed. However, the response reconstruction in the horizontal direction was not as successful as the response reconstruction in the vertical direction. The amplitude of the predicted response is larger than the measured response as indicated by the FFT in figure 4.8 (d). The deviation between the two responses can be related to the accuracy with which the model describes the dynamic characteristics of the system. The modal model is merely a linear approximation of the real system. The main objective was to compute input forces that would reconstruct the response of the tool holder in the vertical direction since the research objective was set to attenuate the response in the vertical direction. Therefore the input forces will facilitate an accurate simulation of the cutting process in the vertical direction of the tool holder. The calculated force signals are presented in figures 4.9 a to d.

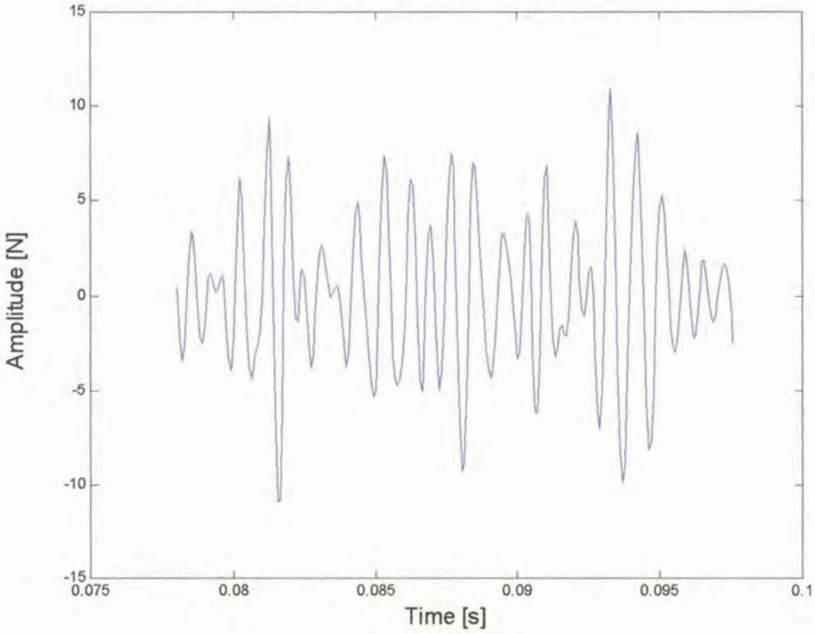

Figure 4.9 (a) *Vertical force signal*

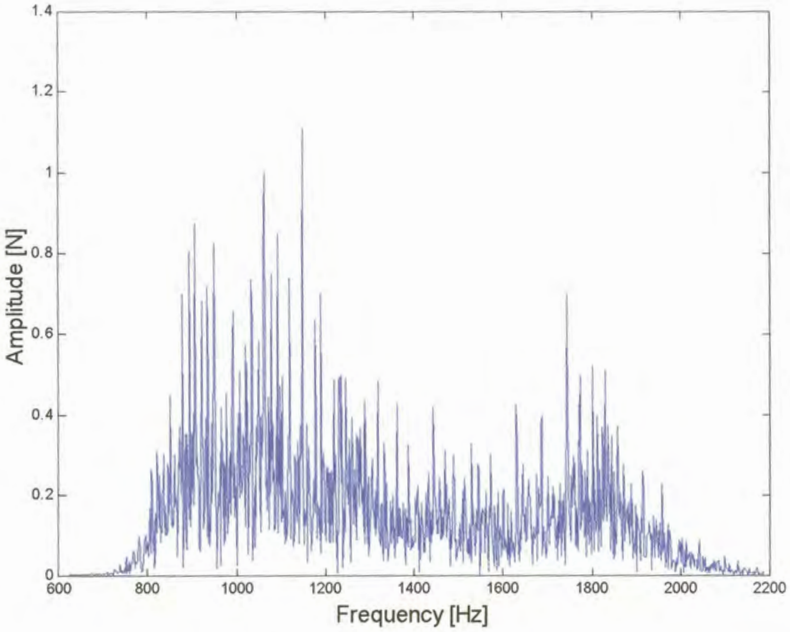

Figure 4.9 (b) *FFT of the vertical force signal*

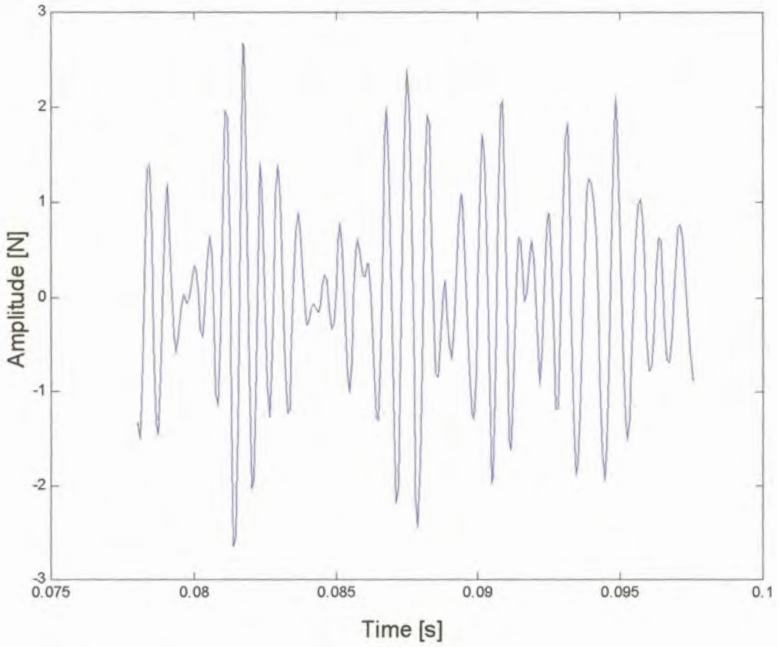

Figure 4.9 (c) *Horizontal force signal*

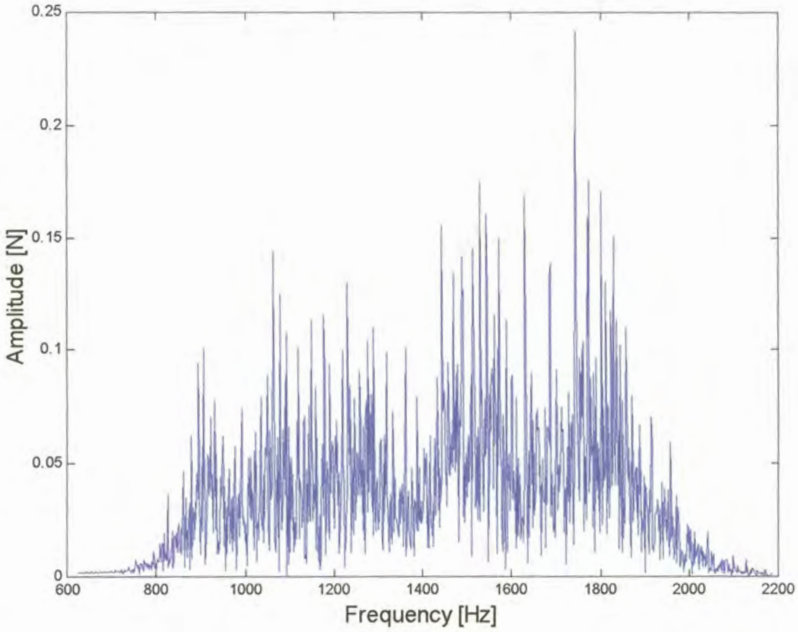

Figure 4.9 (d) *FFT of the horizontal force signal*

Chapter 5

Absorber implementation

The ODS and modal analysis indicated that the most deflection is situated at the tip of the tool in the vertical direction. Therefore the piezoelectric absorber was implemented near the tip of the tool holder in order to manipulate the dynamic stiffness of the cutting edge as much as possible.

A support structure is required to support the actuator in the vertical position. In chapter two the assumption of a rigid support was made since the stiffness of the steel tabletop far exceeded the stiffness of the aluminium beam. However, it is impossible to design a support structure that would fit on the tool changer which would not influence the dynamic characteristics of the system. The influence might improve the dynamic characteristics or it might not. Inevitably an optimal support design is required to ensure optimal performance of the damper in the system. The design of such a support is beyond the scope of the research since the aim is to establish whether the concept is viable.

The support structure is assumed to be rigid in the simulations. Therefore the influence of the support structure is omitted from the modelling process. The influence of the piezoelectric absorber can therefore be determined in isolation. The results obtained from the simulation represents the best scenario, which may be achieved by the implementation of the piezoelectric absorber near the tip of the tool.

5.1 State space modal model of the tool holder and shank

A state space modal model with three force inputs is required to model the structure and the damper. Two of the force inputs are used to simulate the cutting forces of the machining process, as determined in chapter four, while the third input is used in the feedback loop of the piezoelectric damper model. According to Balmės [40] a modal analysis with a collocated transfer function at each force input position is required to construct such a model. Therefore two sets of FRFs were measured with collocated transfer functions at the cutting force input positions, while the third set was measured with a collocated transfer function at the intended actuator position. The modal state space model is an average representation of the modal characteristics of the structure. Figures 5.1 (a) and (b) indicate the transfer function measurements at the collocated point were the actuator would be attached.

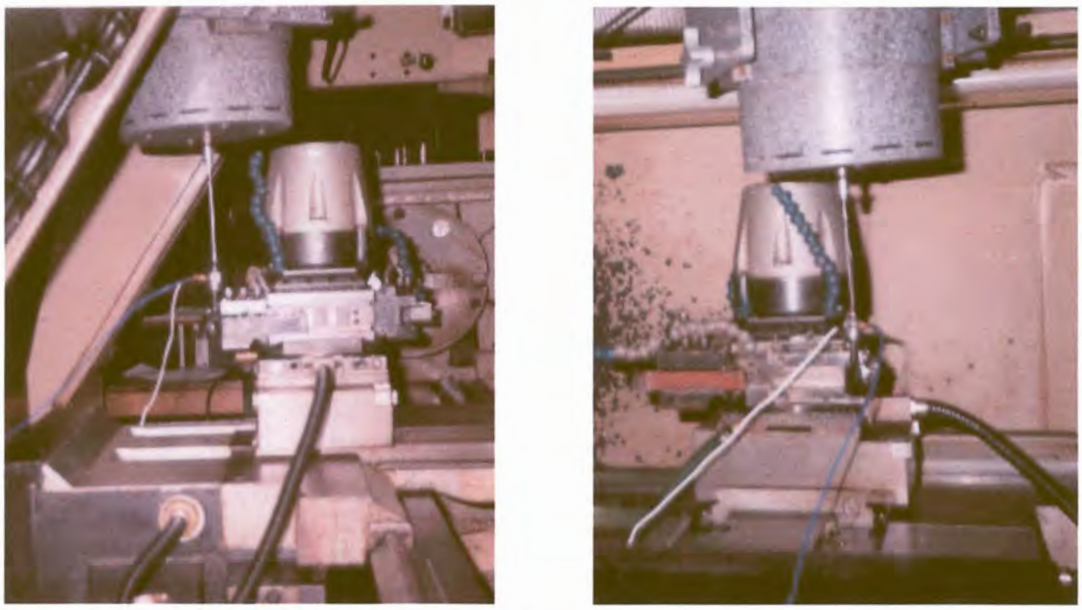

(a) (b)

Figure 5.1 *Transfer function measurement at the actuator attachment position*

5.2 Modelling Process

The objective of the modelling process is to implement and predict the influence of a variety of piezoelectric stack actuators, which are commercially available, as absorbers on the tool holder and shank. The properties of the actuators are substituted in to the feedback loop transfer function of the damper to simulate their behaviour. The optimal resistance and inductance values for the various shunt circuits are determined through inspection. The inspection is based on the transfer function manipulation between the force input and the response at the tool tip in the vertical direction. A schematic representation of the model is shown in figure 5.2.

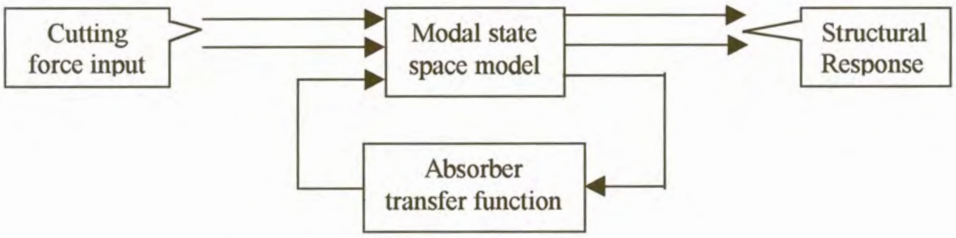

Figure 5.2 *Schematic diagram of the modelling process*

The static stiffness of the actuators is neglected since the open pole static stiffness of the actuators would influence the dynamic characteristics of the tool holder and shank.

To incorporate the open pole static stiffness would be inappropriate since the influence of the support structure is neglected to enable the validation of various dampers on the same structural system. A visual interpretation of the intended configuration is shown in figure 5.3. Note that the static stiffness K of the flow diagram presented in figure 2.1 is neglected in figure 5.3 since the value represents the open pole static stiffness of the actuator.

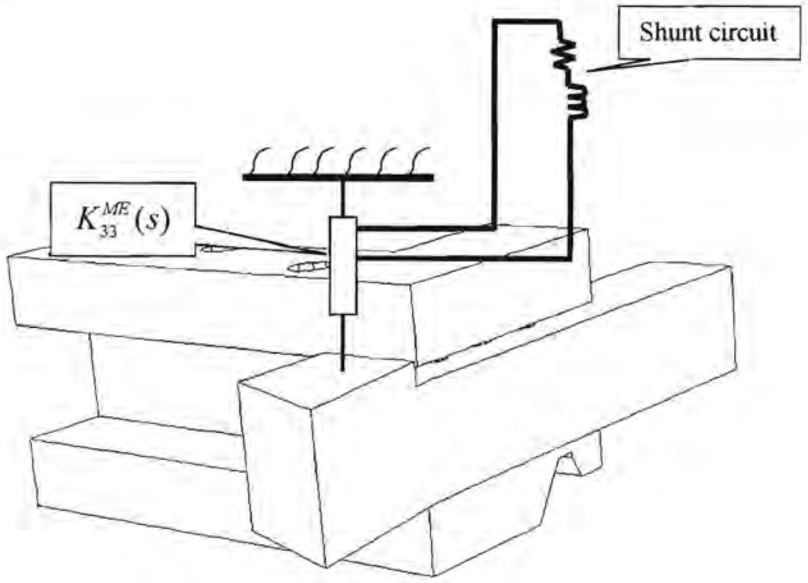

Figure 5.3 *Visual representation of the piezoelectric damper implementation on the tool holder and shank*

A selection of six actuators from Piezomechanik was simulated. The specifications of the actuators are tabled in table 5.1 (a) and (b).

Table 5.1 (a) Piezomechnik piezoelectric stack actuators

Actuator model	Diameter [m]	Number of layers	Layer thickness [m]	Capacitance [F]
500/5/5	0.005	14	3.5×10^{-4}	40×10^{-9}
500/5/15	0.005	42	3.5×10^{-4}	100×10^{-9}
500/5/25	0.005	72	3.5×10^{-4}	150×10^{-9}
500/10/5	0.01	14	3.5×10^{-4}	150×10^{-9}
500/10/15	0.01	42	3.5×10^{-4}	400×10^{-9}
500/10/25	0.01	72	3.5×10^{-4}	600×10^{-9}

Table 5.1 (b) Material properties of the Piezomechnik piezoelectric stack actuators

Relative dielectric constant	4000
Piezoelectric charge constant	500×10^{-12} [m/V]
Young's modulus	60×10^{9} [N/m^2]

5.3 FRF simulation results

The FRF simulation entailed the attenuation of three structural modes with the various piezoelectric absorbers formed with the actuator properties indicated in section 5.2. The three structural mode frequencies and damping levels are presented in table 5.2.

Table 5.2 Structural modes attenuated in the simulations

Mode frequency [Hz]	Damping [%]
1847.2	3.99
1639.9	10.91
1098.7	5.28

The frequency response of the 1639.9 Hz mode is increased when the absorber is tuned to the 1582.2 Hz mode. This can be related to the fact that the mode formed by the absorber is near the mode of the structure at 1639.9 Hz. However if the absorber is tuned to the mode at 1639.9 Hz, it attenuates the FRF at the 1582.2 Hz mode. Therefore the 1639.9 Hz mode was selected for the investigation. The amount of attenuation was measured between the original FRF value at 1582.2 Hz and the peak FRF value at the absorbed mode frequency. The amounts of attenuation for the other two structural modes are measured between the original FRF value of the mode and value of the mode when absorbed.

The results of the simulation are presented in tables 5.3 (a) to (c) and 5.4 (a) to (c). The FRFs for the simulations are displayed in figures 5.4 (a) to (c) and 5.5 (a) to (c).

Table 5.3 (a) Attenuation results at the 1847.2 Hz mode with the 500/5/- series piezoelectric actuators

Actuator	Resistance [Ω]	Inductance [H]	Attenuation [ms^2/N]	Attenuation [%]
500/5/5	80	0.197	2.95	11.68
500/5/15	40	0.099	3.9	15.44
500/5/25	35	0.0764	2.79	11.04

Table 5.3 (b) Attenuation results at the 1639.9 Hz mode with the 500/5/- series piezoelectric actuators

Actuator	Resistance [Ω]	Inductance [H]	Attenuation [ms^2/N]	Attenuation [%]
500/5/5	400	0.234	1.99	9.25
500/5/15	350	0.130	2.56	11.89
500/5/25	220	0.11	2.25	10.40

Table 5.3 (c) Attenuation results at the 1098.7 Hz mode with the 500/5/- series piezoelectric actuators

Actuator	Resistance [Ω]	Inductance [H]	Attenuation [ms^2/N]	Attenuation [%]
500/5/5	350	0.68	2.62	27.5
500/5/15	150	0.345	1.57	16.526
500/5/25	90	0.254	1.04	10.80

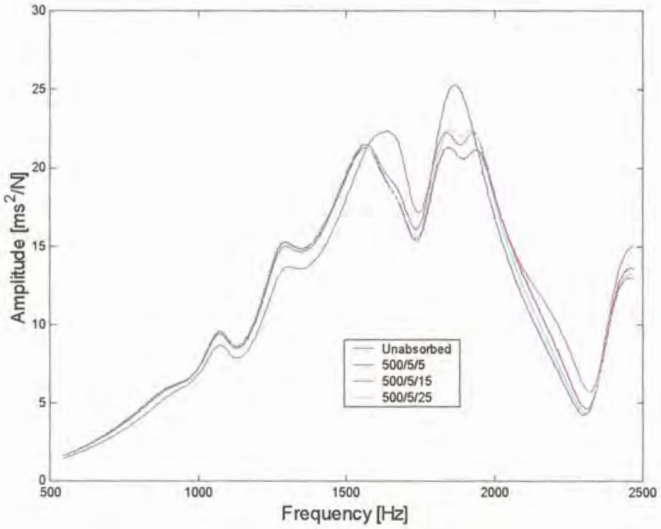

Figure 5.4 (a) *FRFs of the attenuation results at the 1847,2 Hz mode with the 500/5/- series piezoelectric actuators*

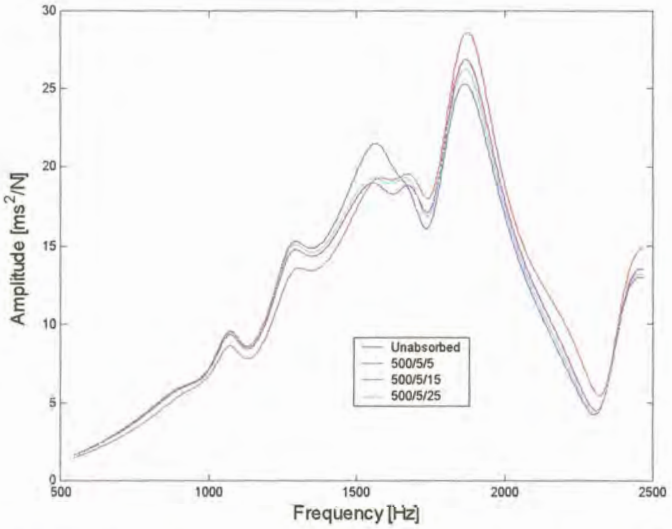

Figure 5.4 (b) *FRFs of the attenuation results at the 1639,9 Hz mode with the 500/5/- series piezoelectric actuators*

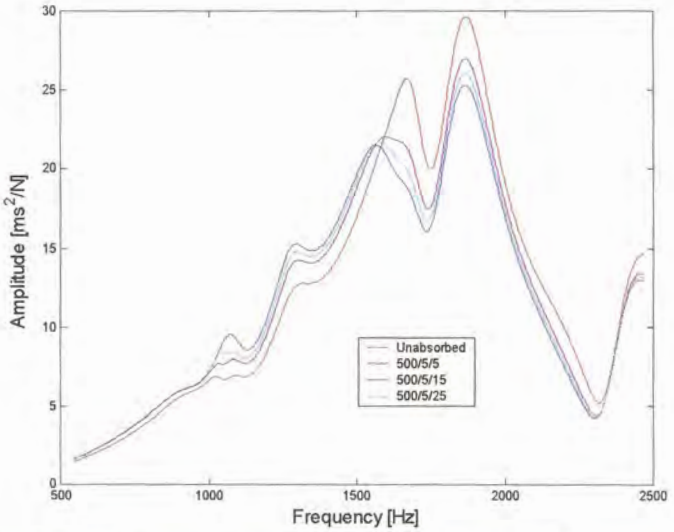

Figure 5.4 (c) *FRFs of the attenuation results at the 1098,7 Hz mode with the 500/5/- series piezoelectric actuators*

Table 5.4 (a) Attenuation results at the 1847.2 Hz mode with the 500/10/- series piezoelectric actuators

Actuator	**Resistance [Ω]**	**Inductance [H]**	**Attenuation [ms^2/N]**	**Attenuation [%]**
500/10/5	19	0.049	Unavailable	Unavailable
500/10/15	10	0.022	4.42	17.5
500/10/25	8	0.017	4.61	18.23

Table 5.4 (b) Attenuation results at the 1639.9 Hz mode with the 500/10/- series piezoelectric actuators

Actuator	**Resistance [Ω]**	**Inductance [H]**	**Attenuation [ms^2/N]**	**Attenuation [%]**
500/10/5	45	0.061	0.94	4.37
500/10/15	60	0.024	2.25	26.84
500/10/25	90	0.021	2.46	11.43

Table 5.4 (c) Attenuation results at the 1098.7 Hz mode with the 500/10/- series piezoelectric actuators

Actuator	**Resistance [Ω]**	**Inductance [H]**	**Attenuation [ms^2/N]**	**Attenuation [%]**
500/10/5	60	0.163	2.45	25.79
500/10/15	40	0.077	2.55	26.84
500/10/25	30	0.059	1.98	20.8

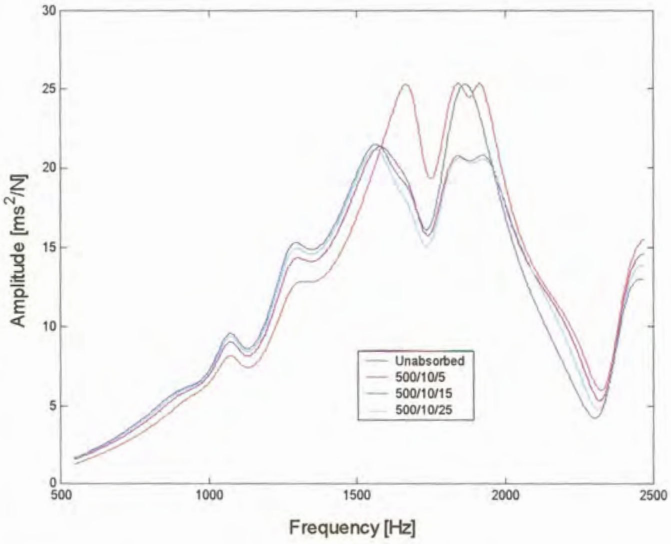

Figure 5.5 (a) *FRFs of the attenuation results at the 1847.2 Hz mode with the 500/10/-series piezoelectric actuators*

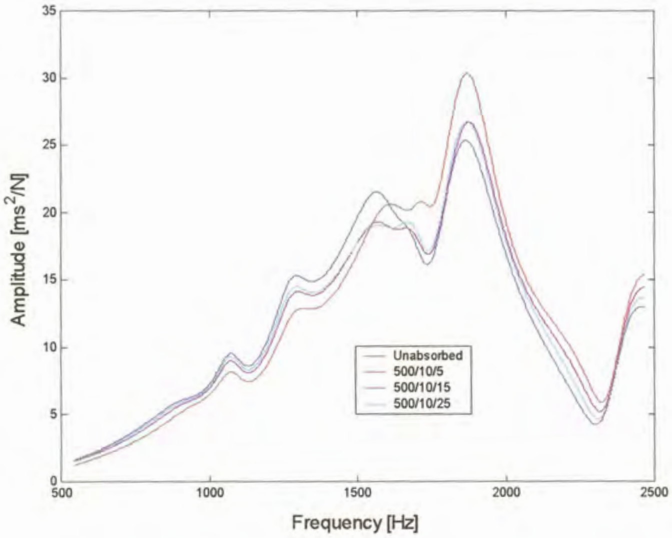

Figure 5.5 (b) *FRFs of the attenuation results at the 1639.9 Hz mode with the 500/10/-series piezoelectric actuators*

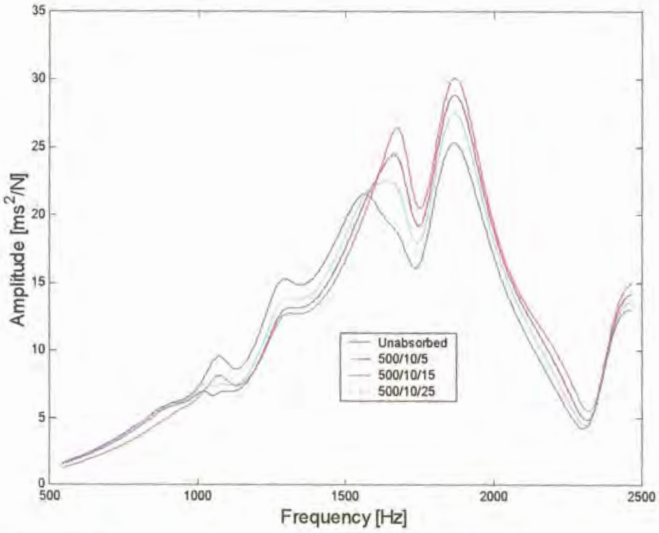

Figure 5.5 (c) *FRFs of the attenuation results at the 1098.7 Hz mode with the 500/10/-series piezoelectric actuators*

The shunt circuit of the piezoelectric absorber is tuned to a specific resonant frequency to absorb a structural mode. However, the resonant frequency of the shunt circuit is a function of the capacitance, inductance and resistance values of the circuit. Therefore, the resistance and inductance values are decreased when the capacitance value of the actuator is increased.

The absorber simulations with the 500/10/- series of actuators on the 1639.9 Hz mode indicated an increase in the resistance values as the capacitance value was increased. Therefore, the previous assumption is invalid when the absorber is influenced by structural modes with frequency values near the mode that is being absorbed.

The amount of damping in the absorber should be more than the amount of inherent damping present in the structural mode, in order to attenuate the structural mode. Resistance is the equivalent of damping in an electrical circuit, and therefore the resistance value of the shunt circuit is related to the inherent damping level present in the absorbed structural mode. The results of the simulations indicate a rise in the resistance values as the inherent mode damping increases.

The resistance values for the various actuator simulations on the three structural modes are shown in tables 5.5 (a) and (b).

Table 5.5 (a) Optimal resistance values for the various modes and actuators of the 500/5/- range

Actuator	Mode 1098.7 Hz Damping 3.99 % Resistance [Ω]	Mode 1639.9 Hz Damping 10.91 % Resistance [Ω]	Mode 1847.2 Hz Damping 5.28 % Resistance [Ω]
500/5/5	80	400	350
500/5/15	40	350	150
500/5/25	35	220	90

Table 5.5 (b) Optimal resistance values for the various modes and actuators of the 500/10/- range

Actuator	Mode 1098.7 Hz Damping 3.99 % Resistance [Ω]	Mode 1639.9 Hz Damping 10.91 % Resistance [Ω]	Mode 1847.2 Hz Damping 5.28 % Resistance [Ω]
500/10/5	19	45	60
500/10/15	10	60	40
500/10/25	8	90	30

Unfortunately, the addition of the piezoelectric absorber may cause an increase in the FRF values at other frequencies of the system. The extent of the phenomena seems to be related to the aspect ratio of the actuator. The definition of the actuator aspect ratio is presented in equation 5.1.

$$\text{Aspect ratio} = \frac{\text{Actuator diameter}}{\text{Actuator length}} \tag{5.1}$$

The increase in the FRF values is tabled in tables 5.6 (a) to (f), along with the aspect ratio of the actuators for the various simulations.

Table 5.6 (a) Increase in the FRF value at 1639.9 Hz, due to the attenuation of the mode at 1847.2 Hz with the 500/5/- series of actuators

Actuator	Capacitance [H]	Aspect ratio	Increase in the FRF value [ms^2/N]
500/5/5	40×10^{-9}	1	0.87
500/5/15	100×10^{-9}	0.33…	No increase
500/5/25	150×10^{-9}	0.2	No increase

Table 5.6 (b) Increase in the FRF value at 1847.2 Hz, due to the attenuation of the mode at 1639.9 Hz with the 500/5/- series of actuators

Actuator	Capacitance [H]	Aspect ratio	Increase in the FRF value [ms^2/N]
500/5/5	40×10^{-9}	1	3.36
500/5/15	100×10^{-9}	0.33…	1.57
500/5/25	150×10^{-9}	0.2	0.97

Table 5.6 (c) Increase in the FRF value at 1847.2 Hz, due to the attenuation of the mode at 1098.7 Hz with the 500/5/- series of actuators

Actuator	Capacitance [H]	Aspect ratio	Increase in the FRF value [ms^2/N]
500/5/5	40×10^{-9}	1	4.37
500/5/15	100×10^{-9}	0.33…	1.70
500/5/25	150×10^{-9}	0.2	0.79

Table 5.6 (d) Increase in the FRF value at 1639.9 Hz, due to the attenuation of the mode at 1847.2 Hz with the 500/10/- series of actuators

Actuator	Capacitance [H]	Aspect ratio	Increase in the FRF value [ms^2/N]
500/10/5	150×10^{-9}	2	3.78
500/10/15	400×10^{-9}	0.66…	No increase
500/10/25	600×10^{-9}	0.4	No increase

Table 5.6 (e) Increase in the FRF value at 1847.2 Hz, due to the attenuation of the mode at 1639.9 Hz with the 500/10/- series of actuators

Actuator	Capacitance [H]	Aspect ratio	Increase in the FRF value [ms^2/N]
500/10/5	150×10^{-9}	2	5.12
500/10/15	400×10^{-9}	0.66…	1.43
500/10/25	600×10^{-9}	0.4	1.46

Table 5.6 (f) Increase in the FRF value at 1847.2 Hz, due to the attenuation of the mode at 1098.7 Hz with the 500/10/- series of actuators

Actuator	Capacitance [H]	Aspect ratio	Increase in the FRF value [ms^2/N]
500/10/5	150×10^{-9}	2	4.79
500/10/15	400×10^{-9}	0.66…	3.57
500/10/25	600×10^{-9}	0.4	2.19

The increase in the FRF values, due to the absorber implementation, decreases as the aspect ratio of the actuator decreases. The 500/10/5 and the 500/5/25 actuators both have a capacitance value of 150×10^{-9} F but has aspect ratios of 2 and 0.2 respectively. Tables 5.6 (c) and (d) indicates that the 500/10/5-actuator ads a minimum of 3.78 ms^2/N to the FRF while the 500/5/25 ads a maximum of 0.97 ms^2/N. Therefore the FRF value increase is primarily related to the aspect ratio of the actuator and not the capacitance value of the actuator.

The attenuation versus capacitance results is presented in table 5.7 (a) and (b). The amount of attenuation increases and decreases when the capacitance value is increased. Therefore the assumption made in section 2.4.2 regarding the increase in attenuation with the increase in capacitance is incorrect for multiple degree of freedom systems.

Table 5.7 (a) Percentage attenuation for each mode versus the capacitance values of the 500/5/- actuator series

Actuator	**Capacitance [H]**	**Aspect ratio**	**Attenuate of the mode at 1847.2 Hz [%]**	**Attenuate of the mode at 1639.9 Hz [%]**	**Attenuate of the mode at 1098.7 Hz [%]**
500/5/5	40×10^{-9}	1	11.68	9.25	27.50
500/5/15	100×10^{-9}	0.33…	15.44	11.89	16.526
500/5/25	150×10^{-9}	0.2	11.04	10.4	10.8

Table 5.7 (b) Percentage attenuation for each mode versus the capacitance values of the 500/10/- actuator series

Actuator	**Capacitance [H]**	**Aspect ratio**	**Attenuate of the mode at 1847.2 Hz [%]**	**Attenuate of the mode at 1639.9 Hz [%]**	**Attenuate of the mode at 1098.7 Hz [%]**
500/10/5	150×10^{-9}	2	Unavailable	4.37	25.79
500/10/15	400×10^{-9}	0.66…	17.50	10.46	26.84
500/10/25	600×10^{-9}	0.4	18.23	11.43	20.80

The average attenuation results vary between ten and twenty percent and the amount of attenuation obtained by the implementation of the absorber is a function of the dynamic properties of the structure, the capacitance and aspect ratio of the actuator. A graphical representation of the results in tables 5.7 (a) and (b) is presented in figures 5.6 (a) and (b).

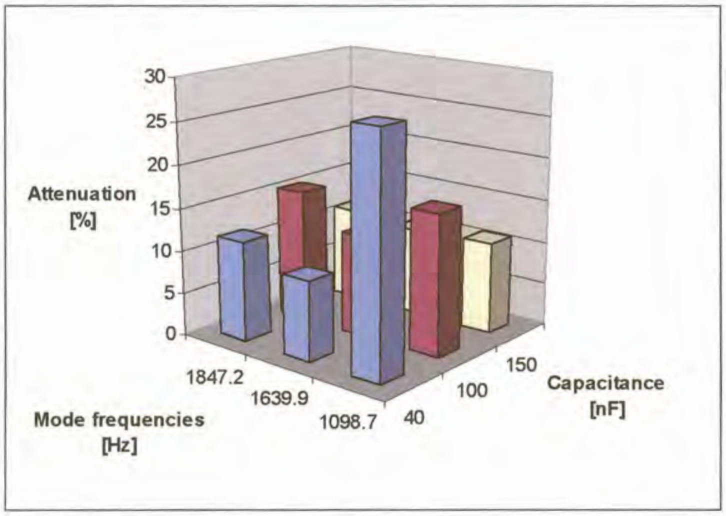

Figure 5.6 (a) *Attenuation results versus the capacitance values for the simulations with the 500/5/- series of actuators*

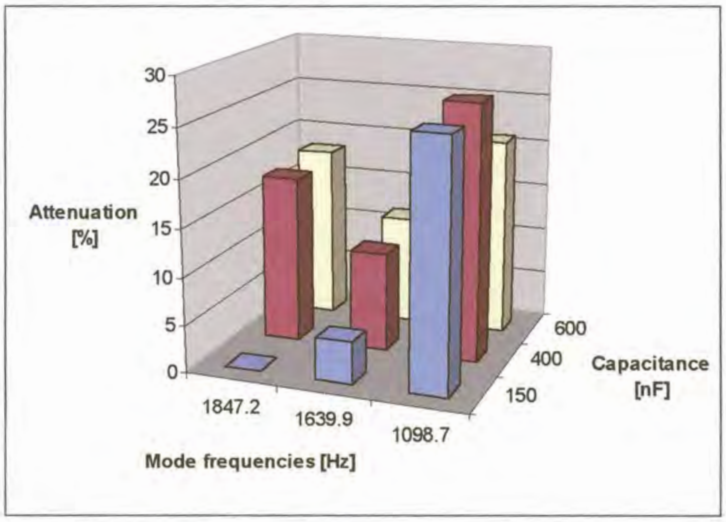

Figure 5.6 (b) *Attenuation results versus the capacitance values for the simulations with the 500/10/- series of actuators*

5.4 Cutting process simulation

The 500/5/15 piezoelectric actuator exhibits superior attenuation ability and minimal disturbance of the FRF over the remainder of the frequency bandwidth. Therefore the actuator was implemented in the cutting process simulation. The results of the simulations are presented in table 5.8 and figures 5.7 (a) to (f).

Table 5.8 Cutting process simulation results

Absorbed mode	FRF attenuation [%]	Amplitude attenuation of the time response signal [$\%_{RMS}$]
1847.2 Hz	15.44	2.93
1639.9 Hz	11.89	3.49
1098.7 Hz	16.53	5.51

Equation 5.2 expresses the amount of attenuation obtained in the cutting process simulation.

$$\text{Atenuation} = \frac{\text{Unabsorbed response amplitude}_{\text{RMS}} - \text{Absorbed response amplitude}_{\text{RMS}}}{\text{Unabsorbed response amplitude}_{\text{RMS}}} \times 100 \quad (5.2)$$

A small amount of attenuation is obtained in the cutting process since the structure is exposed to a wide band excitation of 1200 Hz during the cutting process and the absorber only attenuates an effective frequency bandwidth of approximately 50 to 100 Hz.

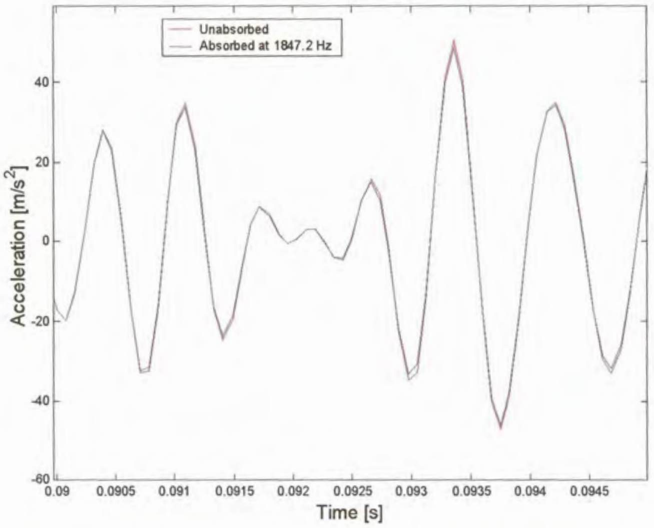

Figure 5.7 (a) *Response in the vertical direction at the tool tip during the cutting simulation with the 1847.2 Hz mode attenuated*

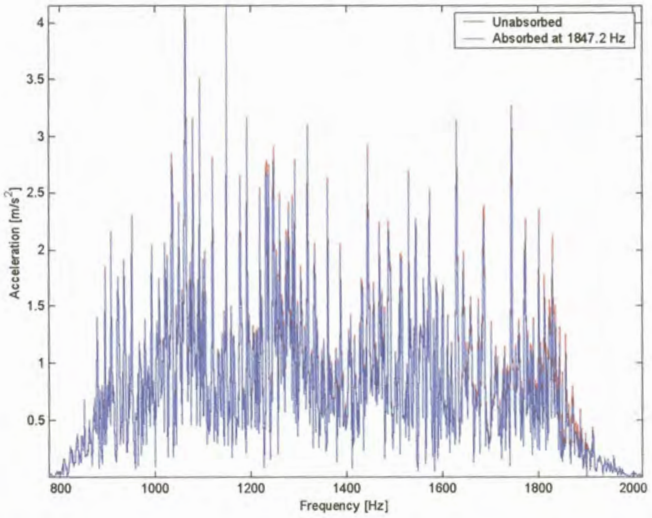

Figure 5.7 (b) *FFT of the response in the vertical direction at the tool tip during the cutting simulation with the 1847.2 Hz mode attenuated*

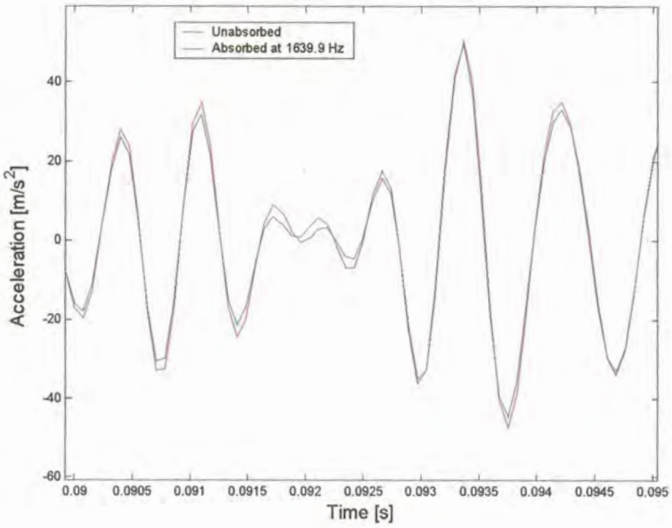

Figure 5.7 (c) *Response in the vertical direction at the tool tip during the cutting simulation with the 1639.9 Hz mode attenuated*

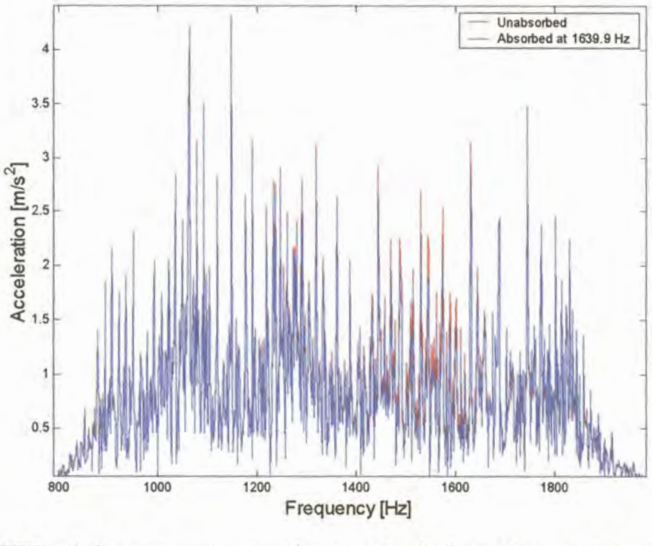

Figure 5.7 (d) *FFT of the response in the vertical direction at the tool tip during the cutting simulation with the 1639.9 Hz mode attenuated*

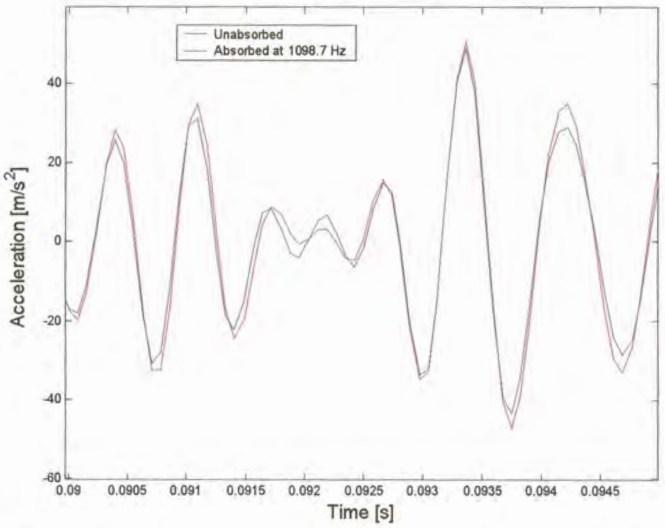

Figure 5.7 (e) *Response in the vertical direction at the tool tip during the cutting simulation with the 1098.7 Hz mode attenuated*

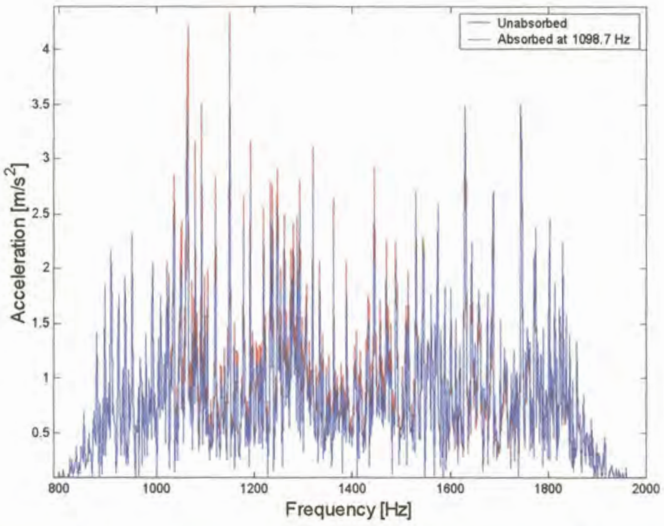

Figure 5.7 (f) *FFT of the response in the vertical direction at the tool tip during the cutting simulation with the 1098.7 Hz mode attenuated*

5.5 Cutting process simulation with multiple absorbers

The objective of the multiple absorber implementation is to increase the effective bandwidth of attenuation. Three absorbers were implemented at the absorber connection point to attenuate the three modes simultaneously, in a bid to improve the attenuation results. Slight changes to the shunt circuit inductance values had to be made since the absorbers influenced one another.

The FRF result of the multiple absorber implementation is displayed in figure 5.8 (a). The amount of attenuation obtained by the absorber implementation at the 1847.2 Hz mode decreased considerably. However the bandwidth of effective attenuation was increased between the 1098.7 Hz and 1639.9 Hz modes.

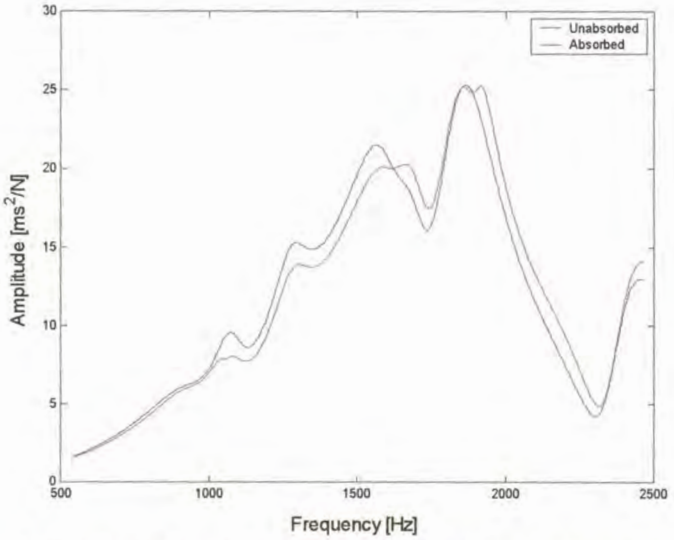

Figure 5.8 (a) *FRF result of the multiple absorber implementation*

The multiple absorber implementation increased the amount of attenuation during the cutting process to 8.76 $\%_{RMS}$. Figures 5.8 (b) and (c) reveal the results obtained by the cutting process.

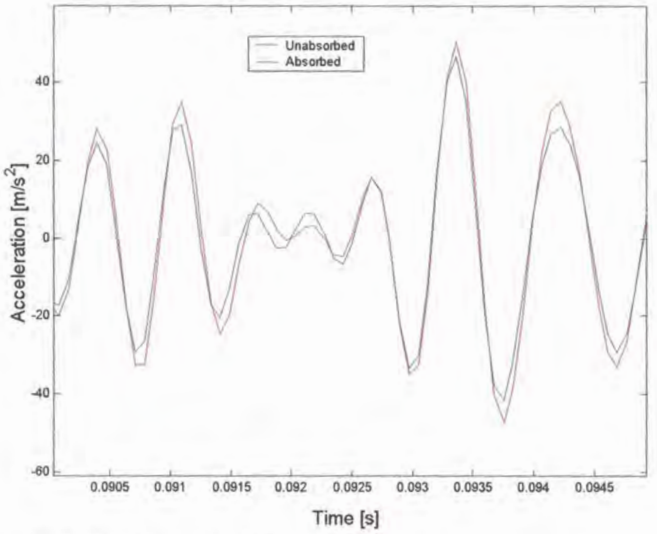

Figure 5.8 (b) Result *of the multiple absorber implementation*

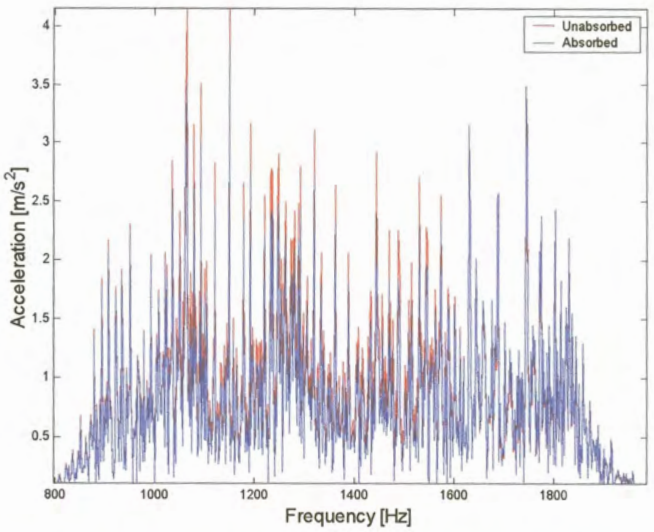

Figure 5.8 (c) R*esult of the multiple absorber implementation*

The attenuation results did not improve as much as expected due to the influence the dampers have on one another.

5.6 Experimental verification

The assembly of the structural support and the piezoelectric stack actuator is presented in figures 5.9 (a) and (b).

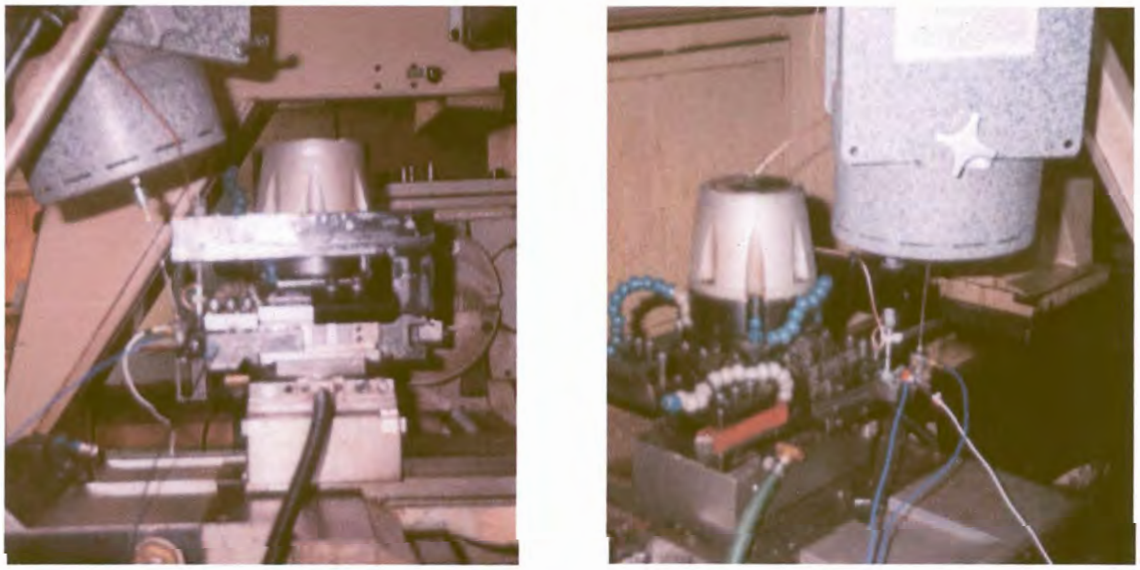

(a) (b)

Figure 5.9 *Piezoelectric absorber implementation on the tool holder for the experimental verification*

A 500/5/15 piezoelectric stack actuator from piezomechanik was implemented in the experimental verification of the piezoelectric absorber on the lathe. The addition of the structural support and piezoelectric stack actuator influenced the dynamic characteristics of the system. A modal analysis was conducted to determine the new modal properties of the system as indicated in figures 5.10 (a) to (e). The mode frequencies of the new system are tabled in table 5.9.

Table 5.9 Mode properties of the system with the structural support in the vertical direction

Mode frequency [Hz]	Damping value [%]
813.2	5.71
1274.6	4.38
1531.5	2.68
1735.8	8.22
1878.8	3.62
1930.8	2.73

The piezoelectric absorber was tuned to absorb the 813.2 Hz, 1735.8 Hz and 1930.8 Hz modes during the experimental verification. Figures 5.10 (a) to (e) displays the point inertance at the tip of the tool holder that were measured to determine the influence of the absorber. The results of the experimental verification are tabled in table 5.10.

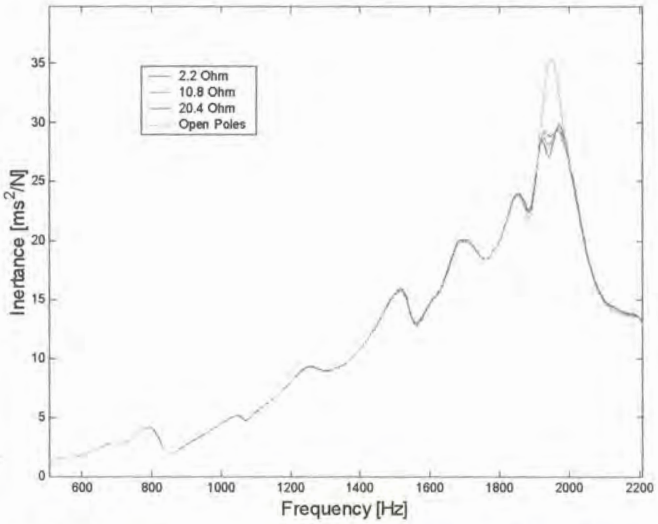

Figure 5.10 (a) Experimental absorption results at the 1930.8 Hz mode

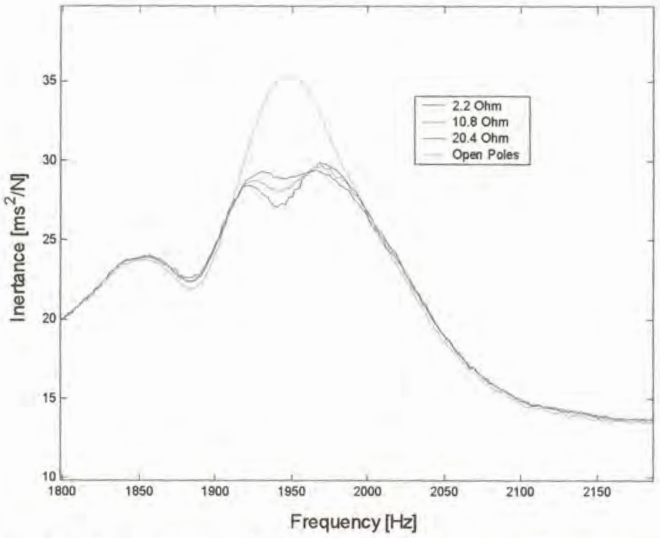

Figure 5.10 (b) Experimental absorption results at the 1930.8 Hz mode

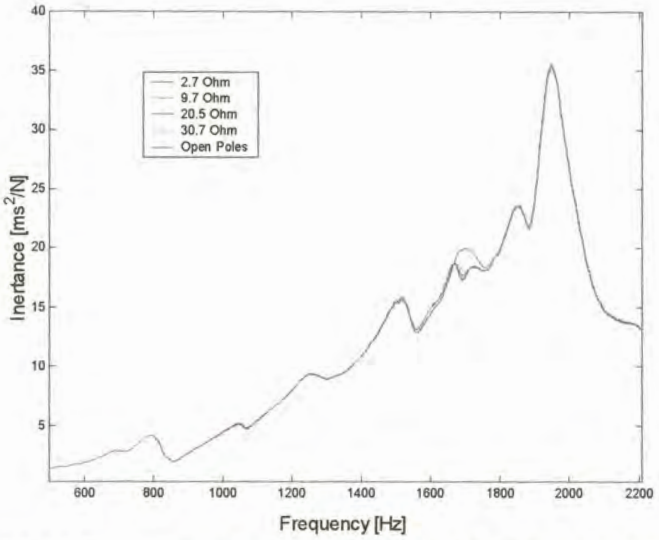

Figure 5.10 (c) Experimental absorption results at the 1735.8 Hz mode

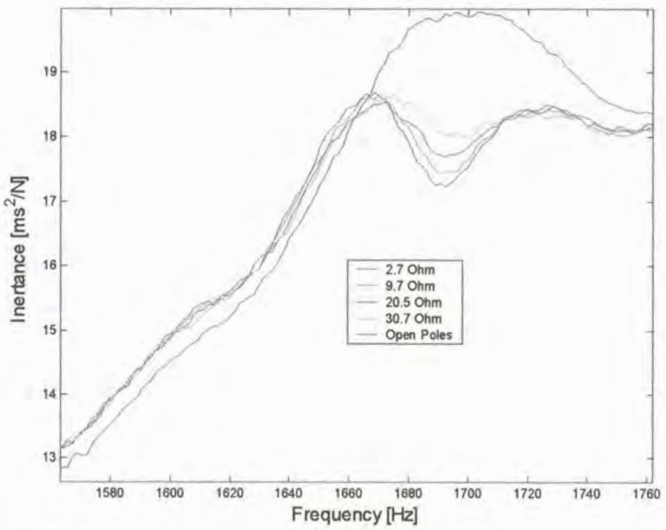

Figure 5.10 (d) Experimental absorption results at the 1735.8 Hz mode

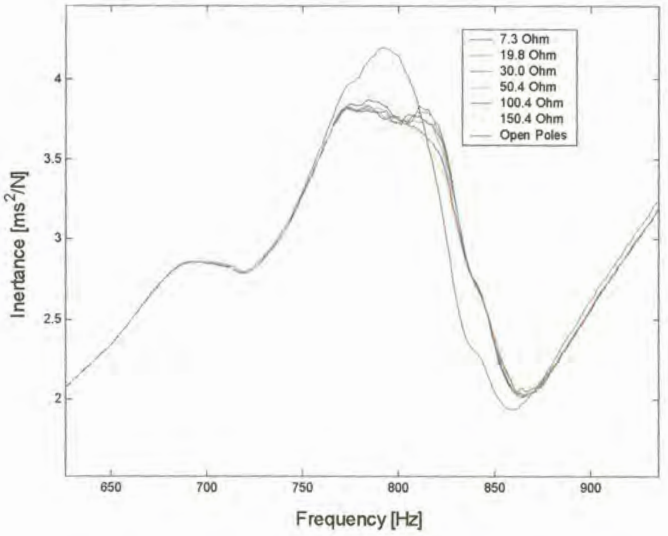

Figure 5.10 (e) Experimental absorption results at the 813.2 Hz mode

Table 5.10 Results of the experimental verification

Mode frequency[Hz]	**Resistance [Ω]**	**Inductance [H]**	**Attenuation [ms^2/N]**	**Attenuation [%]**
813.2	7.3	0.8734	0.37	8.77
1735.8	20.5	0.2221	1.41	7.05
1930.8	20.4	0.1673	6.12	17.23

The experimental implementation of the absorber on the tool holder was successful and the magnitudes of the attenuation results were within the regions predicted by the mathematical simulations. However, the average inductance values required in the shunt circuit of the absorber were higher than the values required in the mathematical simulation since the real capacitance value of the actuator is approximately 74×10^{-9} F. Therefore higher inductance values were required to compensate for the loss in capacitance in order to obtain the correct resonance frequency for the piezoelectric absorber.

Minimal disturbance of the FRF bandwidth was noted in the experimental verification results due to the addition of the support structure and static stiffness of the actuator which influenced the system.

Table 5.11 indicates the optimal shunt resistance versus the damping value of the three structural modes. The experimental results do not verify the conclusion made in section 5.4 about the relationship between the required resistance and the level of inherent damping of the structural mode that is absorbed. The occurrence can also be related to the addition of the support structure and static stiffness of the actuator.

Table 5.11 Mode damping versus the shunt resistance results

Mode frequency[Hz]	**Resistance [Ω]**	**Damping value [%]**
813.2	7.3	5.71
1735.8	20.5	8.22
1930.8	20.4	2.73

Unfortunately the influence of the piezoelectric absorber could not be verified experimentally during the cutting process since no measurements could be made with 5 percent repeatability.

Chapter 6

Conclusion and recommendations for future research

6.1 Conclusion

6.1.1 Analysis procedure

An analysis procedure was developed to investigate the implementation of a shunted piezoelectric actuator that will attenuate the vibrations experienced by a machine tool structure during a machining operation.

The behaviour of the machine tool structure under machining conditions was determined with an ODS analysis which assisted the decision of actuator positioning on the structure. The repeatability of the transmissibility measurements taken for the ODS analysis was superior to normal acceleration measurements on the structure since they are less susceptible to the variation in the excitation force of the cutting process.

A modal analysis was conducted on the structure to determine the dynamic properties of the system and to construct a modal state space model, which is used in the simulation processes. The mode shapes of the modal analysis were used to verify the observations made in the ODS analysis.

A transfer function of the shunted piezoelectric actuator was used in a feedback loop to the modal state space model to simulate the influence of the passively shunted piezoelectric actuator on the structure. The mathematical simulation was based on the assumption that the support structure is rigid. The assumption isolates the system from the influences of the support structure and therefore the influence of the shunted piezoelectric actuators could be determined on a structure with the same dynamic properties.

The original FRF was compared to the compensated FRF at the tool tip to select the optimal actuator and to determine the optimal shunt circuit. The machine tool structure is subjected to wide band excitation during the machining process and therefore the system has to be simulated under machining conditions to determine the effectiveness of the shunted piezoelectric device. The input forces to the simulation process were determined through the SDRR technique proposed by Raath [43].

6.1.2 Mathematical model of the shunted piezoelectric actuator

A mathematical model for a shunted piezoelectric stack actuator was derived and verified experimentally on an aluminium-cantilevered beam. Acceptable correlation was obtained between the mathematical and experimental results. However the addition of the actuator to a structure alters the dynamic properties of the system which makes it difficult to predict the behaviour of the system prior to experimental verification.

The manufacturer's specification on the actuator's rated capacitance value is unfortunately not as accurate as required, and the value has to be obtained experimentally.

The mathematical model of the shunted piezoelectric actuator was developed into a transfer function format in order to incorporate the model with a state space model representation of several different structures. Therefore, no mathematical formulas were derived to estimate the required shunt circuit values, since they are dependent on the structural properties.

6.1.3 FEM of the machine tool structure

A FEM of the structure has to be updated by experimental modal analysis, in order to ensure its integrity. It is necessary to match all of the mode frequencies and shapes for the frequency bandwidth of concern. In some of the published research on machine tool structures, merely a few of the mode frequencies are matched, which is insufficient proof of the FEM's integrity and accuracy. However the reason for the attempts are obvious, since it is extremely difficult to update the multiple modes of the model.

Several attempts were made to model the tool holder and shank of the diplomatic tool changer. Unfortunately, none of the attempts succeeded in passing the MAC test. The failure is caused by the inability to model the interaction between the various connections of the model. The modal model is used in the mathematical simulations due to the inaccuracies of the FEM.

6.1.4 Results of the implementation of the shunted piezoelectric stack actuator the tool holder

A piezoelectric absorber was implemented on the tool holder to attenuate the vibration at the tool tip, since it was more effective than the resistive shunt. The implementation was successful and 17 percent attenuation was obtained at one of the modes during the experimental verification. Attenuation levels of up to 27 percent were obtained with the mathematical simulations.

Due to the wide band excitation, the amount of attenuation obtained during the machining process is reduced to levels between 2 and 5 percent RMS, when comparing the time response to the uncompensated time response. Multiple piezoelectric absorbers were implemented on the tool holder to improve the attenuation results of the cutting process by increasing the effective bandwidth of attenuation.

However the absorbers influenced each other and only 8.76 percent attenuation was obtained. A point inertance was measured at the tool tip to verify the influence of the piezoelectric absorber on the tool holder experimentally. Unfortunately, the influence of the piezoelectric absorber could not be verified experimentally during the cutting process, since no measurements could be made with 5 percent repeatability.

Shunted piezoelectric stack actuators can attenuate machine tool vibration. However, further development is required to improve the attenuation performance during the machining operation, in order to make the concept feasible.

6.2 Recommendations for future research

6.2.1 FEM of the machine tool structure

The accuracy of the finite element model must be improved to enable the development of a design procedure for optimal support structures. The complex interaction of the systems bolted connections is an area of concern and new innovative ideas are required to model the connections.

6.2.2 Multiple resonant shunt circuits

Browning and Wynn [10] developed a wide band passive electronic shunt circuit with which they attenuated twelve modes of a plate structure. It might be possible to manipulate the FRF at the tool tip with such a wide band shunt circuit to improve the attenuation results during the machining process.

6.2.3 Leverage implementation on the piezoelectric absorber

A number of machining operations was performed during the attempts to quantify the influence of the piezoelectric absorber on the tool tip. During the different operations no significant change in the shunt resistor's temperature was observed. The observation raises the question on whether the piezoelectric damper is optimally utilised. The amount of strain applied by the displacement of the tool holder might not be enough to fully utilise the energy capturing ability of the piezoelectric stack actuator. The addition of a leverage system might improve the utilisation of the shunted piezoelectric actuator's energy capturing ability.

6.2.4 Behaviour of the piezoelectric absorber under load conditions

The model developed in the research is merely a linear approximation of the passively shunted piezoelectric actuator's behaviour. The true behaviour of the system under load conditions and the boundaries of the linear approximation are unknown. The behaviour has to be determined before an effective leverage system can be designed.

References

[1] Døssing O. & Staker Operational deflection shapes. Background, measurement and application. *Proceedings of the 5th International Modal Analysis Conference*. 1987.

[2] Smith C. A. & Anderson E. H. Passive damping by smart materials: analysis and practical limitations *SPIE Vol. 2445* pp. 136-148.

[3] Forward R. L. Electronic damping of vibration in optical structures. *Journal of Applied Optics*. 18(5) pp. 690-697.

[4] Hagood N. W. & Von Flotow A Damping of structural vibration with piezoelectric materials and passive electrical networks. *Journal of Sound and Vibration*. 146(2) pp. 243- 268 1991.

[5] Davis C. L. & Lesieutre G. A. A modal strain energy approach to the prediction of resistively shunted piezoceramic damping. *Journal of Sound and Vibration*. 184(1) pp. 129-139 1995.

[6] Lesieutre G. A. Vibration damping and control using shunted piezoelectric materials. *Shock and Vibration Digest*. (30)3 pp. 187-195 1998.

[7] Davis C. L. & Lesieutre G. A. An actively-tuned solid state piezoelectric vibration absorber. *Proceedings of SPIE-Smart structures and materials, Passive damping and isolation*. San Diego CA. 1998.

[8] Warkentin D. J. & Hagood N. W. Nonlinear piezoelectric shunting for structural damping. *Proceedings of SPIE-Smart structures and materials, Smart structures and integrated system*. San Diego CA. pp.747-757 1998.

[9] Inman D. J. Smart structural solutions to vibration problems. *ISMA23 International Conference on Noise and Vibration Engineering. Catholic University of Leaven Belgium*. September 16-18 1998.

[10] Browning D. R. & Wynn W. D. Multiple-mode piezoelectric passive damping experiments for an elastic plates. *Proceedings of the 11th International Modal Analysis Conference Kissimmee*. pp. 1520-1526 1993.

[11] Edburg D. L. Bicos A. S. Fuller C. M. & Tracy J. J. Theoretical and experimental studies of a truss incorporating active members. *Journal of Intelligent Material Systems and Structures*. 3(2) pp. 333-347 1992.

[12] Wojslaw C. F. & Moustakas E. A. *Operational amplifiers the devices and their applications*. John Wiley and sons. *ISBN 0-471-80646-3*. pp. 161-167 1985.

[13] Moschytz G. S. *Linear integrated network design.* Bell telephone laboratories incorporated ISBN 0-442-25582-9. pp. 597-609 1975.

[14] Mulcahey B. & Spangler R. L. Piezos tame tough vibrations. *Machine Design.* pp. 60-63 February 19 1998.

[15] Active Control Experts Inc. Web address http://ACX.com.

[16] Smit D.F. A piezo-ceramic actuator for active vibration control: Design, modeling and control strategies. Masters dissertation. *Department of Mechanical and Aeronautical Engineering of the Faculty of Engineering, University of Pretoria.* 1997.

[17] Sumali H. & Cudney H. H. An active engine mount with a piezoelectric stack actuator. *Collection of technical papers – Proceedings of the AIAA/ASME/AHS/ASC Structures Structural Dynamics and Materials Conference.* pp. 1233-1241 1994.

[18] Sumali H. & Cudney H. H. Electromechanical analysis of an active engine mount incorporating piezoelectric stack actuators. *Adaptive Structures and Composite Materials, Analysis and Application ASME.* AD-Vol. 45 pp. 211-218 1994.

[19] Fuller C. R. Elliott S. J. & P.A. Nelson P.A. *Active control of vibration.* Academic press. ISBN 0-12-269440-6 1996.

[20] Beards C. F. *Engineering vibration analysis with application to control systems.* Edward Arnold. ISBN 0 340 63183 X 1995.

[21] Browning D. R. & Woodson W. D. A Negative capacitance damping circuit for a boring bar with an embedded piezoelectric reaction mass actuator. *Proceedings of the 12th International Modal Analysis Conference.* pp. 511-517 1994.

[22] Pratt J. R. and Nayfeh A.H. Active vibration control for chatter suppression. *Proceedings of the 38th AIAA Structures, Structural Dynamics and Materials Conference. Kissimmee. AIAA paper number 97-1210.* pp. 623-633 1997.

[23] Pratt J. R. and Nayfeh A.H. Experimental system identification and active vibration control of smart machine tools. *Structural Dynamics and Control, Proceedings of the 11th VPI & SU held in Blacksburg Virginia.* May 12-14 1997.

[24] Pratt J. & Nayfeh A. H. Boring bar chatter control. *Proceedings of the 16th International Modal Analysis Conference.* p 215-225 1998.

[25] Hakansson L. Sturesson P-O. H. & Claesson. Active control of machine tool vibration. *Proceedings of the 6th International Conference on Manufacturing Engineering. Melbourne.* November 29 – December 1 1995.

[26] Hakansson L. Sturesson P.-O. H. & Lago T. Active control of chattering in turning – The origin of chatter. *Proceedings of the 17th International Modal Analysis Conference.* p 1799-1805 1999.

[27] Hakansson L. Sturesson P.-O. H. & Lago T. Active control of machine tool chatter. *Proceedings of the 17th International Modal Analysis Conference.* p 1826-1831 1999.

[28] Claesson I. & Hakansson L. Active control of machine tool vibration in a lathe. *Proceedings of the 5th International Conference on Sound and vibration. Adelaide South Australia.* December 15-18 p 501-510 1997.

[29] Claesson I. & Hakansson L Active control of machine tool vibration. *Proceedings of the 6th International Conference on Manufacturing Engineering. Melbourne.* pp.905-910 November 29 – December 1 1995.

[30] Hakansson L. Claesson I. & Sturesson P.-O. H. Adaptive feedback control of machine tool vibration based on the filtered-x LMS-algorithm. *Journal of Low Frequency Noise Vibration and Active Control.* Vol. 17 no. 4 pp. 199-213 1998.

[31] Tobias S. A. *Machine tool vibration.* Blackie & son LTD. 1965.

[32] Tlusty J. & Koenigsberger D. *Machine tool structures volume 1.* Pergamon press. Library of congress catalog card no. 79-84073 1970.

[33] Zatarian M. & Leizaola J. Improvement of the dynamic stiffness of machine tools by adaptively tuned dynamic absorbers. *Noise and Vibration Worldwide.* pp. 12-17 March 1998.

[34] Chung B. Smith, S. & Tlusty J. Active damping of structural modes in high speed machine tools. *Journal of Vibration and Control.* Vol.3 no. 3 pp. 279-295 August 1997.

[35] Martinez David R. Hinnerichs Terry D. & Redmond James M. Vibration control for precision manufacturing using piezoelectric actuators. *Journal of Intelligent Materials and Structures.* Volume 7 pp. 182 to 191 March 1997.

[36] Riehle P. J. & Brown D. Machine tool modification with tuned dampers. *Sound and Vibration.* pp. 34-39 January1984.

[37] Shibo X. & Junbao L. Lingmi Z. Design, modeling and verification of piezoelectric actuator for adaptive truss structures. *Proceedings of the 15th International Modal Analysis Conference.* 1997.

[38] Allemang R. J. & Brown D. L. A correlation coefficient for modal testing. *Proceedings of the 1st International Modal Analysis Conference.* 1983.

[39] Ewins D. J. *Modal testing theory and practice.* John Wiley and sons. ISBN 0 863080 017 3 1984.

[40] Balmés E. *Experimental and analytical structural dynamic toolbox for use with Matlab, User's Guide.* Scientific software group. April 1997.

[41] Friedland B. *Control system design, An introduction to state space methods.* McGraw Hill. ISBN 0-07-022441-2 1986.

[42] Grace A. Laub A. J. Little J. N. & Thomson C. M. *Control system toolbox for use with Matlab User's Guide.* Mathworks Inc. July 1992.

[43] Raath A.D. Structural dynamic response reconstruction in the time domain. PhD thesis. *Department of Mechanical and Aeronautical Engineering, University of Pretoria.* November 1992.

[44] Ljung L. *System identification toolbox for use with Matlab, User's Guide.* Mathworks Inc. May 1995.

[45] Coleman T. Branch M. A. & Grace A. *Optimization toolbox for use with Matlab, User's Guide.* Math works Inc. January 1999.

[46] Bartkowiak R. A. *Electrical circuit analysis.* John Wiley and sons. 1985.

Appendix A

Finite element model updating

In section 2.5.2 the shunted piezoelectric absorber was implemented on a FEM of an aluminium cantilevered beam, in order to verify the mathematical model of shunted piezoelectric absorber. An attempt to model the tool holder of the lathe with finite elements is documented in section 3.3.2. In both cases the structures were modelled with Bernoulli-Euler beam-elements and updated to match experimental results with an optimisation algorithm.

The optimisation algorithm minimised the difference between the EMA and FEM natural frequencies. The matching modes were selected via a MAC test.

A.1 FEM updating results of the cantilevered beam

The finite element model of the cantilevered beam was updated with and without the actuator since, the addition of the actuator had a large influence on the structural modes. The modulus, density, height and width of the beam elements were as variable parameters in the model updating process. A stiffness coefficient was added to the model as a variable parameter, in order to simulate the static influence of the actuator.

A.1.1 FEM updating results without the actuator

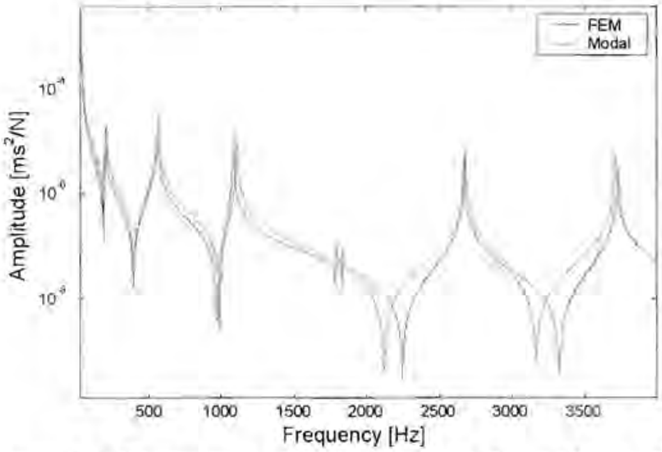

Figure A.1 *Frequency response data at the collocated point*

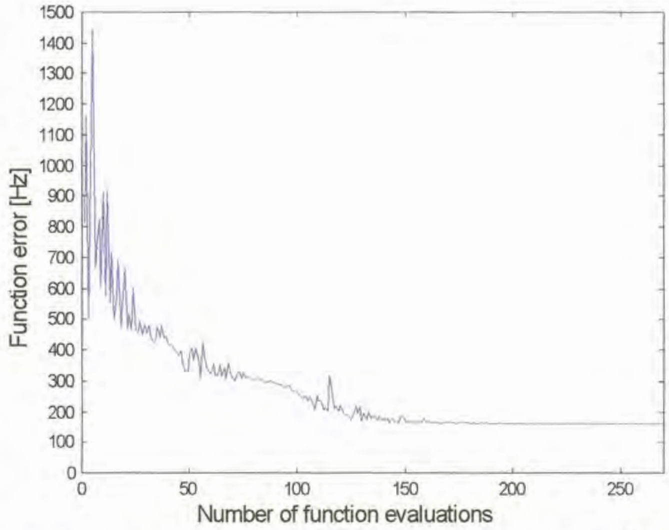

Figure A.2 *The objective function value versus the number of function evaluations*

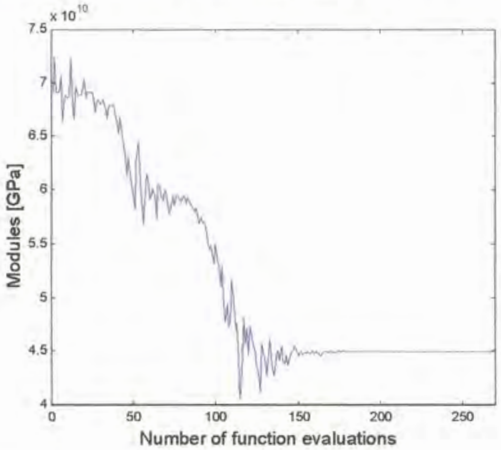

Figure A.3 The Young's modulus value versus the number of function evaluations

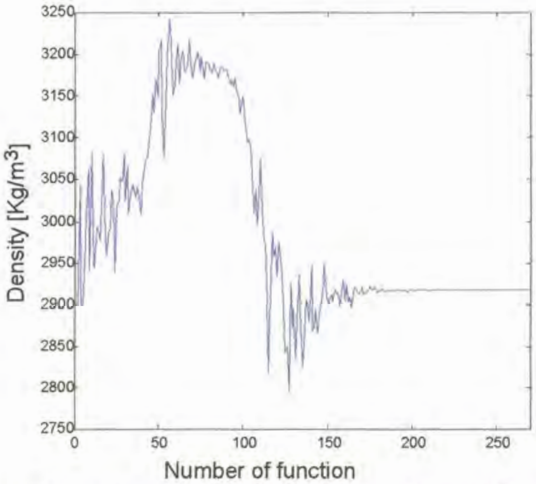

Figure A.4 *The density value versus the number of function evaluations*

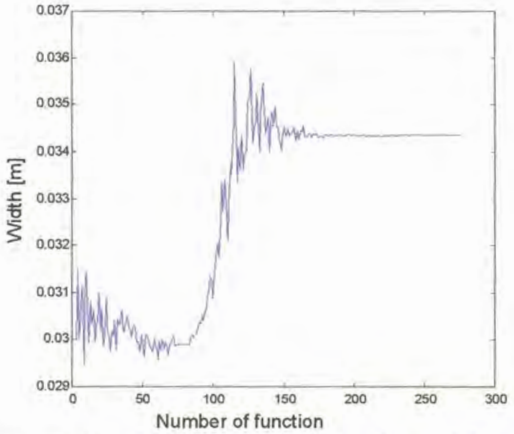

Figure A.5 *The width value versus the number of function evaluations*

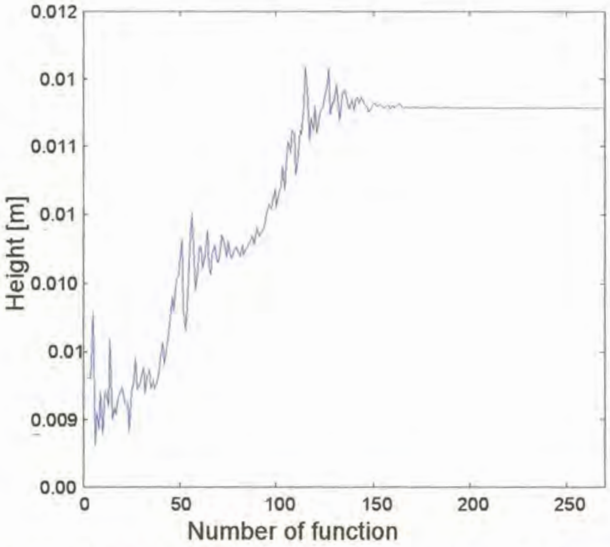

Figure A.6 The height value versus the number of function evaluations

A.1.2 FEM updating results with the actuator

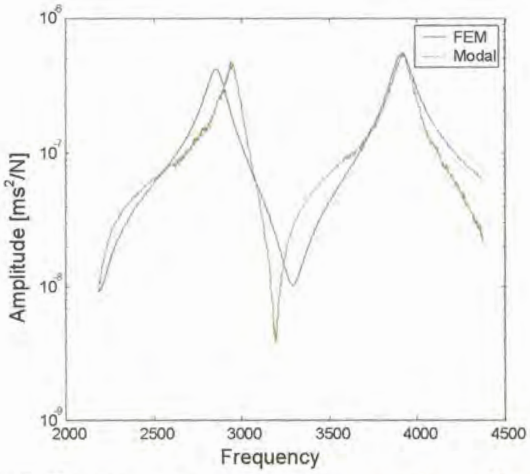

Figure A.7 *Frequency response data at the collocated point*

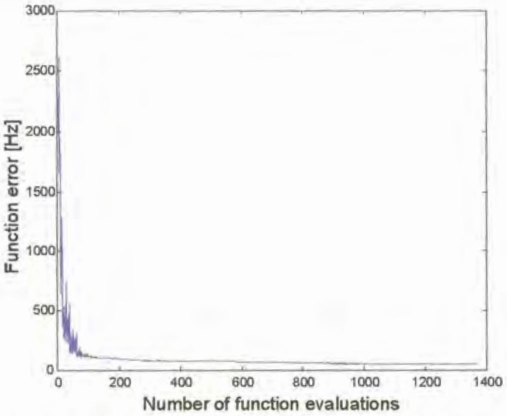

Figure A.8 *The function error value versus the number of function evaluations*

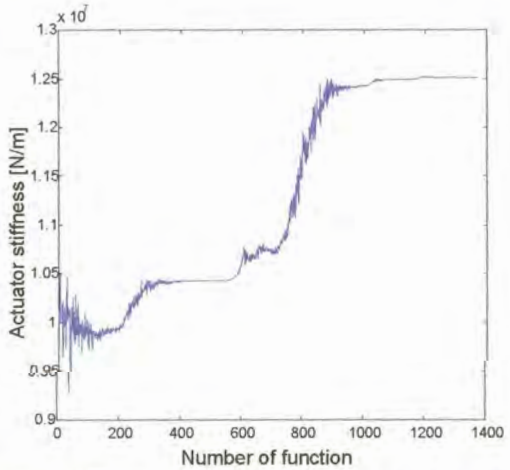

Figure A.9 The actuator stiffness value versus the number of function evaluations

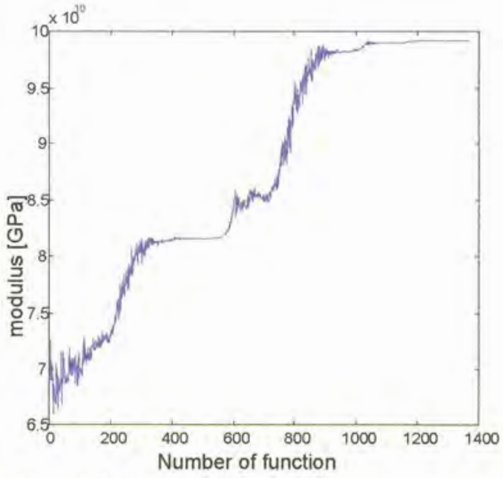

Figure A.10 *The Young's modulus value versus the number of function evaluations*

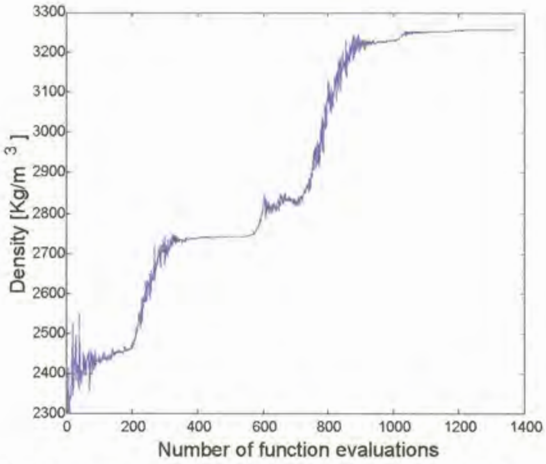

Figure A.11 The density value versus the number of function evaluations

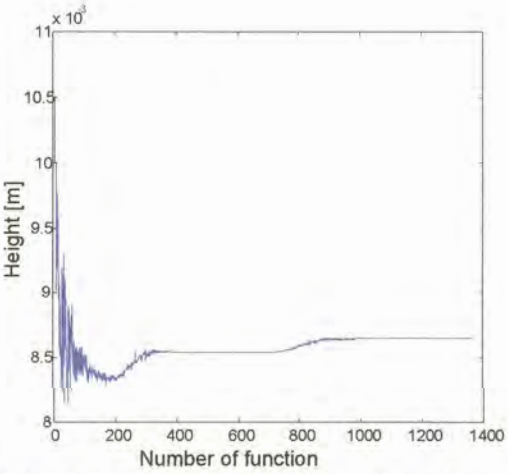

Figure A.12 *The height value versus the number of function evaluations*

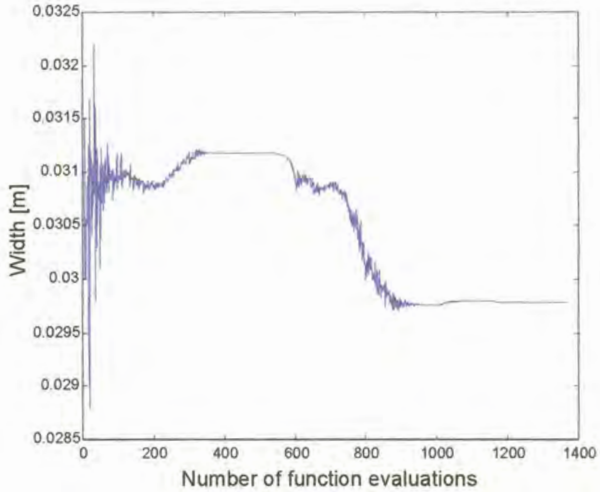

Figure A.13 *The width value versus the number of function evaluations*

A.2 FEM updating results of the tool holder

The tool holder was modelled with beam elements while the support stiffness of the shank and tool changer were represented by 9 spring elements. A schematic diagram of the tool holder is presented in figure A.14.

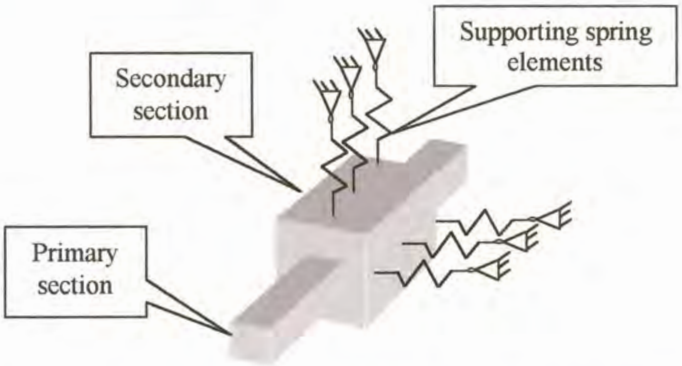

Figure A.14 *Schematic diagram of the tool holder*

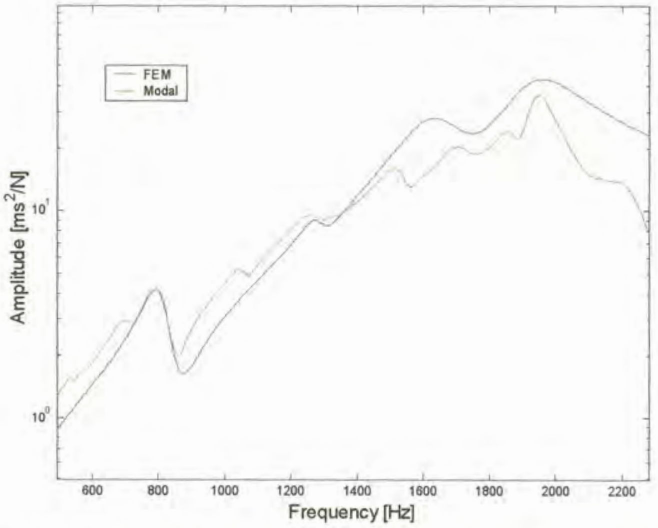

Figure A.15 *FRFs at the tip of the tool holder in the vertical direction*

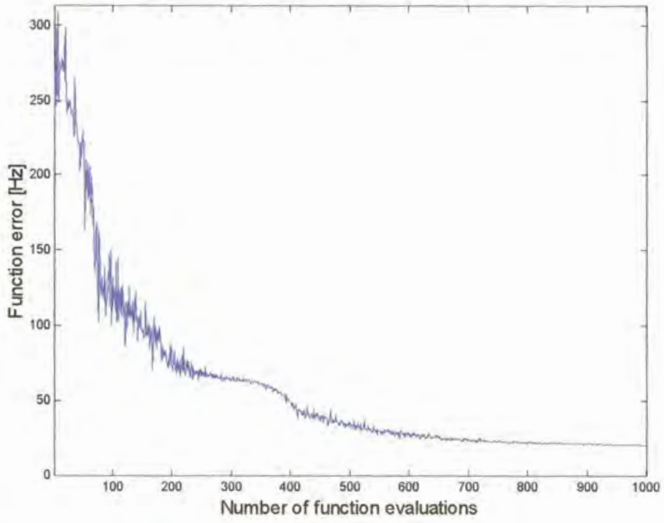

Figure A.16 *Objective function error versus the number of function evaluations*

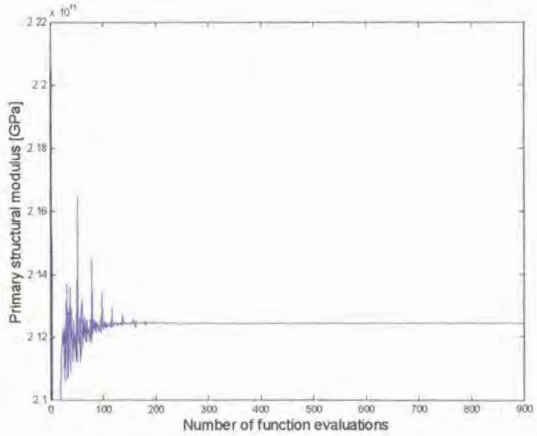

Figure A.17 *Primary structural modulus versus the number of function evaluations*

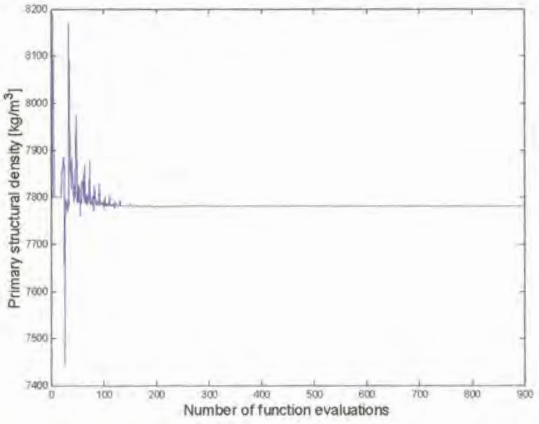

Figure A.18 *Primary structural density versus the number of function evaluations*

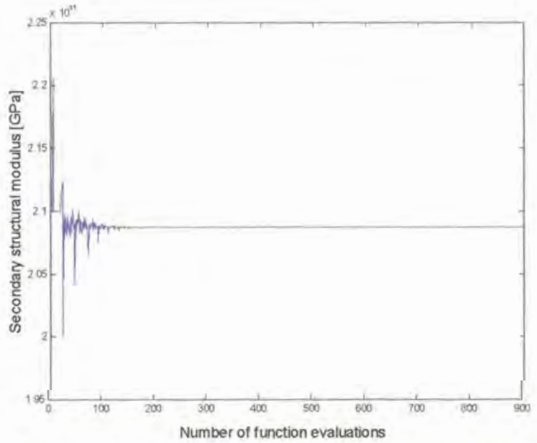

Figure A.19 *Secondary structural modulus versus the number of function evaluations*

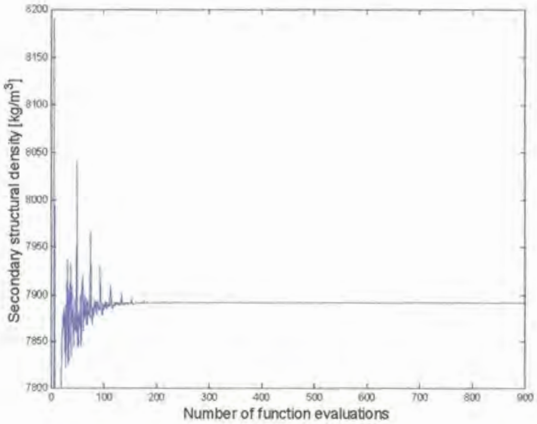

Figure A.20 *Secondary structural density versus the number of function evaluations*

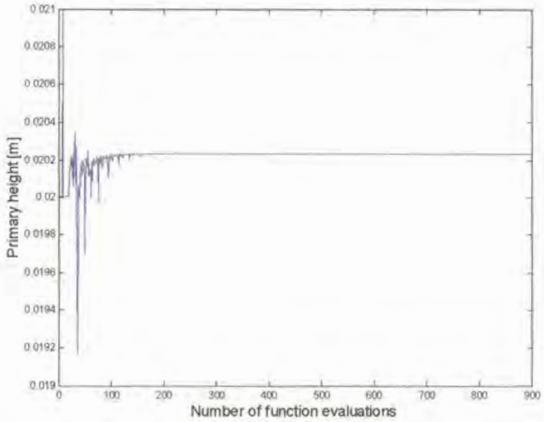

Figure A.21 *Primary beam height versus the number of function evaluations*

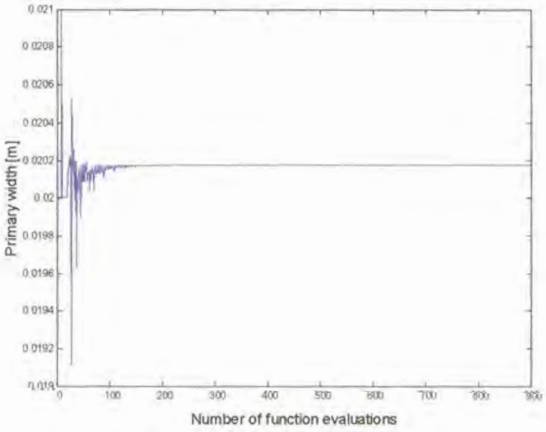

Figure A.22 *Primary beam width versus the number of function evaluations*

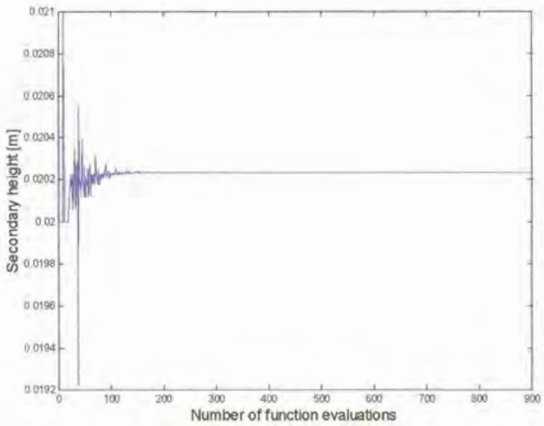

Figure A.23 *Secondary beam height versus the number of function evaluations*

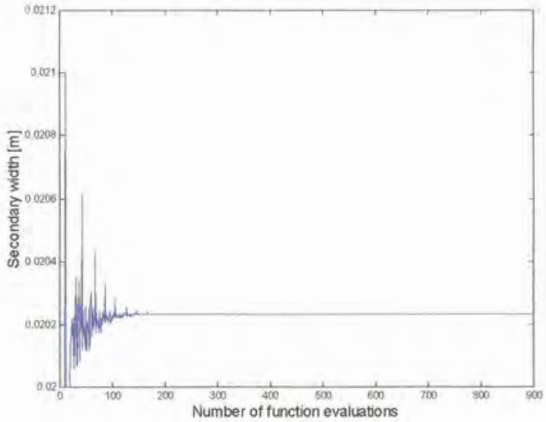

Figure A.24 *Secondary beam width versus the number of function evaluations*

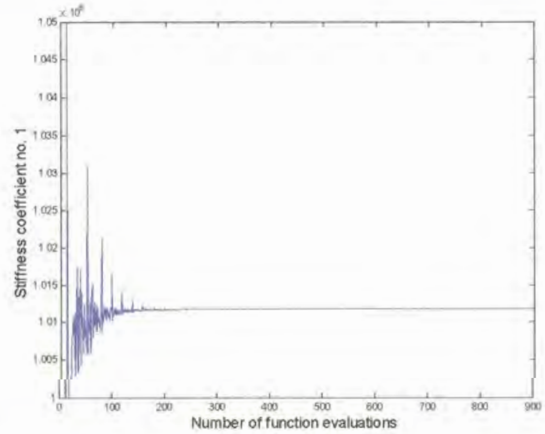

Figure A.25 *Stiffness coefficient number 1 versus the number of function evaluations*

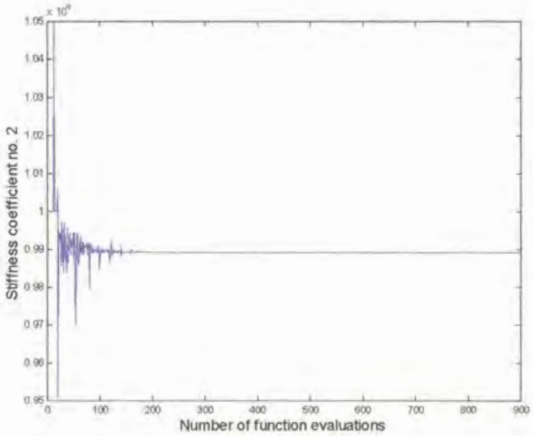

Figure A.26 *Stiffness coefficient number 2 versus the number of function evaluations*

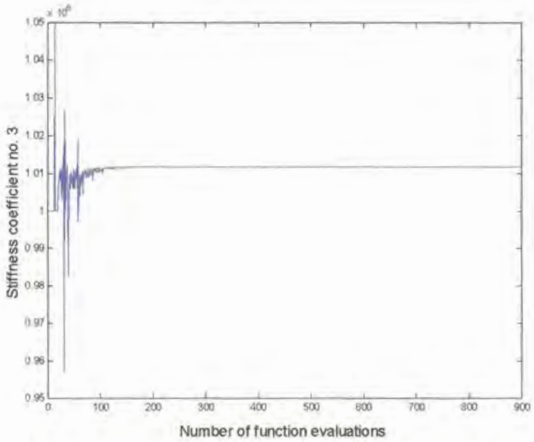

Figure A.27 *Stiffness coefficient number 3 versus the number of function evaluations*

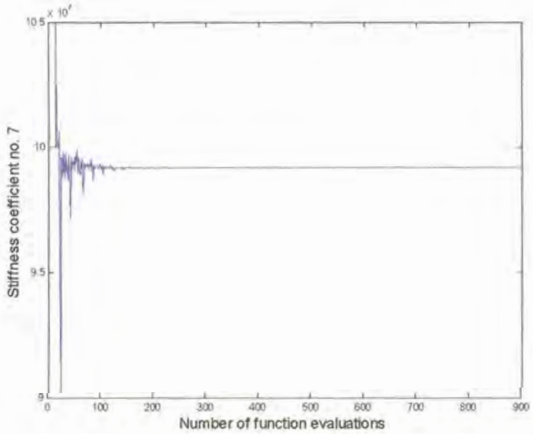

Figure A.28 *Stiffness coefficient number 7 versus the number of function evaluations*

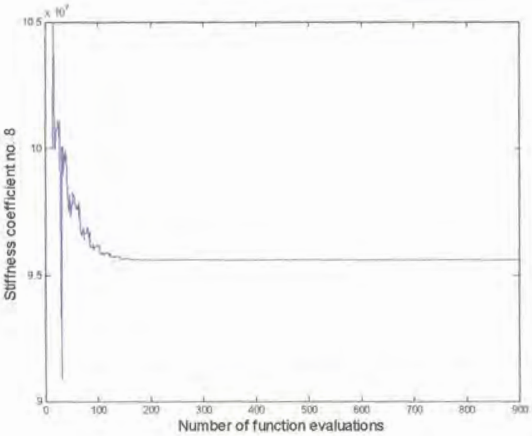

Figure A.29 *Stiffness coefficient number 8 versus the number of function evaluations*

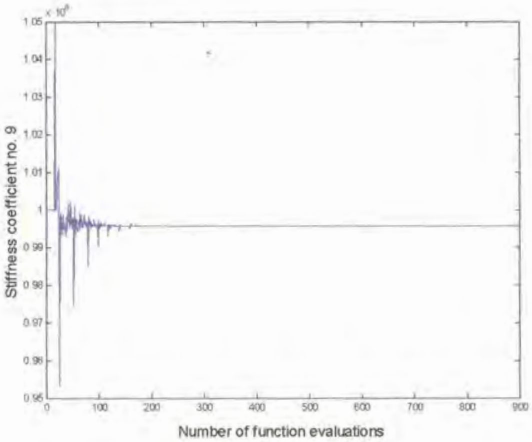

Figure A.30 *Stiffness coefficient number 9 versus the number of function evaluations*

Appendix B

Transmissibility measurements

The transmissibility functions were measured to construct the ODS. The topic is discussed in section 3.1. Details of the machining process is tabled in table 3.1. The figures in the appendix display the measured transmission functions during two separate machining runs under the same machining conditions.

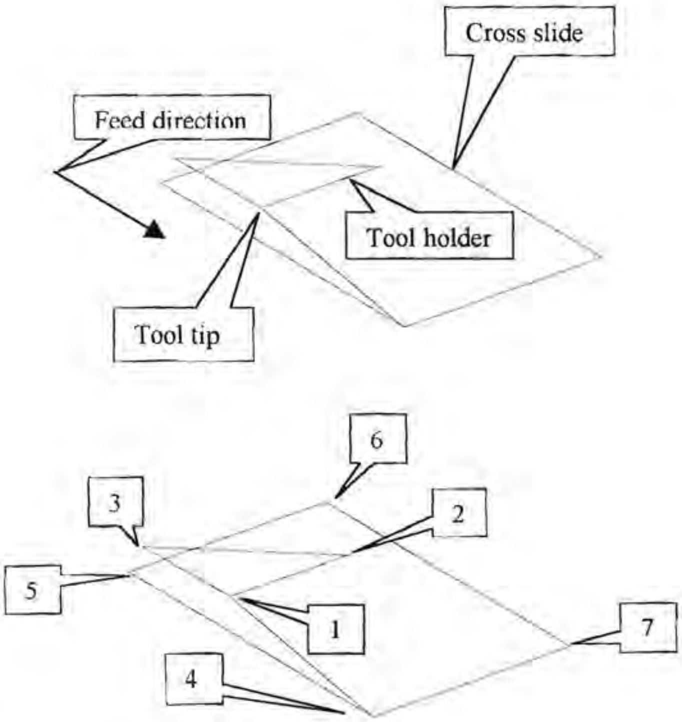

Figure B.1 *Schematic diagram of the transmissibility measurement points*

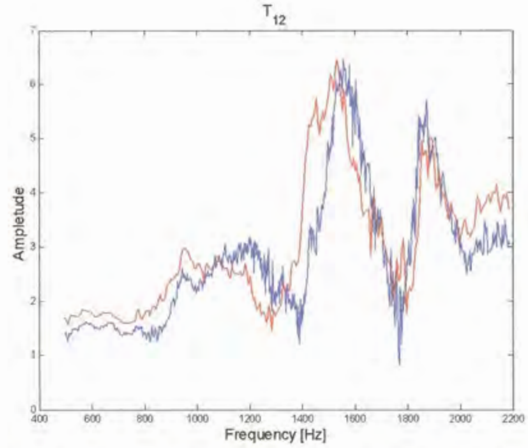

Figure B.2 *Transmissibility function between point 2 and 1 in the horizontal direction*

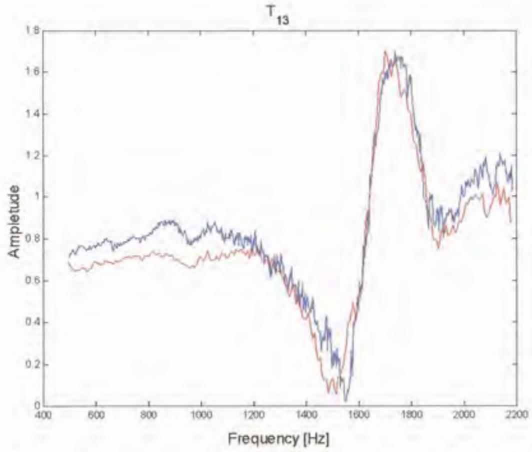

Figure B.3 *Transmissibility function between point 3 and 1 in the horizontal direction*

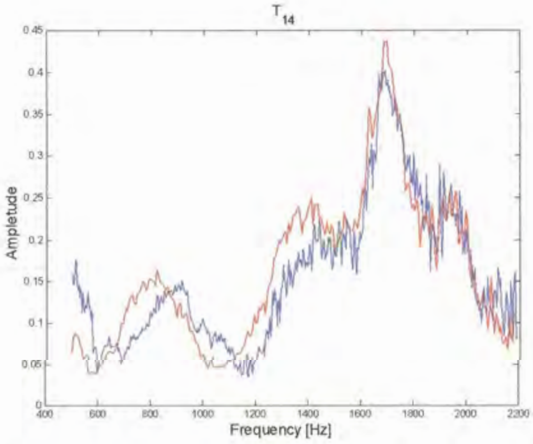

Figure B.4 *Transmissibility function between point 4 and 1 in the horizontal direction*

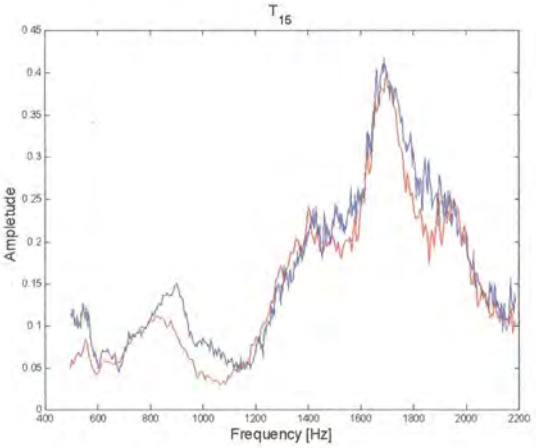

Figure B.5 *Transmissibility function between point 5 and 1 in the horizontal direction*

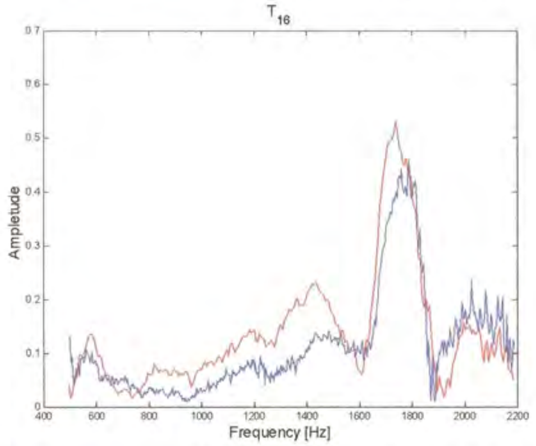

Figure B.6 *Transmissibility function between point 6 and 1 in the horizontal direction*

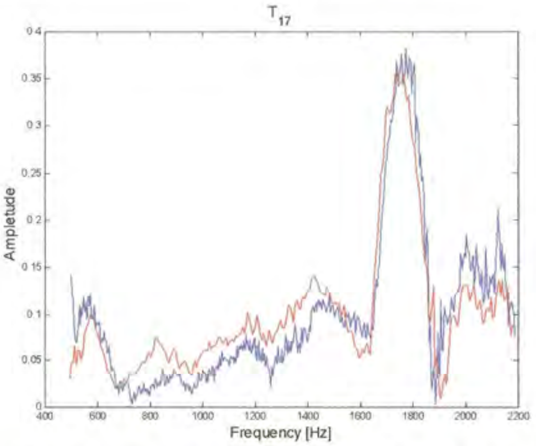

Figure B.7 *Transmissibility function between point 7 and 1 in the horizontal direction*

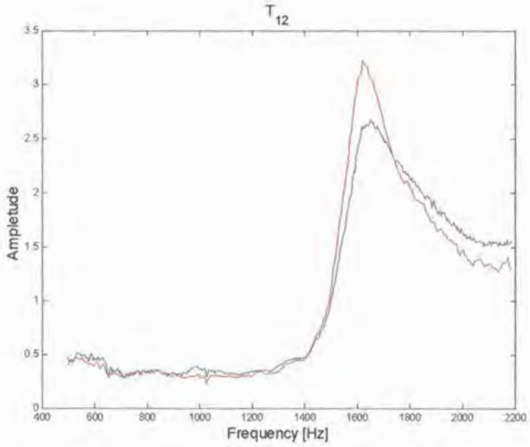

Figure B.8 *Transmissibility function between point 2 and 1 in the vertical direction*

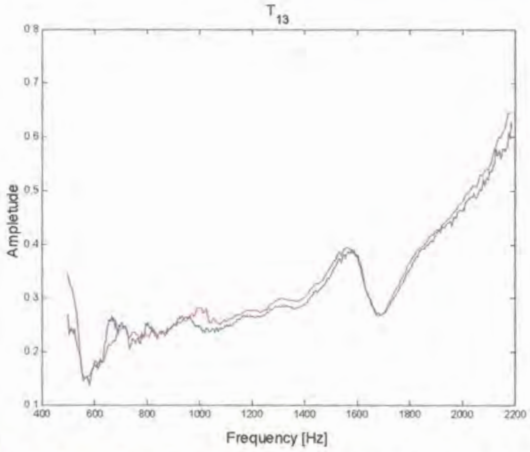

Figure B.9 *Transmissibility function between point 3 and 1 in the vertical direction*

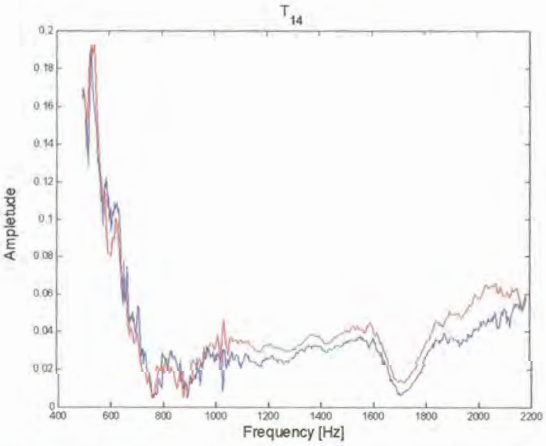

Figure B.10 *Transmissibility function between point 4 and 1 in the vertical direction*

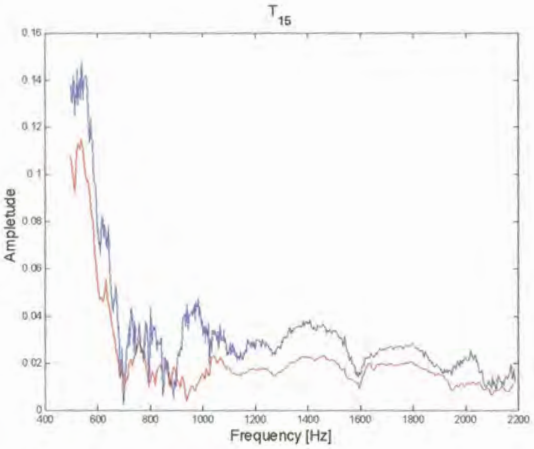

Figure B.11 *Transmissibility function between point 5 and 1 in the vertical direction*

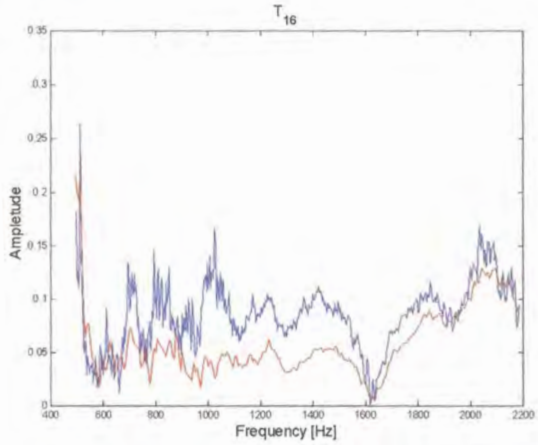

Figure B.12 *Transmissibility function between point 6 and 1 in the vertical direction*

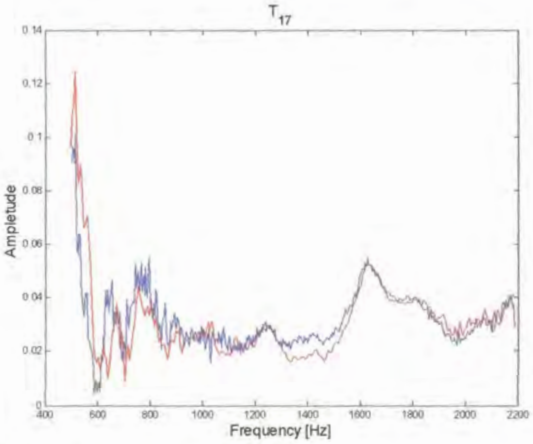

Figure B.13 *Transmissibility function between point 7 and 1 in the vertical direction*